DYNAMIC RESERVOIR CHARACTERIZATION OF NATURALLY FRACTURED RESERVOIRS FROM AN INTER-WELL TRACER TEST

A Thesis

by

UFUK KILICASLAN

Submitted to the Office of Graduate and Professional Studies of
Texas A&M University
in partial fulfillment of the requirements for the degree of

MASTER OF SCIENCE

Chair of Committee,	David S. Schechter
Committee Members,	Robert A. Wattenbarger
	Yuefeng Sun
Head of Department,	A. Daniel Hill

December 2013

Major Subject: Petroleum Engineering

ABSTRACT

After field redevelopment in the Sherrod Unit of the Spraberry Trend Area, an inter-well tracer test was conducted at the field scale in order to understand the fracture system, which forms preferential flow paths for better management of waterflooding. The test consisted of 13 injection wells and more than 110 producing wells that were sampled, with each injector having its own unique tracer.

A wide range of tracer responses was observed in terms of tracer recovery, breakthrough time, and tracer velocity. Additional noise on tracer data was noticed due to reinjection of produced water. In this study, a comprehensive workflow is presented for dynamic reservoir characterization of naturally fractured reservoirs from an inter-well tracer test by incorporation of analytical interpretation, streamline simulation, and streamline-based optimization techniques. Categorized tracer responses were mapped according to analytical analysis, and dominating flow trends were detected in E-W and NE-SW directions before the simulation study. The constructed three-phase, dual-porosity model was simulated by a streamline simulator. Certain parameters in the model were modified based on high tracer response until a reasonable match was obtained for an inverted nine-spot pattern and breakthrough time of the injected tracer. Once the model became capable of matching historical field production, a 1-year prediction run was conducted for optimization. Cumulative oil production was increased by 8,000 bbl by allocating more water toward efficient producers, and 10,000 bbl less water was produced for the optimized case.

DEDICATION

I dedicate this work to Hz. Hussein who laid down his life to protect essence of the Islam and to Mustafa Kemal Ataturk who established Turkish Republic as an independent country. I also dedicate this work to my family, to Aylin, and to my best friends.

ACKNOWLEDGEMENTS

I would like to thank my committee chair, Dr. David Schechter, and my committee members, Dr. Wattenbarger and Dr. Sun, for their guidance and support throughout the course of this research.

I would like to also thank Turkish Petroleum Corporation for scholarship to be a graduate student at Texas A&M University and Pioneer Natural Resources, which provided the data set in this study.

Thanks also go to Aymen who taught me so many things as well as Hisham, Kanfar, Zuhair, Alkouh, Suliman and roommates in 815, and colleagues and the department faculty and staff for making my time at Texas A&M University a great experience.

I also want to extend my gratitude to the Room 112; Mehmet, Savas and Sezer, and to the KANKAS seniors; Cagri, Serkan, Gorkem, Ismail and Mutlu, and to KANKAS juniors; Atalay, Can, Gizem, Semih, Sezgi and Zalo. Also, many thanks go to Turkish friends in College Station; Abdulkadir, Basri, Gokhan, Mustafa and Yasin.

Finally, thanks to my family for their encouragement and to Aylin for her patience and love.

NOMENCLATURE

C	tracer concentration in parts per trillion
e_i	injection efficiency
e_{min}	lower injection efficiency limit
e_{max}	upper injection efficiency limit
q_{inj}	injection rate of injector in stb/day
q_{prod}	production rate of producer in stb/day
k_{rwe}	relative permeability of water at residual oil saturation
k_{rw}	relative permeability of water
k_{ro}	relative permeability of oil
L_x	fracture spacing in x-direction, ft
L_y	fracture spacing in y-direction, ft
L_z	fracture spacing in z-direction, ft
S_w	water saturation
S_{wr}	connate water saturation
S_{or}	residual oil saturation
S_n	normalized water saturation
w_i	increase/decrease in weight
w_{max}	maximum weight at e_{max}
w_{min}	minimum weight at e_{min}

W_{inj}	cumulative injected water from injector in stb
ΔW_{inj}	cumulative injected water for one time interval
W_{prod}	cumulative water production of producer in stb
ΔW_{prod}	cumulative produced water for one time interval
Δt	elapsed time after tracer injection in days
α	exponent
σ	sigma, matrix-fracture interaction coefficient
$\emptyset_m$	matrix porosity, fraction
$\emptyset_f$	fracture porosity, fraction

UNITS

bbl	barrel
ft	feet
L	liter
ppt	parts per trillion
stb	stock tank barrel

TABLE OF CONTENTS

Page

LIST OF FIGURES

Page

LIST OF TABLES

Page

CHAPTER I

INTRODUCTION

Most of the oil fields in the world are now being operated by either secondary or tertiary recovery methods to produce remaining oil after primary depletion. No matter which technique is used, overall efficiency increases by having accurate reservoir characterization capable of reflecting actual fluid flow in the reservoir.

Fluid flow in a porous medium is affected by any kind of heterogeneity within rock fabrics. The presence of fractures further triggers the complexity of fluid flow in a porous medium. As a result, characterization of naturally fractured reservoirs becomes more challenging. To overcome difficulty in comprehending fluid flow phenomena in naturally fractured reservoirs, a variety of static and dynamic data are incorporated to understand overall reservoir heterogeneity and to decide the best option for recovery enhancement.

The basic requirement for managing waterflood is to understand how injection wells displace oil to producing wells. However, reservoir-originated effects such as faulting, structure, permeability, influx, and boundaries beside the wellbore make fluid movements complicated to diagnose. Active management of the displacement process can be accomplished by quantifying these complicated fluid movements (Grinestaff, 1999).

An inter-well tracer test has many distinctive advantages for reservoir characterization because it could detect reservoir heterogeneity and provide useful

information such as volumetric sweep, directional flow trends, and delineation of flow barriers to optimize tertiary recovery in terms of design, control, and implementation (Wagner, 1977).

Streamline simulation is the best option for modeling an inter-well water tracer test due to its nature of tracing. It directly assesses dynamic injector-producer connectivity with respect to sweep efficiency, allocation factor, and injection efficiency, so the inter-well tracer test provides reliable, definitive, and unambiguous information on injector-producer connectivity (Guan et al., 2005).

1.1. Project Overview

The conservative tracer test was conducted in the Sherrod Unit of the Spraberry Field, as shown in Fig. 1. The project area includes 13 injectors and more than 110 production wells, with each injection well having its own unique tracer. The general pattern is an inverted nine-spot design. A tracer concentration of 50 parts per trillion (ppt) was determined as a low detection limit. In Table 1, the injection schedule of tracers is illustrated by injection well, injection date, tracer type, and amount of tracer injected in liters. However, they were injected as slug with a ratio of 10%.

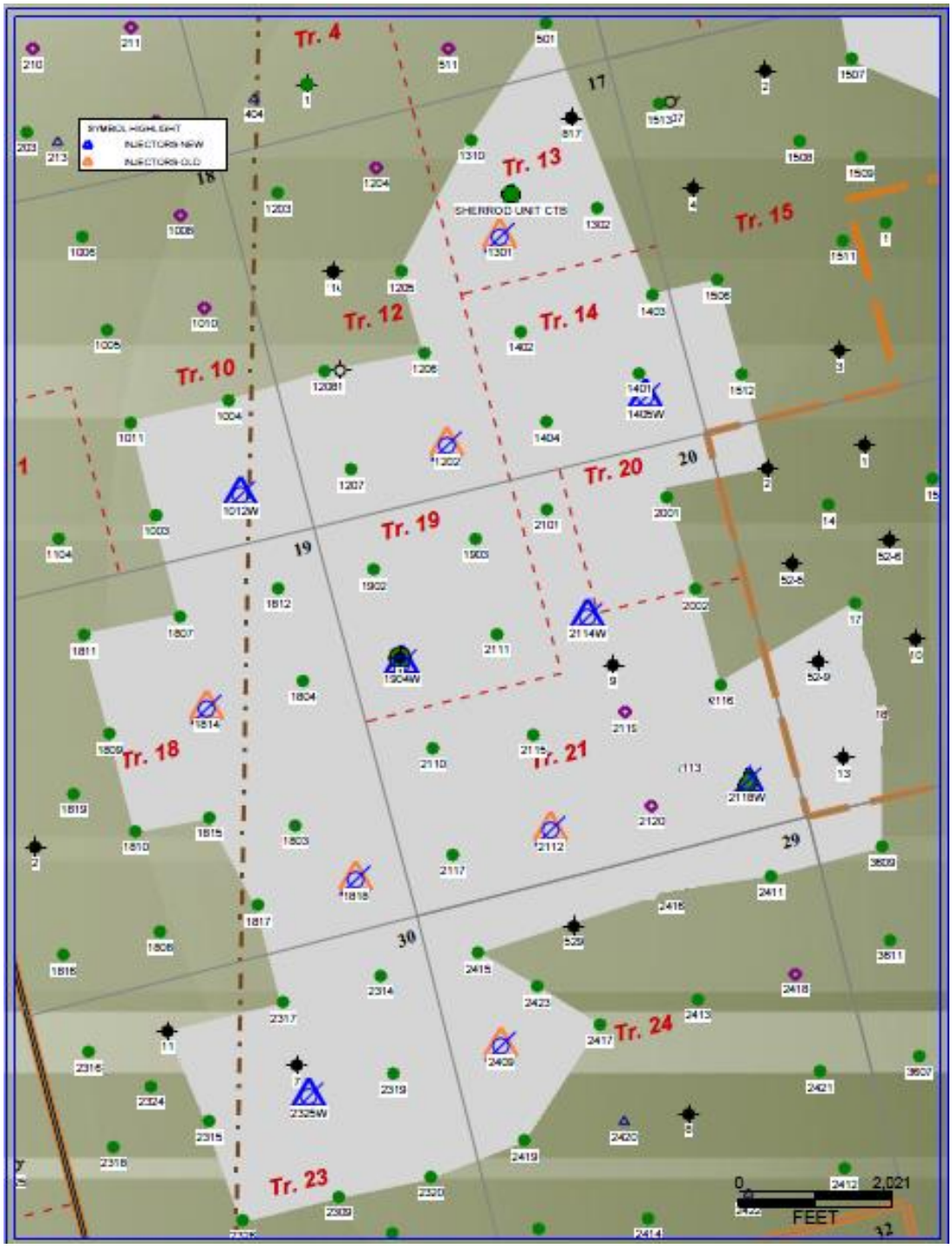

Fig. 1: Extent Of Tracer Test In Sherrod Unit

Table 1: Summary Of Tracer Injection Program

Well Name	Injection date	Tracer type	Amount (L)	Amount (gram)
Sherrod U 1814W	25-Apr-11	IWT-1900	200	20000
Sherrod U 1202W	25-Apr-11	IWT-2400	118	11800
Sherrod U 1818W	26-Apr-11	IWT-1100	212	21200
Sherrod U 2112W	26-Apr-11	IWT-1700	193	19300
Sherrod U 2409W	26-Apr-11	IWT-1200	231	23100
Sherrod U 1904W	27-Apr-11	IWT-2200	159	15900
Sherrod U 2114W	27-Apr-11	IWT-2500	128	12800
Sherrod U 2325W	28-Apr-11	IWT-1000	273	27300
Sherrod U 2118W	28-Apr-11	IWT-1600	148	14800
Sherrod U 1012W	28-Apr-11	IWT-2100	154	15400
Sherrod U 701W	28-Apr-11	IWT-2000	168	16800
Sherrod U 1301W	1-May-11	IWT-1400	88	8800
Sherrod U 1405W	1-May-11	IWT-1300	92	9200

1.2. Research Objectives

- Analyze inter-well tracer response by using analytical techniques to characterize reservoir heterogeneity, sweep efficiency, and connectivity.
- Conduct a series of simulation jobs by FrontSim™ for assessing flow dynamics in a naturally fractured reservoir based on tracer observations.
- Use the optimization suite FrontSim for a history-matched pattern in order to enhance waterflood performance in fractured reservoirs.

1.3. Thesis Outline

The content of each chapter is summarized below.

Chapter I is a brief introduction to research the topic, project overview, and its objectives.

Chapter II is a literature review about the tracer and its analyzing techniques for both fractured and non-fractured reservoirs. It also includes modeling of naturally fractured reservoirs and streamline simulation. Finally, a general description of the Spraberry Trend Area is given.

Chapter III illustrates results and conclusions from interpretation of tracer response by analytical methods. Moreover, historical reservoir performance was evaluated at the field scale before attempting simulation work.

Chapter IV describes construction of a dual-porosity model and initial sensitivity analyses on reservoir parameters in FrontSim. It also presents a case study for history-matching work. Then, a comparison is shown between the observed and final history-matched model.

Chapter V provides application of the Pattern Flood Management (PFM) suite for the history-matched model and suggestions for maximizing waterflood performance.

Chapter VI shows conclusions from this study and recommendations for future work.

CHAPTER II

LITERATURE REVIEW

In this chapter, general information is given about tracers and their applications. It reviews previous research conducted on tracer interpretation techniques in both non-fractured and fractured reservoirs. Also, it shows progress in modeling naturally fractured reservoirs through time. Finally, a review of the Spraberry Trend Area is presented in many aspects.

2.1. Background

After primary recovery, bypassed oil is recovered by secondary and tertiary recovery methods. In order to be successful in these applications, fluid dynamics and flow paths in the reservoir should be well understood. Much information can be obtained from seismic, geology, and well logs, as well as from reservoir simulation; however, pressure transient tests and inter-well tracer tests provide actual distribution of the fluid transmissibility of a reservoir. Unlike averaged estimation of reservoir parameters from pressure transient tests, inter-well tracer tests can detect preferential flow paths and reservoir heterogeneity between injection and production wells, which is why it increases reservoir resolution in detail and provides better reservoir characterization.

Tracers can be categorized into two main types: radioactive and chemical tracers. Radioactive tracers are chemical compounds that contain radioactive isotopes, and the

time they take to disintegrate to a stable state, called “decay time,” is used for analysis. Chemical tracers for water are classified as dyes, ionic, and organic tracers. However, in terms of application, the two main categories for tracers are conservative and partitioning tracers.

In the case of the conservative tracer or water tracer, it moves only with water without interaction with other phases. The use of these tracers can give more information about flow paths and permeability distribution between wells. However, the partitioning tracer has an interaction with not only water but also other in-situ phases. The chromatographic delay due to a diffused tracer’s reversal movement from in-situ phases to injected water is used to estimate residual oil saturation and fluid distribution.

In industry, these partitioning tracers are referred to as single-well partitioning tracer tests (SWPTTs) and partitioning inter-well tracer tests (PITTs). A SWPTT is an in-situ method to measure fluid saturation in the reservoir and is useful to assign target oil saturation for enhanced oil recovery (EOR) operations. For SWPTT, water that carries chemical tracers is injected into a single well and produced back from same single well for measuring residual oil saturation and connate water saturation. Unlike SWPTT, both conservative and partitioning tracers are injected into the reservoir and are observed from production wells. In-situ oil distribution in the tracer-swept area can be deduced from the separation between elution curves of conservative and partitioning tracers, which relies on the amount and distribution of oil contacted by the partitioning tracers and the partitioning coefficient of tracer (Oyerinde, 2005).

2.2. Tracer Test Interpretation

Depending on tracer type and application, various interpretation techniques exist in the literature. These interpretations include analytical methods, semi-analytical methods, and numerical methods. Inverse modeling has been also used to determine reservoir parameters from tracer response.

Cooke (1971) used the chromatographic method to determine residual oil saturation. Tomich et al. (1973) provided a description of a method to measure residual oil saturation from a single-well chemical tracer in watered-out reservoirs. Deans and Shallenberger (1974) made some modifications to this method in order to determine connate water saturation of a formation producing oil almost without water. Deans (1978) proposed a new technique to estimate fractional flow versus saturation in a reservoir near residual oil saturation by using chemical tracers. The "dead-end" pore model was modified by Deans and Carlisle (1986) to quantitatively evaluate a single-well tracer response in carbonate reservoirs by assuming that diffusion is the only way to access a non-flowing pore system.

For inter-well tracer test analysis, Brigham and Smith Jr. (1965) derived specific equations to quantitatively analyze tracer performance in a single layer in a five-spot flood, which has a unit mobility ratio. Unlike the method by Brigham and Smith Jr. (1965), Baldwin Jr. (1966) developed a model that considers not only divergent flow, but also convergent flow by applying an approximate solution of the dispersion equation to subdivided radial elements to predict tracer flow in a five-spot pattern. Yuen et al.

(1979) demonstrated an algorithm that deconstructs overall tracer profile into individual layer responses and can compute permeability thickness and porosity thickness products for a multi-layered reservoir from five-spot responses. Another approach to a multi-layered reservoir was illustrated by Abbaszadeh-Dehghani and Brigham (1984). They (1984) proposed a correlation of tracer breakthrough curves and pattern breakthrough curves of any homogenous pattern system with a unit mobility ratio into a single curve formed by defining a simple correlation parameter, and they applied an optimization technique to produce equivalent layering for the same system. Lichtenberger (1991) used a steady-state layered tube model to match inter-well responses conducted in EOR pilot areas and observed that this practical model could present permeability distribution of the layers. Agca (Agca, 1987; Agca et al., 1990) added a tracer option to the three-dimensional (3D) UTCHEM compositional simulator developed at the University of Texas at Austin to model laboratory experiments and small-scale field tracer projects. Allison et al. (1991) used this simulation, which can allow for physical dispersion, variable rate, areal permeability variation, and mobile oil unlike streamline simulation in order to quantitatively analyze multiple tracers at the field scale. Datta-Gupta and King (1995) proposed a semi-analytical approach for tracer test analysis, in which an evolution equation is solved exactly along each piece of approximated hyperbolic intervals from streamlines of velocity field obtained from a finite difference simulator. After determining tracer transient time of a production well, tracer response and swept area can be calculated from simple integral expression. A type-curve application based on a different theory was suggested by Gupta et al. (1995). Type curves of transfer

function and phase spectrum formed by using the frequency domain theory for convective transport could be used for estimating heterogeneity and pore volume from a two-well tracer test. Sato and Abbaszadeh (1996) studied how fractures and barriers affect pressure distribution and reservoir displacement performance with a unit mobility ratio for different well patterns by using a complex-variable boundary element method. Akin (2001) used simple spreadsheet models to evaluate tracer flow from injection well to production well in heterogeneous reservoirs.

Although many analytical tools mentioned above could provide information about different reservoir features from a conservative tracer test, the method of moments (MOM) is a robust and simple analytical technique to accurately determine swept volume, which is most crucial information for the success of secondary and tertiary recovery. Initially, Danckwerts (1953) used MOM to calculate swept volume for reactor beds. Deans (1978) introduced this method to the oil industry. Asakawa (2005) provided a 3D derivation of it for any kind of heterogeneous reservoir.

Inverse modeling is another common technique for modeling tracer transport. Mostly, the streamline-based inversion approach has been preferred because of computation efficiency for parameter sensitivity. Many authors (Datta-Gupta et al., 2002; Vasco et al., 1999; Yoon et al., 1999) used the streamline-based inverse model TAMU developed at Texas A&M University. The residual oil saturation distribution of Ranger Field was estimated from PITT data by using this inverse model (Iliassov et al., 2001). Oyerinde (2005) added new derivations to the TAMU inverse model to calculate mobile oil saturation and coupled it with ECLIPSE™ to analyze multi-well PITT in

Ranger Field. The overall idea is that an obtained match for the conservative tracer gives permeability distribution. Saturation distribution is changed until a match is obtained for the partitioning tracer. Altinay (2005) combined both MOM and inverse modeling such that the initial guess of the inverse model for oil saturation was obtained from MOM.

2.2.1. Tracer Test Interpretation in Naturally Fractured Reservoirs

Due to the presence of fractures, fluid flow is a complex phenomenon in these types of reservoirs. Many previous models were not capable of assigning fracture and matrix systems accurately. Grove and Beetem (1971) and Tang et al. (1981) worked on quantitatively estimating reservoir parameters from tracer flow in fractured reservoirs. Ramirez et al. (1993) came up with analytical solutions to tracer flow in naturally fractured reservoirs by considering diffusion, convection, adsorption, and radioactive decay mechanism. The solutions were shown for linear flow of vertical fractures, radial flow of horizontal fractures, and cubic block matrix-fracture geometry. While dispersion and convection occur in the mobile region (i.e., fracture), only diffusion and adsorption were allowed in the immobile or stagnant region (i.e., matrix). Shinta and Kazemi (1993) developed a single-porosity, two-dimensional (2D), two-phase simulation model coupled with a tracer transport model, in which a dual-porosity model was reduced to a single-porosity model for better identifying the flow characteristics of a fracture system from a tracer test. Ramirez-S. et al. (1995) coupled a cubic matrix-fracture geometry model with the Rosenbrock non-linear regression method (Rosenbrock, 1960) to evaluate a tracer

test during radial flow regime and used this composed model for estimating fracture and matrix parameters in a practical sense. Samaniego et al. (2005) provided short- and long-term analytical solutions of proposed models for tracer flow in both homogenous and naturally fractured reservoirs under a constant mass flux condition. Lange et al. (2005) used the 3D discrete fracture network (DFN) flow simulator developed by Lange et al. (2004) to compute tracer flow in fractured reservoirs. Stalgorova and Babadagli (2011) used a modified Random Walk Particle Tracking (RWPT) algorithm to model field-scale tracer injection in a naturally fractured reservoir.

2.3. Modeling Naturally Fractured Reservoirs

Many different simulation techniques have been developed to predict the performance of naturally fractured reservoirs. The three main methods, continuum approach, discrete fracture approach, and integrated approach, have been used for flow modeling of naturally fractured reservoirs.

First, Barenblatt et al. (1960) used a dual-continuum or dual-porosity approach for modeling by assuming that quasi-steady-state flow occurs from matrix to fracture. Warren and Root (1963) assumed pseudo-steady-state flow conditions and introduced two dimensionless parameters, inter-porosity flow coefficient (λ) and storage capacity of secondary porosity (ω). Unlike the model presented by Warren and Root (1963), Gilman and Kazemi (1983) considered a variable matrix block size and calculated shape factor for their dual-porosity, two-phase flow model as

$$\sigma = 4\left[\frac{1}{L_x^2} + \frac{1}{L_y^2} + \frac{1}{L_z^2}\right],$$

where L_x, L_y and L_z are matrix block dimensions.

A 3D, three-phase model was developed by Thomas et al. (1983) in order to simulate fluid flow in naturally fractured reservoirs. The model uses Warren and Root's shape factor and considers gravity, capillary pressure, and viscous forces.

Another approach for modeling fluid flow in naturally fractured reservoirs is the discrete fracture model illustrated by Long et al. (1985) and Dershowitz and Doe (1988). Although fracture representation is close to the actual case, the model assumes that flow occurs only through a connected fracture system and ignores matrix permeability and isolated fracture contribution. Furthermore, it has other limitations on applications in terms of size, speed, and complexity compared with the continuum approach.

Several authors (Dershowitz et al., 2000; Jensen et al., 1998; Lee et al., 1997; Lee and Lough, 1999; Ouenes and Hartley, 2000; Sarda et al., 2002) presented different techniques for coupling the dual-continuum approach and the discrete fracture approach in order to retain their own advantages on modeling. A DFN simulator, which combines both approaches in a certain fashion, was developed by Lange et al. (2004).

2.4. Streamline Simulation

Streamline simulation solves the flow equation based on the IMPES formulation, in which the pressure equation is solved first with an implicit numerical method and then

the saturation equation is solved explicitly. After obtaining a pressure solution from input data, instantaneous velocity field is generated to trace the streamlines. Traced streamlines form a new coordinate system called "time-of-flight coordinates," which is a novelty of streamline simulation. Once transformation is done from the 3D coordinate system into one-dimensional (1D) time-of-flight coordinates along the streamline, the 1D transport equation is solved in the time-of-flight coordinate, either analytically or numerically. Calculated saturation along the streamline is mapped back onto the original 3D physical grid. This procedure is followed for each time step or each pressure update.

The streamline approach in fluid flow calculation has been used for many years. Speed advantage was the early focus for streamline simulation rather than flow physics. A second stage focused more on fluid flow physics, extending application of streamline simulation to more complex flow issues such as compositional and thermal simulations. Currently, the focus is using streamline simulation as a complement to finite difference simulation in order to obtain vital information for reservoirs such as drainage areas, flood optimization and sweep efficiency enhancement, uncertainty quantification, etc. (Al-Najem et al., 2012).

Streamlines are defined as integrated curves tangential to a defined velocity field at a given instant in time (Datta-Gupta and King, 2007). Early description of the analytical equation, which defines stream function and potential function for incompressible flow in a 2D domain, was provided by Muskat and Wyckoff (1934). In order to predict two-phase flow in a simple 2D, two-well homogeneous model, Fay and Pratts (1951) established a numerical model based on those descriptions. Introduction of

the streamtube approach by Higgins and Leighton (1962), a solution of Buckley-Leverett along this 1D system, was used for modeling multiphase flow in porous media. Numerical advantage and computation speed of analytical solution techniques are employed by Thiele et al. (1996), Peddibhotla et al. (1996) and Jessen and Orr (2002). However, assumptions for an analytical solution do not take into consideration gravity, changing well conditions, and non-uniform initial conditions. Batycky (1997) and Batycky et al. (1997) were the first to develop a 3D, two-phase streamline simulator by using numerical solutions along streamlines, combined with operator splitting techniques, to model these field-scale phenomena properly. For two-phase incompressible flow including capillary effects, Rodriguez et al. (2003) developed a full 3D streamline simulator such that gravity and capillary effects are separated from convective terms via advances in operator splitting. A modified pressure and saturation equation, including capillary and gravity effects to the streamline simulator, was tested (Berenblyum et al., 2003). A streamline-based dual-porosity simulator was developed by Donato et al. (2003) for modeling waterflooding in fractured reservoirs. Likewise, to account for capillary, gravity, and matrix-fracture transfer function, another 3D incompressible streamline simulator was used to model water-oil displacement in dual-porosity reservoirs (Moreno et al., 2004). Cheng et al. (2006) proposed a solution for modeling compressible flow in reservoirs by streamline simulation. They introduced an "effective density" term along streamlines, which takes a part in the streamline saturation equation as a density-dependent source term, and used this information for incorporating cross-streamline effects via pressure and remapping saturations. An API

tracking option was included by Beraldo et al. (2007) into a incompressible 3D streamline simulator for modeling variation in oil composition. They (Beraldo et al., 2008) extended this work to the case of compressible flow, with formulation provided by Cheng et al. (2006) and Osako and Datta-Gupta (2007). The difference was using cumulative streamtube volumes as the distance coordinate for the transport solution along the streamline instead of using time-of-flight. Extension to a streamline simulator by Thiele et al. (2010) allowed modeling polymer flooding at the field scale.

Application of streamline simulation in reservoir engineering can be categorized into three major groups: (1) history matching, which varies from the simple use of streamline-delineated drainage zones in traditional history matching to the sophisticated use of streamline information for data integration, (2) reservoir management and surveillance in terms of sweep efficiency, rate optimization, well placement, and EOR and (3) upscaling, ranking, and characterization of fine-scale static models for validation of the flow simulation model (Al-Najem et al., 2012). Several examples for the application of streamline simulation can be found in the literature (Datta-Gupta and King, 2007).

2.5. Review of Spraberry Trend Area

The Spraberry Trend Area was a candidate for the largest oil field in the world as it covers a 2,500-mi^2 area in the Permian Basin (Fig. 2). Even though estimated oil in the

Spraberry reservoir was originally more than 10 billion bbl, the recovery factor is less than 10% (Schechter, 2002).

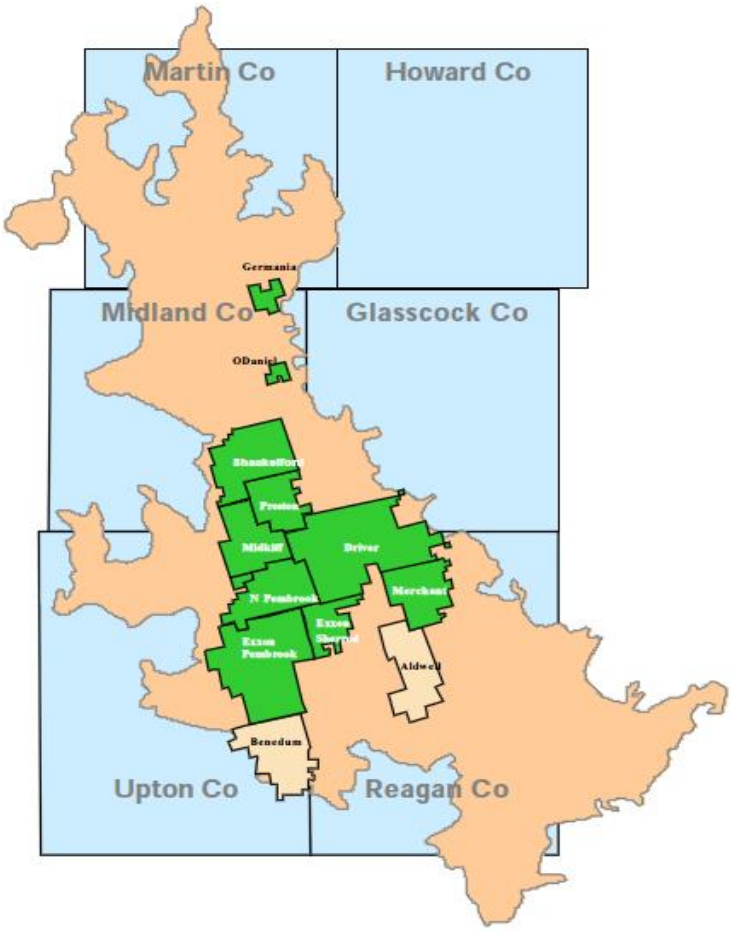

Fig. 2: Map Of Spraberry Trend Area

2.5.1. Geology

The deposition of Spraberry sand, which had been derived from relatively low-lying border lands south of the Midland Basin, occurred in an elongated basin bordered by mildly unstable shelves and platforms during the Permian age. These fine-grained sands are interbedded with shales, laminated siltstones, silty sandstones, thin limestones, shaly limestones, and dolomites. The low porosity and low permeability of them is due to close initial packing, pressurizing, and tight cementation (Warn and Sidwell, 1953).

The Lower, Middle and Upper Spraberry formations are subdivisions of the Spraberry found since its discovery at depths of approximately 7,000–8,000 ft. Further subdivisions within each of the submarine fan complexes were done by Tyler and Gholston (1988) to distinguish operational units. Among six operational units in the Upper Spraberry, only two of them (1U and 5U) are oil-productive zones. A log example is shown in Fig. 3 (Baker et al., 2000) in terms of petrophysical units.

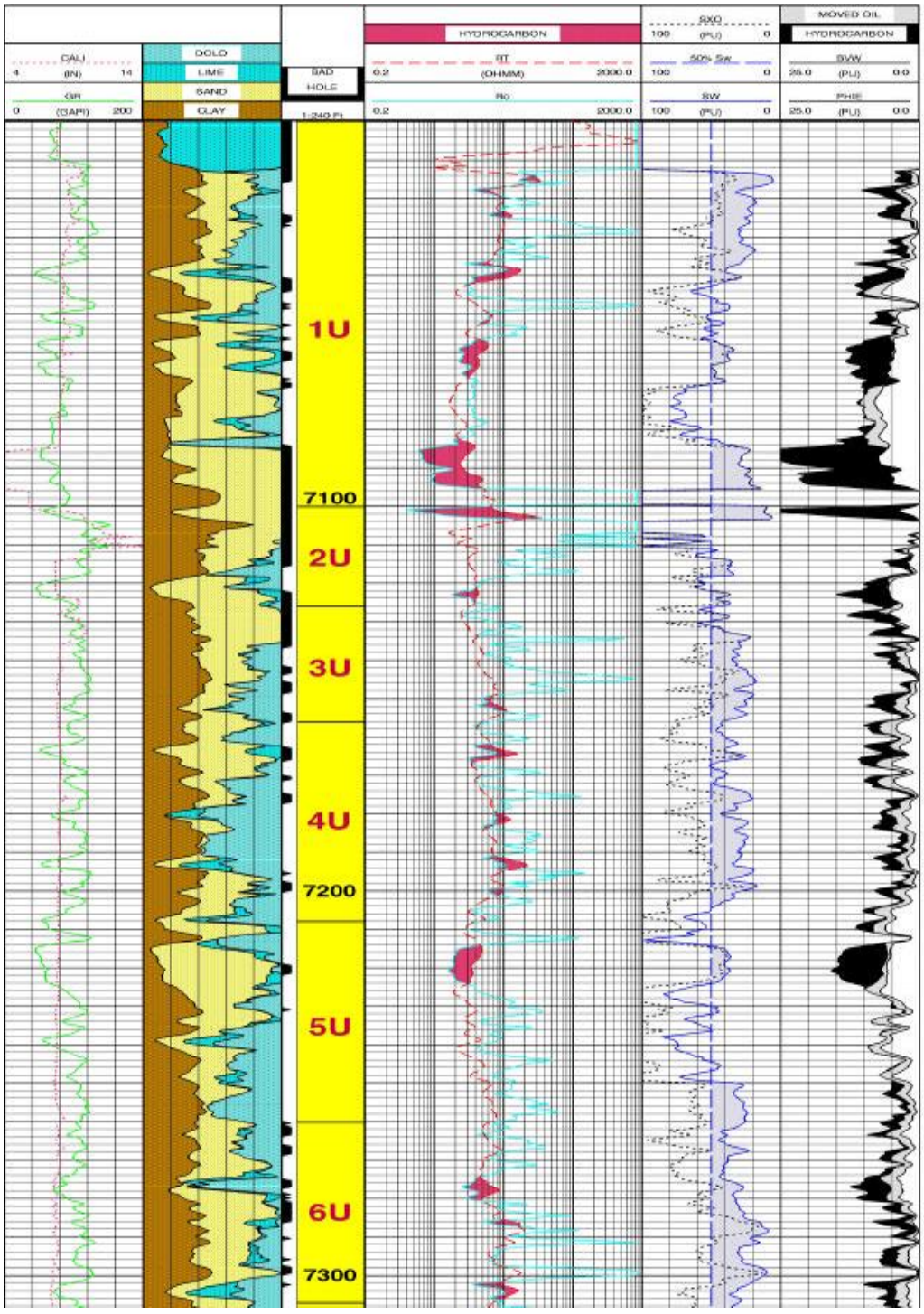

Fig. 3: Petrophysical Analysis Of A Type Log

2.5.2. Reservoir Characterization

At the development stage of the field, much work was done to characterize the reservoir in terms of rock, fracture, and fluid properties. Additional characterization attempts have been done by the aids of development in technology.

The Spraberry sands are closely packed and tightly cemented. The range of porosity for these sands is between 7 and 17% (Warn and Sidwell, 1953). Matrix permeability is less than 1 mD (Banik and Schechter, 1996; Brownscombe and Dyes, 1952; Christie and Blackwood, 1952; Dyes and Johnston, 1953). The cut-off criteria for fluorescing zones in terms of shale volume, shaliness factor, and effective porosity was determined as < 15, < 0.15, and $> 7\%$, respectively, by coupling core and log data (Banik and Schechter, 1996). Sponge core (used for estimating current oil saturation) from the E.T. O'Daniel #37 well showed the rock to be weakly water-wet, as opposed to strongly water-wet as was previously believed (Schechter et al., 1996b).

An extensive vertical fracture system, which makes the field commercial under this low matrix permeability, exists in the pay zones. The interference test by Sohio Petroleum in Driver Field showed that shut-in test wells and regular producing wells have the same trend in terms of pressure decline in the reservoir, decrease in productivity index, and rapid increase in GOR, which is an indication of good reservoir communication regardless of distance (Elkins, 1953). The resulting effective permeability from a build-up analysis of 16 Upper Spraberry wells in the Driver Area is between 2 and 183 mD due to the presence of vertical fractures, while matrix

permeability is around 0.5 mD (Dyes and Johnston, 1953). By matching breakthrough time for wells in the Humble waterflood pilot area, the permeability along and perpendicular to the main fracture trend oriented in a NE-SW direction that was observed in cores; its ratio was determined to be 144:1 (Barfield et al., 1959). The defined permeability isotropy ratio varying from 6:1 to 144:1 provided a better match between calculated and measured pressures of new wells from mathematical analysis of pressure transients in the Driver Area (Elkins and Skov, 1960). During production period or in a low-pressure area, the average effective permeability is close to the matrix permeability, which is in a range of 0.01–0.1 mD; however, it was measured between 2 and 16 mD at a reasonably high injection rate because of stress-sensitive fractures, a fact observed by many field tests (Baker et al., 2000).

Fracture orientation varies from N36°E to N76°E based on analysis of pressure interference, water injection, and gas injection in the field (Elkins and Skov, 1960). Fracture spacing was estimated as a few inches to a few feet from the frequency observed in the 3.5 in. of core (Elkins, 1953). Based on analysis of oriented horizontal core from the E.T. O'Daniel #28 well in the Upper Spraberry, the average strike of the fracture system in the upper pay zone (1U) was determined as 43°NE, with an average fracture spacing of 3.17 ft. On the other hand, for the bottom pay zone (5U), there are two distinct fracture sets: the average fracture orientation of the first one at 32°NNE with an average fracture spacing of 1.62 ft and the second with an average spacing of 3.79 ft at 70°ENE. Moreover, it was observed that the NE fracture set is mineralized through the 1U pay zone, except at the base of it. However, the ENE fracture set and the NNE

fracture do not have any mineralization (McDonald et al., 1997). Many field test measurements showed high-permeability anisotropy and heterogeneity in the fracture system and generally agree with horizontal core analysis (Schechter, 2002). The general fracture system of the Upper Spraberry is presented in Fig. 4.

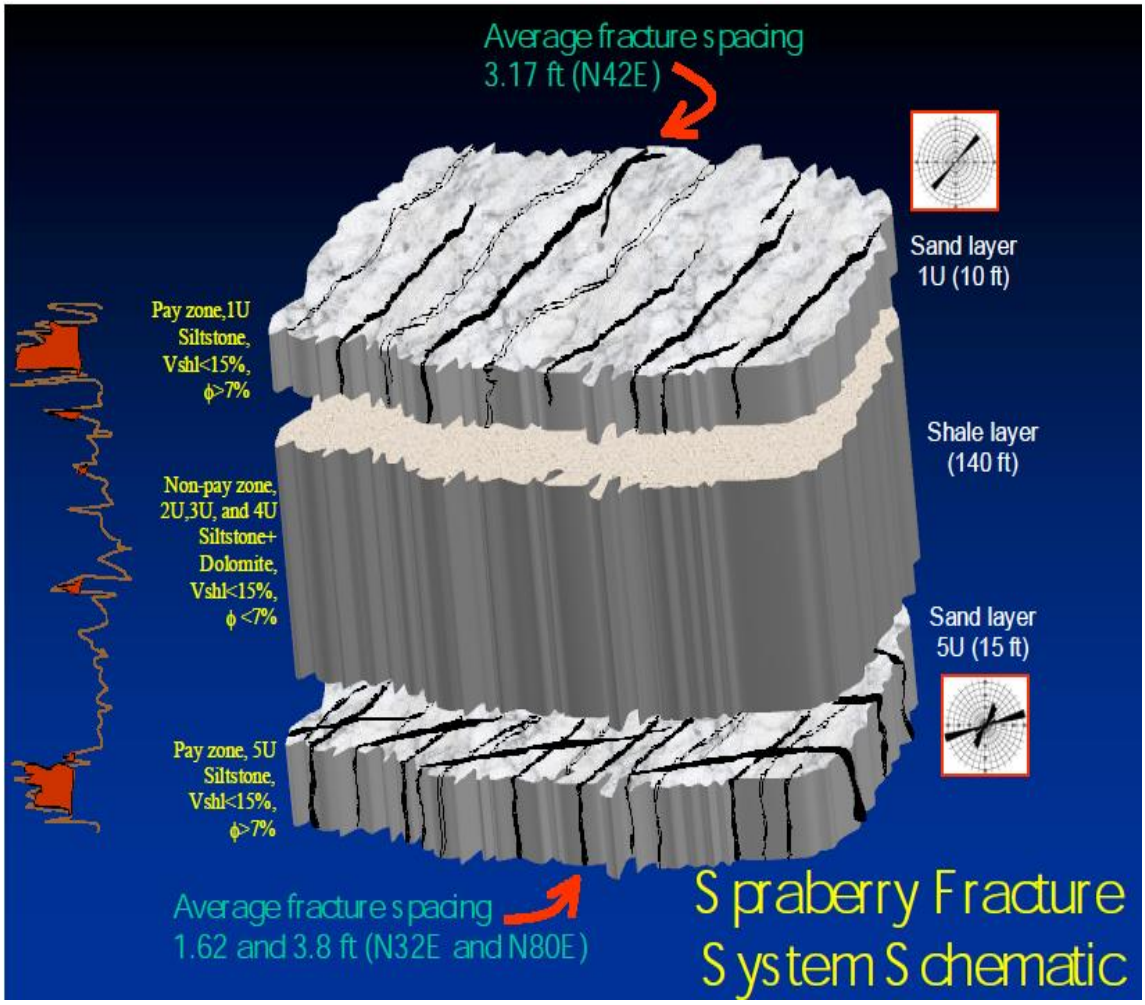

Fig. 4: Schematic Diagram Of Fracture System In Upper Spraberry

The initial reservoir pressure was between 2,319 and 2,390 psi, depending on location. The temperature of the reservoir is 138 degF. The reservoir initially was under-saturated with a saturation pressure of 1,900 psi, and its dissolved GOR was 730 ft^3/bbl. The formation volume factor is 1.4 with the corresponding unit. The gravity of the oil is between 36.5 and 38.5 API°. The average gravity of the flashed gas is 1.09, and the specific gravity of separator gas is 0.853 (Christie and Blackwood, 1952).

2.5.3. Primary Production

The first discovery of oil from Spraberry sand was in January 1949 in Spraberry Deep Field in eastern Dawson County. Tex Harvey Field was the second discovery of Spraberry in eastern Midland County. After this discovery, field development started in Tex Harvey, and many new fields were discovered, such as Germania, Midkiff, Pembrook, etc. during 1950. In 1951, activities continued in Midland, Glasscock, Upton, and Regan Counties. At the end of the 1951, cumulative production from all Spraberry fields reached 12,103,489 bbl (Christie and Blackwood, 1952). At the beginning of 1953, the field had produced some 45 million bbl of oil from 2,234 drilled wells (Elkins, 1953). The general production profile of Spraberry wells showed a rapid decline in production within 1 year because of partial closing of the fractures around the low-pressure well vicinity. GOR exceeded 100,000 ft^3/bbl for some of the wells when reservoir pressure was less than bubblepoint pressure (Chowdhury, 2002).

2.5.4. Secondary Production

After low primary recovery, Atlantic's research and development division suggested the water imbibition method as a secondary recovery method over water or gas injection in the case of conventional reservoirs because the Spraberry Trend Area has a very tight matrix and a high-density fracture system, which can lead to excessive channeling. This method could be successful under these conditions: water-wet rock, adjusted water injection rate according to the imbibition rate, and both intense and uniform fracture systems (Brownscombe and Dyes, 1952). Many attempts have been made by operators for water injection in the Spraberry. Generally, they located injection wells along the main fracture trend, while production wells were aligned perpendicular to that trend in order to push removed oil by water toward a production well. No significant increase in oil production of those production wells was observed for any injection test except for the Humble pilot test in 1955. The central producer of the five-spot showed a dramatic increase in oil production after the injection program done by Humble Oil & Refining Company (Barfield et al., 1959). This successful pilot test led to other waterflood operations. The large-scale cyclic waterflood operation in the Driver Unit by Sohio Petroleum was successful for producing oil more than 50% faster and a lower water-cut value than in the case of water imbibition at a stable reservoir pressure. The production mechanism for this cycle operation, decline in reservoir pressure that is restored by water injection, causes expansion of rock and reservoir fluids while capillary forces have a tendency to keep water in the rock. This mechanism contrasts with

imbibition of water into rock and counter flow of oil due to capillary forces during pressure balance (Elkins and Skov, 1962). Increase in oil production was not substantial compared with the Humble pilot test. However, production wells aligned on-trend with injection wells along the main fracture direction, showing a good response to water injection, while off-trend wells had unfavorable responses for almost all early waterflood in the Spraberry. Also, oil production of some wells located along the primary fracture system increased under low-rate water injection in the Spraberry (Schechter, 2002).

Although more than 50 years of waterflooding took place, low oil recovery, which is less than 15% in the Spraberry, was attributed to lack of pattern confinement and injection well density, incorrect well pattern alignment, fracture mineralization (Schechter et al., 1996a), low permeability to oil after waterflooding of the gas-saturated reservoir (Baker, 1996), and stress-sensitive fracture conductivity (Elkins and Skov, 1962; Guo and Schechter, 1997).

CHAPTER III

ANALYTICAL INTERPRATATION TECHNIQUES FOR THE TRACER TEST

Before starting simulation work, a quantitative analysis for the tracer date can provide crucial information for building the reservoir model and adjusting reservoir parameters. From observed tracer data, we can easily calculate swept pore volume by MOM, tracer recovery, and tracer velocity. Based on magnitude and distribution of those, both static and dynamic reservoir models could be modified.

3.1. Method of Moments Analysis

MOM was used to calculate swept volume for reactor beds (Danckwerts, 1953). In the oil industry, Deans (1978) first applied this method. A general derivation of MOM for 3D for any kind of heterogeneous reservoir was provided by Asakawa (2005).

3.1.1. Derivation of Method of Moments

Swept volume can be calculated by using the first temporal moments of produced conservative tracer concentration. Asakawa (2005) proved that the mass conversion equation for the single-porosity model is exactly same for the dual-porosity model. In other words, the first temporal moment or mean residence time of a conservative tracer

can be used to calculate pore volume contacted by injected fluids for naturally fractured reservoirs.

The pore volume swept between a given injector and producer for any case of variable injection/production rates, multiple producers, and partial tracer recovery from a slug tracer can be calculated by the following equation:

$$\overline{V_s} = \frac{m_p}{M_{inj}} \frac{\int_0^\infty qCtdt}{\int_0^\infty Cdt} - \frac{V_{slug}}{2} \tag{3.1}$$

In the field, the duration for detecting the tracer is limited. Therefore, a complete tracer profile is not available to interpret. However, this is solved by an exponential fit to the tail of the tracer curve because the concentration of the tracer generally declines exponentially. For this reason, the tail of the tracer elution curve can be expressed as

$$C(t) = be^{-at} \ \ for\ t > t_b \tag{3.2}$$

So, Eq.3.1 can be written as

$$\overline{V_s} = \frac{m_p}{M_{inj}} \frac{\int_0^{t_b} qCtdt \int_{t_b}^\infty qCtdt}{\int_0^{t_b} Cdt \int_{t_b}^\infty Cdt} - \frac{V_{slug}}{2} \tag{3.3}$$

Substituting Eq. 3.2 in the rightmost terms of the numerator and denominator of Eq. 3.3 and evaluating the integral in the closed form results in

$$\overline{V_s} = \frac{m_p}{M_{inj}} \frac{\int_0^{t_b} qC(t)tdt + q\frac{b}{a^2}e^{-at_b}(1+at_b)}{\int_0^{t_b} C(t)dt + \frac{b}{a}e^{-at_b}} - \frac{V_{slug}}{2} \tag{3.4}$$

Eq.3.4 is used for estimation of average swept pore volume (Shook et al., 2009).

3.1.2. Swept Volume Calculation

It was seen that only 52 wells out of 110 sampled wells showed at least one of the tracer responses out of 13 different tracers injected in the Sherrod Unit. Because a large number of injector-producer pairs is available, one sample calculation is shown in Table 2.

Table 2: MOM Sample Calculation For Sherrod 1003–1012W

Well	Tracer	SampleDate	Δt	q_{inj}	W_{inj}	ΔW_{inj}	C	ΔW_{inj} xC	ΔW_{inj} xCxW_{inj}
			days	stb/d	stb	stb	ppt	g	bbl*g
1003	IWT-2100	29-Apr-11	1	351	351	351	769803.0	43.0	15076.8
		3-May-11	5	344	1727	1376	513879.9	112.4	194127.7
		7-May-11	9	341	3091	1364	538189.9	116.7	360714.9
		11-May-11	13	340	4451	1360	376701.8	81.4	362501.1
		25-May-11	27	334	9127	4676	193386.0	143.8	1312026.8
		22-Jun-11	55	346	18815	9688	138043.0	212.6	4000073.0
		20-Jul-11	83	344	28447	9632	89784.0	137.5	3910813.2
		4-Aug-11	98	252	32227	3780	71145.0	42.8	1377752.6
				Swept Pore Volume, bbl			SUM	890.1	11533086.1
							$\frac{\sum \Delta Winj\ xCxWinj}{\sum \Delta Winj\ xC}$		12957.3

In Table 2, Δt is the elapsed time after the tracer injection in days, q_{inj} is the injection rate of the injector in stb/day, W_{inj} is the cumulative injected water from injector in stb, ΔW_{inj} is the cumulative injected water for one time interval, and C is the observed tracer concentration in ppt. Based on the integral formula provided, swept pore volume is calculated. It is important to highlight that because many tracers have an inclining trend during the late time, exponential decline cannot be applied. Therefore, terms representing exponential decline were omitted, and calculation was only done for observed data.

For a full-field scale, swept volume for each production-injector pair is listed on Table 3. For a better understanding, swept volumes are normalized by dividing its maximum value, as shown in Table 4.

Table 3: Swept Pore Volume Calculation For Full Field

	1814	1202	1818	2112	2409	1904	2114	2325	2118	1012	701	1301	1405
	IWT-1900	IWT-2400	IWT-1100	IWT-1700	IWT-1200	IWT-2200	IWT-2500	IWT-1000	IWT-1600	IWT-2100	IWT-2000	IWT-1400	IWT-1300
Ruby 18	17502	17757	18477	18707	18077	20872	14920	7994	13405	14742	10925	21195	19255
Ruby 19	28826	27015	26218	26345	25715	0	25258	11142	22655	22573	0	0	23731
Sherrod 711	22224	24028	24019	25432	24044	0	14253	11691	23344	22141	6570	25544	22864
Sherrod 1003	13833	14181	15274	17928	14747	15033	9811	6834	14680	12957	8257	20467	13139
Sherrod 1004	27868	29902	27240	29652	29064	0	25050	14669	30018	25899	0	29525	27908
Sherrod 1205	18767	19392	19962	20514	19005	21578	14328	9270	18755	17006	11492	14651	18318
Sherrod 1206	31921	28870	30855	38049	34228	0	31153	20359	38068	28947	0	42172	35756
Sherrod 1207	16470	15391	18360	19243	17526	16579	8297	7585	16259	14781	8929	21826	15016
Sherrod 1208	23484	22626	23997	27354	24995	22153	20293	13296	26260	23132	19971	31691	25467
Sherrod 1302	20627	21425	21641	22209	21284	21592	16227	10341	21326	19609	0	18334	20141
Sherrod 1310	0	15510	0	0	21770	0	20808	12857	32354	23641	0	25831	22962
Sherrod 1402	29472	22584	27945	31470	29884	28497	26934	16403	31638	30277	0	37308	31587
Sherrod 1403	40013	29359	35551	47620	40257	30360	37833	21241	41914	38932	24810	51578	40291
Sherrod 1404	18624	16126	19205	18213	18065	16697	12161	8973	18560	14906	9109	22972	15442
Sherrod 1506	23671	24050	23295	24242	24108	0	18661	11515	23851	22415	0	17894	18454
Sherrod 1511	0	0	0	0	0	0	0	17521	0	39072	0	0	34249
Sherrod 1512	16666	16316	16599	15867	15697	18988	14817	8526	17116	12812	8778	21024	12913
Sherrod 1513	0	35499	0	0	41497	0	36151	20231	42274	36134	0	32902	28680
Sherrod 1804	14368	17546	19283	20680	18792	13355	12128	9153	18732	15045	8732	21799	18178
Sherrod 1807	22431	19978	20576	22121	20214	21592	14949	9861	19852	15766	0	26633	20589
Sherrod 1809	14662	16890	20828	22531	19799	17748	8472	8718	19448	16008	9629	23909	18010
Sherrod 1810	30673	20059	18365	23156	21034	10158	20582	8466	25303	26757	5448	17842	24203
Sherrod 1811	0	0	0	0	0	0	0	0	0	20655	0	0	0
Sherrod 1812	22583	28850	26911	32605	29129	19237	24425	16472	31188	28423	0	36408	30546
Sherrod 1815	20899	22111	24726	29511	24920	25118	21001	14317	27023	24781	24014	33349	28234
Sherrod 1817	16131	16022	13416	17690	15182	15997	10764	7383	15185	13381	8954	19544	13922
Sherrod 1819	18395	18990	27109	27383	26174	18885	21804	10425	26144	21658	9561	28529	25551
Sherrod 1902	18789	16533	18741	19983	20046	13814	15748	10622	19810	18774	0	22254	17419
Sherrod 1903	31080	31321	31228	32609	32544	21363	26880	16524	33917	31705	0	0	27539
Sherrod 2001	28211	22582	27083	27351	28367	0	23753	18704	30508	28450	0	39062	29652
Sherrod 2002	19438	25979	13246	6844	25571	16507	16910	3069	26217	24648	0	0	26524
Sherrod 2101	20574	20803	20680	20384	20398	21578	16904	9937	20511	17872	0	24494	16244
Sherrod 2110	31735	30599	24000	35041	32550	23354	32072	19069	35480	34213	0	38489	36809
Sherrod 2111	13315	12308	15540	11717	14075	10973	8611	6659	13759	12282	7756	18291	11303
Sherrod 2113	19031	20045	22066	22697	20673	17578	11880	9358	15418	17105	9392	23422	16698
Sherrod 2115	29309	27005	20815	32710	29078	29010	28843	17866	31688	29574	0	38057	32676
Sherrod 2116	34914	33776	31070	30098	34375	21978	30922	19737	37772	35275	24926	44451	35991
Sherrod 2117	20183	20547	17758	18582	21984	17780	14563	9752	20265	17706	12016	22740	19011
Sherrod 2309	20231	21243	21735	20908	15080	21091	19004	9590	21689	17783	9951	24539	18087
Sherrod 2313	35987	35322	32948	46203	34960	0	28314	17707	39024	36571	0	0	41279
Sherrod 2314	33279	31977	24974	22741	32826	0	37313	15860	35759	35908	0	42223	36874
Sherrod 2315	16243	17097	13681	19785	18282	19280	10570	6689	18203	14283	9429	23620	17032
Sherrod 2317	31701	30344	25332	34635	31986	31560	30616	21288	33449	33733	0	39189	35353
Sherrod 2319	17824	18160	17658	19358	15343	17022	12590	7394	18384	15527	9067	22377	16166
Sherrod 2320	22003	22259	22597	22574	18510	0	17333	10695	22731	19934	0	28836	18788
Sherrod 2324	0	0	30881	0	0	0	0	15820	0	39072	0	0	0
Sherrod 2326	31366	34716	31538	33847	33029	22618	24494	15355	34118	33631	11866	32852	33102
Sherrod 2411	32878	23846	36484	41532	20292	31560	36691	23631	40525	40091	24922	48210	46220
Sherrod 2415	28609	29272	27525	31882	31211	3690	28394	14085	33628	32479	0	38279	33143
Sherrod 2416	32968	29121	31950	32791	31188	0	29725	17595	27123	31332	0	42374	33601
Sherrod 2417	19776	19848	20460	20547	16168	19765	18324	9177	21195	16681	11852	23821	16012
Sherrod 2423	25216	26435	25429	25417	19058	20450	14151	11499	24837	22867	0	29302	23984

Table 4: Normalized Swept Volume For Full Field

	1814	1202	1818	2112	2409	1904	2114	2325	2118	1012	701	1301	1405
	IWT-1900	IWT-2400	IWT-1100	IWT-1700	IWT-1200	IWT-2200	IWT-2500	IWT-1000	IWT-1600	IWT-2100	IWT-2000	IWT-1400	IWT-1300
Ruby 18	0.339	0.344	0.358	0.363	0.350	0.405	0.289	0.155	0.260	0.286	0.212	0.411	0.373
Ruby 19	0.559	0.524	0.508	0.511	0.499	0.000	0.490	0.216	0.439	0.438	0.000	0.000	0.460
Sherrod 711	0.431	0.466	0.466	0.493	0.466	0.000	0.276	0.227	0.453	0.429	0.127	0.495	0.443
Sherrod 1003	0.268	0.275	0.296	0.348	0.286	0.291	0.190	0.132	0.285	0.251	0.160	0.397	0.255
Sherrod 1004	0.540	0.580	0.528	0.575	0.563	0.000	0.486	0.284	0.582	0.502	0.000	0.572	0.541
Sherrod 1205	0.364	0.376	0.387	0.398	0.368	0.418	0.278	0.180	0.364	0.330	0.223	0.284	0.355
Sherrod 1206	0.619	0.560	0.598	0.738	0.664	0.000	0.604	0.395	0.738	0.561	0.000	0.818	0.693
Sherrod 1207	0.319	0.298	0.356	0.373	0.340	0.321	0.161	0.147	0.315	0.287	0.173	0.423	0.291
Sherrod 1208	0.455	0.439	0.465	0.530	0.485	0.430	0.393	0.258	0.509	0.448	0.387	0.614	0.494
Sherrod 1302	0.400	0.415	0.420	0.431	0.413	0.419	0.315	0.200	0.413	0.380	0.000	0.355	0.390
Sherrod 1310	0.000	0.301	0.000	0.000	0.422	0.000	0.403	0.249	0.627	0.458	0.000	0.501	0.445
Sherrod 1402	0.571	0.438	0.542	0.610	0.579	0.552	0.522	0.318	0.613	0.587	0.000	0.723	0.612
Sherrod 1403	0.776	0.569	0.689	0.923	0.781	0.589	0.734	0.412	0.813	0.755	0.481	1.000	0.781
Sherrod 1404	0.361	0.313	0.372	0.353	0.350	0.324	0.236	0.174	0.360	0.289	0.177	0.445	0.299
Sherrod 1506	0.459	0.466	0.452	0.470	0.467	0.000	0.362	0.223	0.462	0.435	0.000	0.347	0.358
Sherrod 1511	0.000	0.000	0.000	0.000	0.000	0.000	0.000	0.340	0.000	0.758	0.000	0.000	0.664
Sherrod 1512	0.323	0.316	0.322	0.308	0.304	0.368	0.287	0.165	0.332	0.248	0.170	0.408	0.250
Sherrod 1513	0.000	0.688	0.000	0.000	0.805	0.000	0.701	0.392	0.820	0.701	0.000	0.638	0.556
Sherrod 1804	0.279	0.340	0.374	0.401	0.364	0.259	0.235	0.177	0.363	0.292	0.169	0.423	0.352
Sherrod 1807	0.435	0.387	0.399	0.429	0.392	0.419	0.290	0.191	0.385	0.306	0.000	0.516	0.399
Sherrod 1809	0.284	0.327	0.404	0.437	0.384	0.344	0.164	0.169	0.377	0.310	0.187	0.464	0.349
Sherrod 1810	0.595	0.389	0.356	0.449	0.408	0.197	0.399	0.164	0.491	0.519	0.106	0.346	0.469
Sherrod 1811	0.000	0.000	0.000	0.000	0.000	0.000	0.000	0.000	0.000	0.400	0.000	0.000	0.000
Sherrod 1812	0.438	0.559	0.522	0.632	0.565	0.373	0.474	0.319	0.605	0.551	0.000	0.706	0.592
Sherrod 1815	0.405	0.429	0.479	0.572	0.483	0.487	0.407	0.278	0.524	0.480	0.466	0.647	0.547
Sherrod 1817	0.313	0.311	0.260	0.343	0.294	0.310	0.209	0.143	0.294	0.259	0.174	0.379	0.270
Sherrod 1819	0.357	0.368	0.526	0.531	0.507	0.366	0.423	0.202	0.507	0.420	0.185	0.553	0.495
Sherrod 1902	0.364	0.321	0.363	0.387	0.389	0.268	0.305	0.206	0.384	0.364	0.000	0.431	0.338
Sherrod 1903	0.603	0.607	0.605	0.632	0.631	0.414	0.521	0.320	0.658	0.615	0.000	0.000	0.534
Sherrod 2001	0.547	0.438	0.525	0.530	0.550	0.000	0.461	0.363	0.591	0.552	0.000	0.757	0.575
Sherrod 2002	0.377	0.504	0.257	0.133	0.496	0.320	0.328	0.060	0.508	0.478	0.000	0.000	0.514
Sherrod 2101	0.399	0.403	0.401	0.395	0.395	0.418	0.328	0.193	0.398	0.347	0.000	0.475	0.315
Sherrod 2110	0.615	0.593	0.465	0.679	0.631	0.453	0.622	0.370	0.688	0.663	0.000	0.746	0.714
Sherrod 2111	0.258	0.239	0.301	0.227	0.273	0.213	0.167	0.129	0.267	0.238	0.150	0.355	0.219
Sherrod 2113	0.369	0.389	0.428	0.440	0.401	0.341	0.230	0.181	0.299	0.332	0.182	0.454	0.324
Sherrod 2115	0.568	0.524	0.404	0.634	0.564	0.562	0.559	0.346	0.614	0.573	0.000	0.738	0.634
Sherrod 2116	0.677	0.655	0.602	0.584	0.666	0.426	0.600	0.383	0.732	0.684	0.483	0.862	0.698
Sherrod 2117	0.391	0.398	0.344	0.360	0.426	0.345	0.282	0.189	0.393	0.343	0.233	0.441	0.369
Sherrod 2309	0.392	0.412	0.421	0.405	0.292	0.409	0.368	0.186	0.421	0.345	0.193	0.476	0.351
Sherrod 2313	0.698	0.685	0.639	0.896	0.678	0.000	0.549	0.343	0.757	0.709	0.000	0.000	0.800
Sherrod 2314	0.645	0.620	0.484	0.441	0.636	0.000	0.723	0.307	0.693	0.696	0.000	0.819	0.715
Sherrod 2315	0.315	0.331	0.265	0.384	0.354	0.374	0.205	0.130	0.353	0.277	0.183	0.458	0.330
Sherrod 2317	0.615	0.588	0.491	0.672	0.620	0.612	0.594	0.413	0.649	0.654	0.000	0.760	0.685
Sherrod 2319	0.346	0.352	0.342	0.375	0.297	0.330	0.244	0.143	0.356	0.301	0.176	0.434	0.313
Sherrod 2320	0.427	0.432	0.438	0.438	0.359	0.000	0.336	0.207	0.441	0.386	0.000	0.559	0.364
Sherrod 2324	0.000	0.000	0.599	0.000	0.000	0.000	0.000	0.307	0.000	0.758	0.000	0.000	0.000
Sherrod 2326	0.608	0.673	0.611	0.656	0.640	0.439	0.475	0.298	0.661	0.652	0.230	0.637	0.642
Sherrod 2411	0.637	0.462	0.707	0.805	0.393	0.612	0.711	0.458	0.786	0.777	0.483	0.935	0.896
Sherrod 2415	0.555	0.568	0.534	0.618	0.605	0.072	0.551	0.273	0.652	0.630	0.000	0.742	0.643
Sherrod 2416	0.639	0.565	0.619	0.636	0.605	0.000	0.576	0.341	0.526	0.607	0.000	0.822	0.651
Sherrod 2417	0.383	0.385	0.397	0.398	0.313	0.383	0.355	0.178	0.411	0.323	0.230	0.462	0.310
Sherrod 2423	0.489	0.513	0.493	0.493	0.369	0.396	0.274	0.223	0.482	0.443	0.000	0.568	0.465

In order to analyze the overall response for the full field, the distribution of normalized swept volume can be seen in Fig. 5.

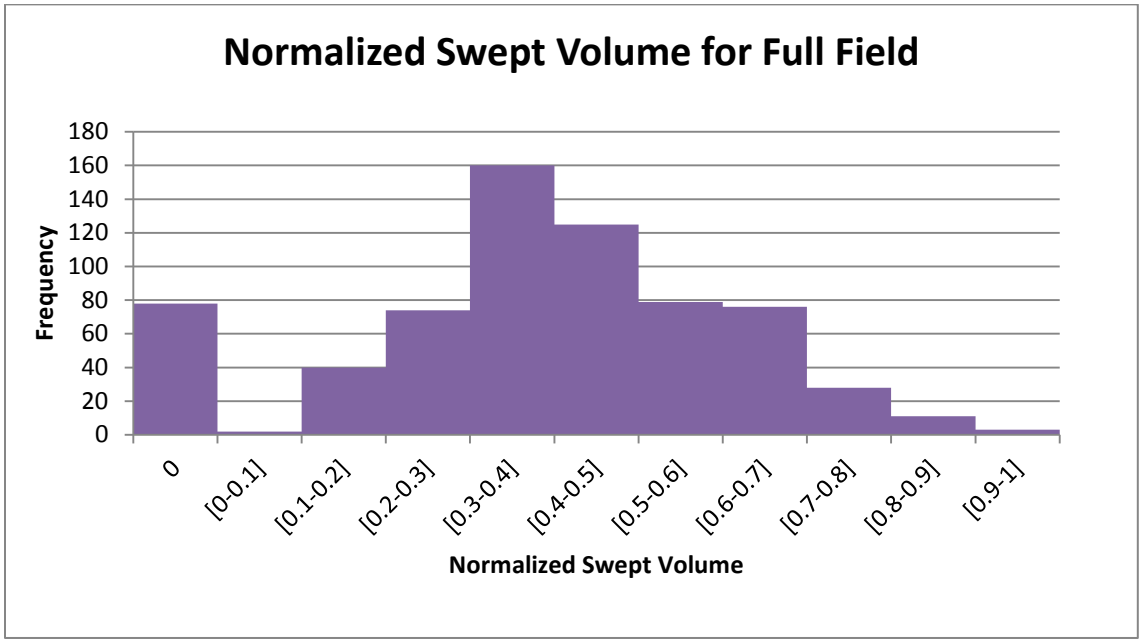

Fig. 5: Distribution Of Normalized Swept Volume For Full Field

Normalized swept volume for the full field almost shows a normal distribution within a range of 0.3 to 0.7, and this distribution can represent fracture distribution, which controls fluid flow in the reservoir. Some of the tracers show maximum frequency in the range of 0 to 0.2. This low-range swept volume could be related to either poor connectivity with sampled wells or remaining injected water in the reservoir. However, some of the wells have a normalized swept volume higher than 0.7, which is most probably an indication of preferential flow paths for injected water.

Mapping of these trends between injector and producer might provide a general understanding of fluid flow in the Sherrod Unit. However, the injected volume base formulation of the MOM theory could mask other important details in tracer response, such as tracer recovery, tracer velocity, and number of peaks where those details are distinctive for identifying flow heterogeneity within the reservoir. As a result, these details will be analyzed and categorized in the following sections for better description of flow dynamics.

3.2. Tracer Recovery Analysis

Contrary to swept volume calculation, tracer recovery in an offset well offers a clear picture of the relationship between injector and producer. Tracer recovery by percentage for a producer actually equals the percentage of injected water produced by that producer. In other words, tracer recovery can show how many barrels of injected water are produced by an offset well and how many barrels of injected water stay in the reservoir. It also elucidates the amount of water production due to injected water and due to the reservoir itself for a producer. Regarding those relations, one sample calculation is shown in Table 5.

In Table 5, Δt is the elapsed time after tracer injection in days, q_{prod} is production rate of the producer in stb/day, W_{prod} is cumulative water production of the producer in stb, ΔW_{prod} is cumulative water production of the producer for one time interval, and C

is observed tracer concentration in ppt. In order to convert the $\Delta W_{prod} \times C$ product from bbl×ppt to the mass unit of g, $42 \times 3{,}785/10^{12}$ was multiplied with that product as a conversion factor, where 42 represents the conversion of bbl to galUS, 3,785 represents the conversion of galUS to L, and 10^{12} represents the conversion of ppt to the mass fraction in g. Finally, a summation of the recovered tracer in g at the last sampled date is divided by the total injected tracer in g, and the resulting fraction is multiplied by 100 to obtain total tracer recovery of the well by percentage.

Table 5: Tracer Recovery Calculation For Sherrod 1003-1012W

Well	Tracer	SampleDate	Δt	q_{prod}	W_{prod}	ΔW_{prod}	C	ΔW_{prod} xC
			days	stb/d	stb	stb	ppt	g
1003	IWT-2100	29-Apr-11	1	107.18	107.18	107.18	769803	13.12
		3-May-11	5	110.79	550.35	443.17	513880	36.20
		7-May-11	9	114.97	1010.23	459.88	538190	39.35
		11-May-11	13	119.37	1487.72	477.49	376702	28.59
		25-May-11	27	131.69	3331.32	1843.60	193386	56.68
		22-Jun-11	55	119.57	6679.20	3347.88	138043	73.47
		20-Jul-11	83	149.42	10863.06	4183.86	89784	59.72
		4-Aug-11	98	167.26	13371.90	2508.84	71145	28.37
		Injected Tracer, L		154	**SUM**			335.49
		Injected Tracer, g		15400	**Tracer Recovery %**			2.18

Similarly, this calculation procedure was followed to calculate tracer recovery for each injector-production well pair. As illustrated in Fig. 6, the maximum tracer recovery for any injector is less than 10%. Having a low tracer recovery is unlikely for the Sherrod Unit, where a highly conductive and highly intense fracture system is thought to

be responsible for high water-cut values observed in the field. This kind of low recovery can be attributed to confinement of tracer in the reservoir. For the confinement of tracer, the injected tracer stays in the reservoir without production by sampled wells. This could be achieved by either the presence of a very low-conductivity fracture system, in which tracers have not reached wells, or by having a good matrix-fracture interaction mechanism, where a large amount of water imbibes into the matrix system. However, none of the reservoir properties mentioned above was common for the Spraberry Trend Area. Therefore, the injected tracer either moved outside the project area or it was produced by non-sampled wells. Another reason could be the dilution of the injected tracer, which will be highlighted in later sections.

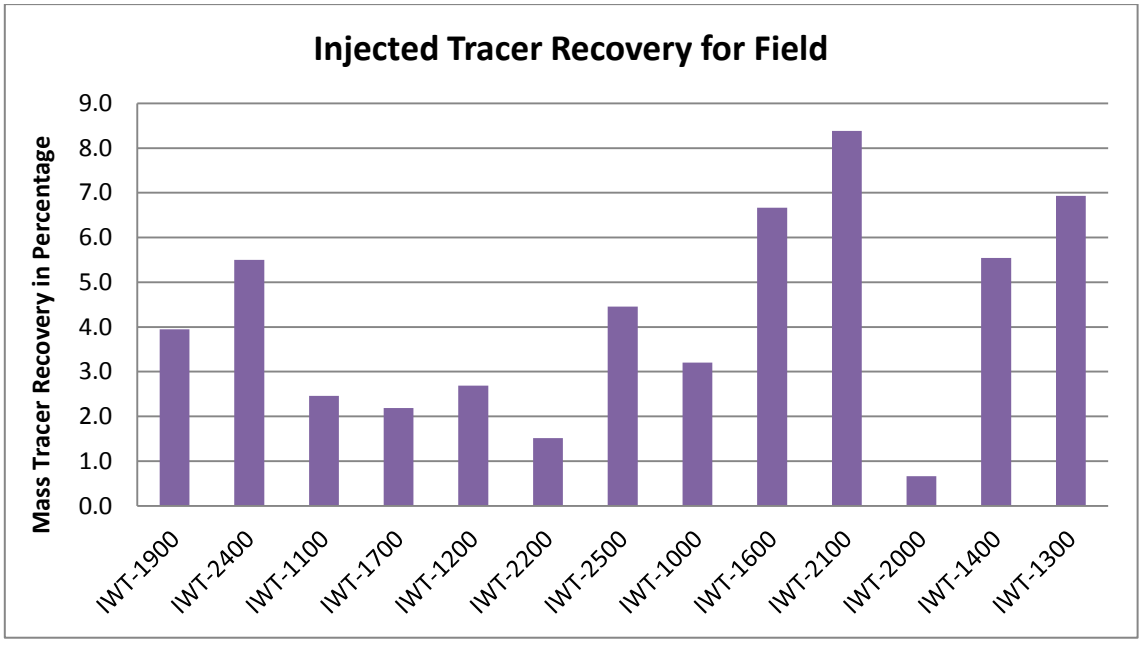

Fig. 6: Distribution Of Tracer Recovery For All Injector In Percentage

The overall injected tracer recovery for the field was categorized based on recovery percentage. Table 6 presents the number of wells in each category for corresponding injectors. A histogram of recovered tracer in the field based on defined categories is shown in Fig. 7.

Table 6: Field Scale Frequency Of Tracer Recovery

Injection Well	1814	1202	1818	2112	2409	1904	2114	2325	2118	1012	701	1301	1405	FIELD
Mass of Tracer Recovery (%)	IWT 1900	IWT 2400	IWT 1100	IWT 1700	IWT 1200	IWT 2200	IWT 2500	IWT 1000	IWT 1600	IWT 2100	IWT 2000	IWT 1400	IWT 1300	TOTAL
<0.01	25	21	29	32	25	33	19	19	24	15	23	30	17	312
[0.01-0.05]	10	10	12	9	11	1	14	16	14	14	1	10	17	139
[0.05-0.1]	4	7	2	2	6	0	5	6	4	6	0	2	3	47
[0.1-0.5]	6	8	4	2	6	1	9	9	5	14	0	1	11	76
[0.5-1]	2	2	1	2	1	2	1	1	0	1	1	0	0	14
[1-2]	0	1	0	0	0	0	1	0	1	1	0	0	1	5
2+	0	0	0	0	0	0	0	0	1	1	0	2	1	5

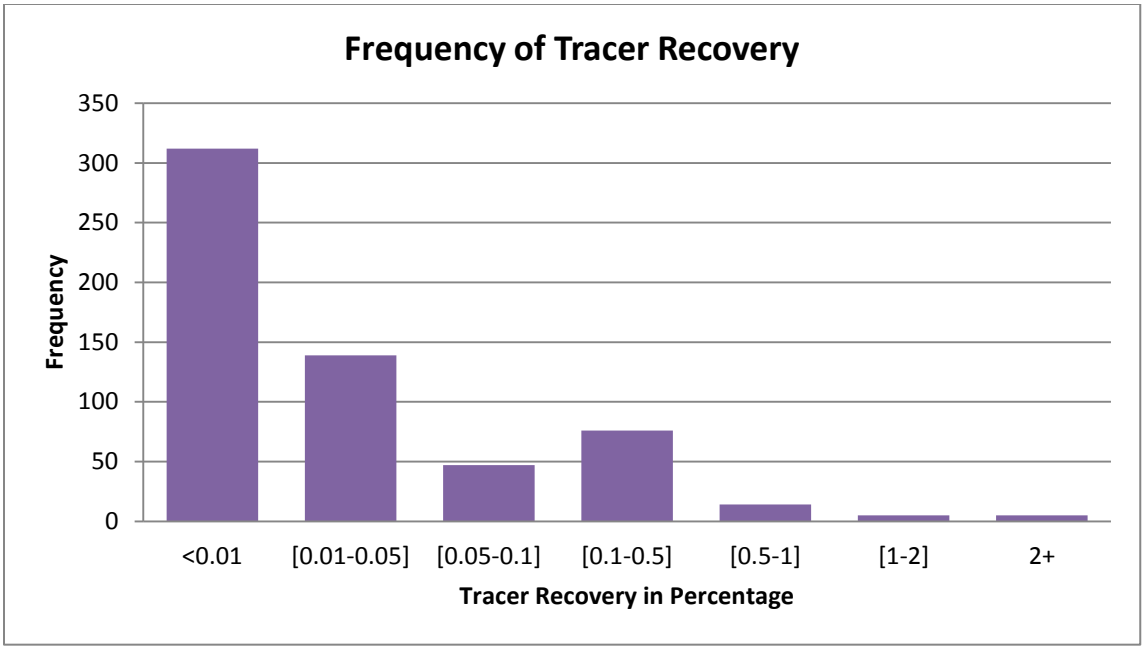

Fig. 7: Distribution Of Field Tracer Recovery In Percentage

According to the histogram, tracer recovery within 0.1–0.5% does not follow the general trend of the frequency. This range is a turning point in terms of reflecting a different fracture system. As a result, another categorization for tracer recovery was done based on this range. The new categorization consists of three different recovery ranges: tracer recovery less than 0.1%, tracer recovery between 0.1% and 0.5%, and tracer recovery higher than 0.5%. The first group constitutes higher than 83% of the overall response; however, the amount of received water calculated from this range is extremely low for understanding the source of water for wells. The second category, which is in the range of 0.1–0.5%, is the turning point and covers 12.5% of tracer responses. The remaining group is tracer recovery higher than 0.5%. Even though the last two categories are relatively rare at the field scale, they are the most reliable

responses among overall tracer tests in order to characterize the fracture system and to understand the water source of the wells because they constitute a large portion of total recovered tracer in terms of amount.

Tracer recovery by percentage for the field scale is illustrated in Table 7 and is colored according to the categories mentioned above. Yellow represents tracer recovery less than 0.1%, green shows tracer recovery in the range of 0.1–0.5%, and recovery higher than 0.5% is colored by light blue.

To understand the main fracture system in the reservoir, the last two categories of recovered tracer are mapped separately. Each injector has a unique color, which is the same as the arrow starting from that injector. The map for the second category, shown in Fig. 8, reveals that recovered tracer in the range of 0.1–0.5% flowed through very complex fractures. It is impossible to make a uniform fracture realization over the study area that allows this kind of fluid movement. Characterizing such a complex system requires further knowledge about geology, especially for responses far away from the injector.

Table 7: Full Field Tracer Recovery In Percentage

	1814	1202	1818	2112	2409	1904	2114	2325	2118	1012	701	1301	1405
	IWT-1900	IWT-2400	IWT-1100	IWT-1700	IWT-1200	IWT-2200	IWT-2500	IWT-1000	IWT-1600	IWT-2100	IWT-2000	IWT-1400	IWT-1300
Ruby 18	0.082	0.134	0.027	0.024	0.071	0.002	0.105	0.106	2.864	0.303	0.001	0.032	0.130
Ruby 19	0.002	0.006	0.001	0.001	0.004	0.000	0.006	0.009	0.453	0.026	0.000	0.000	0.009
Sherrod 711	0.007	0.018	0.003	0.003	0.009	0.000	0.019	0.020	0.011	0.063	0.623	0.002	0.030
Sherrod 1003	0.256	0.340	0.076	0.061	0.196	0.017	0.354	0.229	0.221	2.184	0.010	0.119	0.324
Sherrod 1004	0.002	0.003	0.001	0.001	0.002	0.000	0.004	0.003	0.002	0.120	0.000	0.001	0.005
Sherrod 1205	0.034	0.059	0.010	0.010	0.031	0.000	0.063	0.044	0.037	0.143	0.000	2.291	0.060
Sherrod 1206	0.003	0.005	0.001	0.001	0.003	0.000	0.005	0.005	0.004	0.429	0.000	0.005	0.009
Sherrod 1207	0.143	1.705	0.047	0.041	0.121	0.007	0.267	0.171	0.142	0.912	0.004	0.071	0.224
Sherrod 1208	0.027	0.040	0.008	0.006	0.021	0.001	0.041	0.030	0.025	1.078	0.001	0.016	0.044
Sherrod 1302	0.035	0.069	0.012	0.012	0.035	0.000	0.066	0.055	0.046	0.175	0.000	2.631	0.090
Sherrod 1310	0.000	0.000	0.000	0.000	0.000	0.000	0.000	0.000	0.000	0.001	0.000	0.006	0.000
Sherrod 1402	0.011	0.764	0.005	0.004	0.011	0.000	0.023	0.019	0.014	0.054	0.000	0.005	0.027
Sherrod 1403	0.001	0.126	0.000	0.000	0.001	0.000	0.002	0.003	0.001	0.007	0.000	0.000	0.015
Sherrod 1404	0.046	0.895	0.016	0.016	0.049	0.001	0.086	0.061	0.050	0.190	0.001	0.019	1.541
Sherrod 1506	0.000	0.001	0.000	0.000	0.001	0.000	0.001	0.001	0.001	0.004	0.000	0.000	0.173
Sherrod 1511	0.000	0.000	0.000	0.000	0.000	0.000	0.000	0.000	0.000	0.000	0.000	0.000	0.013
Sherrod 1512	0.085	0.126	0.026	0.026	0.080	0.003	0.140	0.095	0.088	0.281	0.002	0.034	2.452
Sherrod 1513	0.000	0.000	0.000	0.000	0.000	0.000	0.000	0.000	0.000	0.001	0.000	0.007	0.001
Sherrod 1804	0.936	0.116	0.021	0.017	0.056	0.815	0.120	0.080	0.069	0.268	0.002	0.027	0.117
Sherrod 1807	0.004	0.004	0.001	0.001	0.002	0.000	0.005	0.003	0.003	0.195	0.000	0.001	0.004
Sherrod 1809	0.847	0.135	0.028	0.022	0.066	0.006	0.135	0.089	0.082	0.249	0.004	0.046	0.128
Sherrod 1810	0.029	0.003	0.001	0.000	0.002	0.000	0.003	0.029	0.002	0.007	0.000	0.001	0.005
Sherrod 1811	0.000	0.000	0.000	0.000	0.000	0.000	0.000	0.000	0.000	0.008	0.000	0.000	0.000
Sherrod 1812	0.344	0.089	0.003	0.002	0.006	0.004	0.014	0.012	0.009	0.036	0.000	0.003	0.018
Sherrod 1815	0.259	0.012	0.003	0.002	0.006	0.001	0.012	0.008	0.007	0.023	0.000	0.005	0.012
Sherrod 1817	0.033	0.060	0.922	0.008	0.041	0.001	0.072	0.046	0.043	0.132	0.000	0.011	0.058
Sherrod 1819	0.369	0.072	0.012	0.009	0.029	0.003	0.053	0.037	0.027	0.095	0.002	0.019	0.048
Sherrod 1902	0.001	0.066	0.000	0.000	0.000	0.000	0.001	0.001	0.001	0.002	0.000	0.000	0.001
Sherrod 1903	0.000	0.002	0.000	0.000	0.001	0.003	0.002	0.003	0.002	0.009	0.000	0.000	0.229
Sherrod 2001	0.010	0.025	0.004	0.005	0.012	0.000	0.687	0.022	0.017	0.064	0.000	0.004	0.030
Sherrod 2002	0.000	0.001	0.000	0.001	0.000	0.004	0.023	0.008	0.001	0.003	0.000	0.000	0.001
Sherrod 2101	0.005	0.011	0.002	0.002	0.007	0.000	0.011	0.011	0.008	0.030	0.000	0.002	0.490
Sherrod 2110	0.002	0.004	0.155	0.001	0.002	0.009	0.011	0.004	0.003	0.011	0.000	0.001	0.005
Sherrod 2111	0.139	0.215	0.045	0.054	0.118	0.529	1.404	0.143	0.128	0.364	0.005	0.076	0.172
Sherrod 2113	0.086	0.133	0.031	0.028	0.078	0.004	0.131	0.112	1.698	0.290	0.002	0.045	0.153
Sherrod 2115	0.004	0.007	0.321	0.001	0.004	0.000	0.011	0.006	0.004	0.018	0.000	0.002	0.008
Sherrod 2116	0.005	0.014	0.003	0.617	0.009	0.101	0.320	0.023	0.013	0.062	0.000	0.002	0.035
Sherrod 2117	0.018	0.033	0.316	0.700	0.015	0.000	0.036	0.026	0.024	0.078	0.000	0.007	0.037
Sherrod 2309	0.009	0.013	0.003	0.002	0.176	0.000	0.015	0.009	0.010	0.027	0.000	0.004	0.012
Sherrod 2313	0.000	0.001	0.000	0.000	0.000	0.000	0.001	0.113	0.001	0.002	0.000	0.000	0.001
Sherrod 2314	0.003	0.007	0.065	0.252	0.004	0.000	0.007	0.220	0.005	0.018	0.000	0.001	0.010
Sherrod 2315	0.022	0.023	0.009	0.004	0.013	0.001	0.026	0.272	0.016	0.049	0.000	0.006	0.023
Sherrod 2317	0.004	0.009	0.245	0.001	0.006	0.000	0.009	0.061	0.007	0.023	0.000	0.002	0.011
Sherrod 2319	0.057	0.095	0.025	0.018	0.714	0.002	0.107	0.676	0.062	0.217	0.001	0.025	0.107
Sherrod 2320	0.001	0.003	0.001	0.001	0.095	0.000	0.003	0.003	0.002	0.008	0.000	0.000	0.004
Sherrod 2324	0.000	0.000	0.002	0.000	0.000	0.000	0.000	0.002	0.000	0.000	0.000	0.000	0.000
Sherrod 2326	0.003	0.004	0.002	0.001	0.003	0.000	0.004	0.032	0.004	0.006	0.000	0.002	0.003
Sherrod 2411	0.001	0.002	0.001	0.000	0.018	0.000	0.002	0.002	0.001	0.004	0.000	0.001	0.002
Sherrod 2415	0.003	0.005	0.002	0.222	0.003	0.000	0.006	0.261	0.004	0.015	0.000	0.001	0.009
Sherrod 2416	0.003	0.008	0.003	0.002	0.005	0.000	0.008	0.010	0.432	0.028	0.000	0.001	0.012
Sherrod 2417	0.013	0.022	0.004	0.004	0.312	0.000	0.023	0.017	0.017	0.047	0.000	0.005	0.022
Sherrod 2423	0.005	0.010	0.002	0.002	0.252	0.000	0.011	0.010	0.007	0.025	0.000	0.002	0.014
TOTAL	3.949	5.499	2.462	2.187	2.690	1.517	4.453	3.206	6.666	8.382	0.659	5.541	6.930

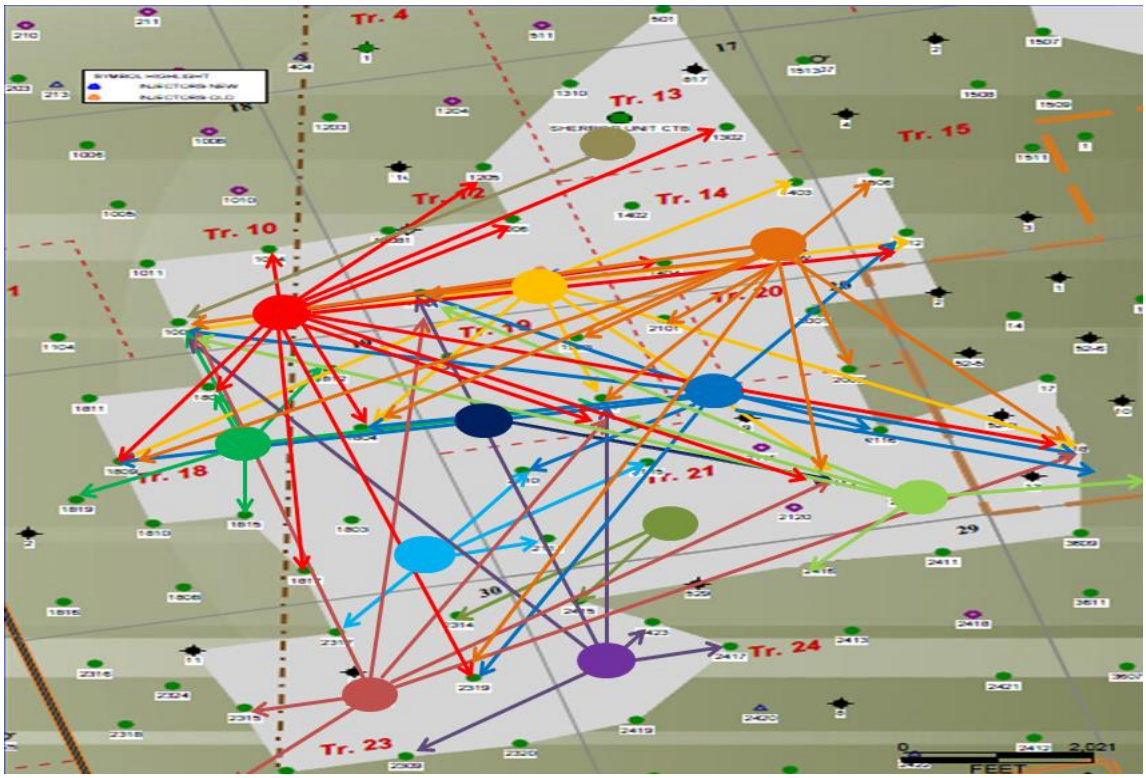

Fig. 8: Field Tracer Map For Tracer Recovery In The Range Of 0.1-0.5 %

However, this complexity disappears when tracer recovery higher than 0.5% is mapped at the field scale. As illustrated by Fig. 9, no matter their location, all injectors have the same flow trend. This observation proves the existence of a highly conductive fracture system in the E-W direction. Although it is not as common as the E-W direction, injection wells 1012W, 1202W, 2114W, and somehow 2112W showed another fracture system in the NE-SW direction. These fracture trends are very close to what is observed from the analysis of horizontal core in the O'Daniel Unit.

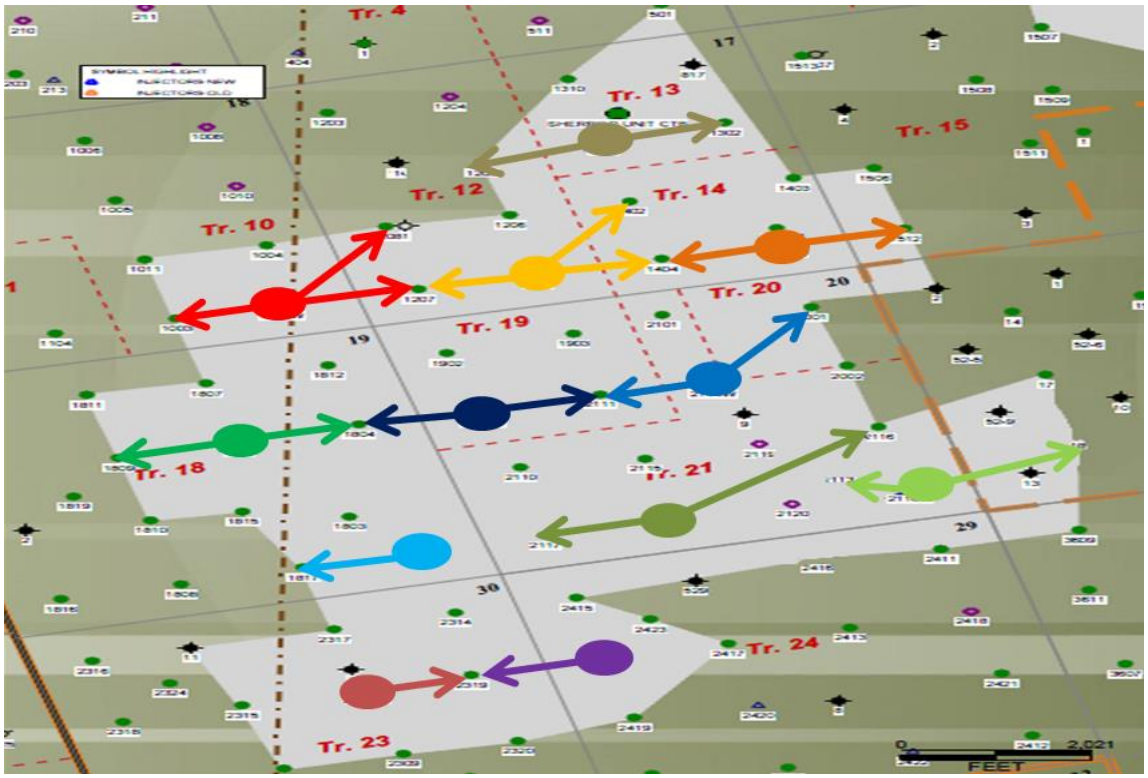

Fig. 9: Field Tracer Map For Tracer Recovery Higher Than 0.5 %

For investigation of a NE-SW-oriented fracture system in the reservoir, mapping tracer recovery is done for the last two categories, which are recoveries of 0.1–0.5% (shown by dashed arrows) and recoveries higher than 0.5% (shown by regular arrows). However, this time-mapping of recoveries does not cover all observed wells; it is limited to the inverted nine-spot area in order to analyze them confidently. As demonstrated in Fig. 10, this limited mapping makes clear the existence of another set of fracture systems in the NE-SW direction in addition to that in the E-W direction.

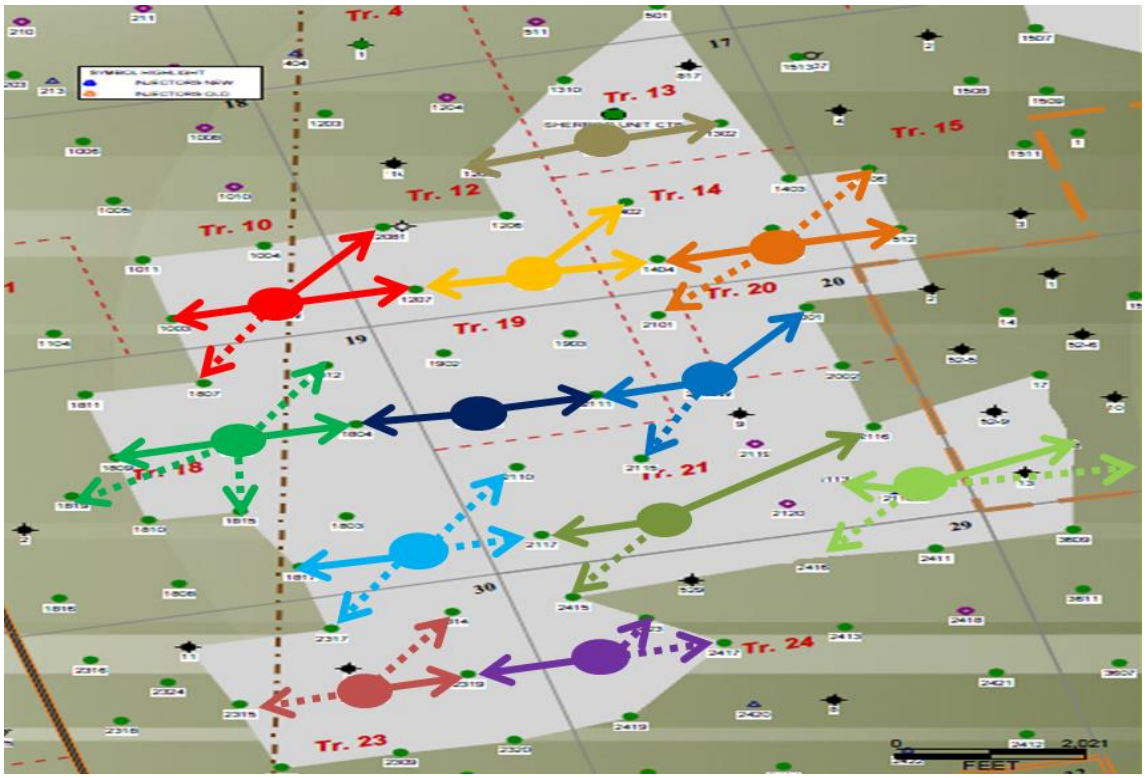

Fig. 10: Pattern Based Full Field Map For High Tracer Recovery

3.3. Traced Water Production

Once tracer recovery in mass is calculated proportionally to the total amount of injected tracer, the obtained fraction can be used to estimate the amount of received water from a particular injector by the amount of injected water with that fraction. Even though high-recovery wells received a certain amount of water, that amount is very low compared with total water production. Maximum tracer recovery is less than 5% for any well in the field, which means that only 5% of injected water was produced by

corresponding wells. Therefore, remaining water should come from the reservoir or from external water flux.

For deep investigation of traced water, the Sherrod 1003-1012W well pair, which has the highest tracer, was selected for analysis. In order to assign water contribution of the injector to the producer accurately, only tracer response at the breakthrough time was taken into account because other responses are highly affected by change in flow distribution or streamlines due to change in well rates. The advantage of this well pair is that breakthrough occurred just 1 day after injection. Another positive aspect of it is that there is no injector located around it (shown in Fig. 11), which can have an impact on both tracer response and water production.

In Table 5, recovered tracer at the breakthrough time was calculated as 13.12 g. A fraction of 0.00085 was obtained after dividing 13.12 g of recovered tracer by the 15,400 g of total injected tracer. When this fraction is multiplied by the water injection rate of 351 bbl at the corresponding time, the total amount of injected water produced by Sherrod 1003 is 0.3 bbl because breakthrough was only 1 day. However, the water production rate of it was 107 bbl. Basically, the injector of Sherrod 1012W had no impact on the water production of Sherrod 1003, and this well produces water from either the reservoir or from an external water source according to the tracer result.

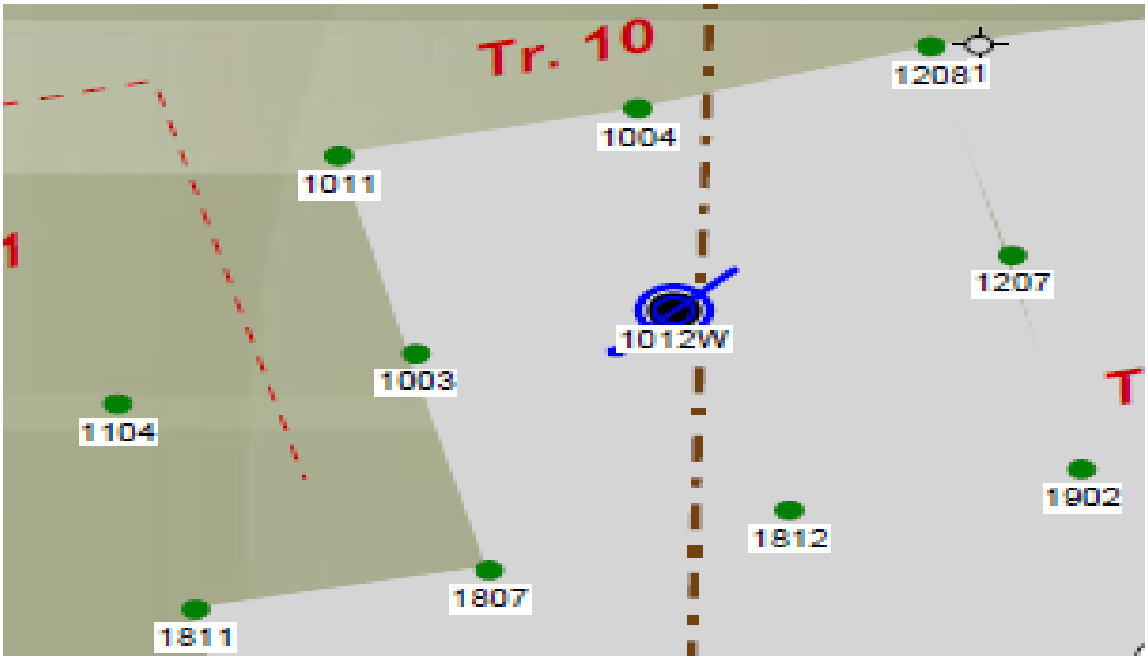

Fig. 11: Map For Well Pair Of Sherrod 1003-1012W

In order to validate this observation, the water cut of Sherrod 1003 was analyzed before and after injection was introduced. As seen from Fig. 12, before starting injection of 1012W, Sherrod 1003 had an average water cut of 0.88. However, it reached up to 100% of water production after injection started by August 1, 2010. In addition to an increase in water cut, the production rate of Sherrod 1003 was tripled from an average of 20 stb/day during the pre-injection period to 60 stb/day after just 1 month, illustrated in Fig. 13. This large amount of change in water production observed after introducing injector cannot be explained by only water influx to Sherrod 1003. More water was received from the injector than was calculated based on tracer. In other words, calculation of water production based on tracer underestimates water production due to injector. This highlights that the injected tracer was exposed to excessive dilution. As a

result, further precaution is required during evaluation of water allocation according to the magnitude of tracer response.

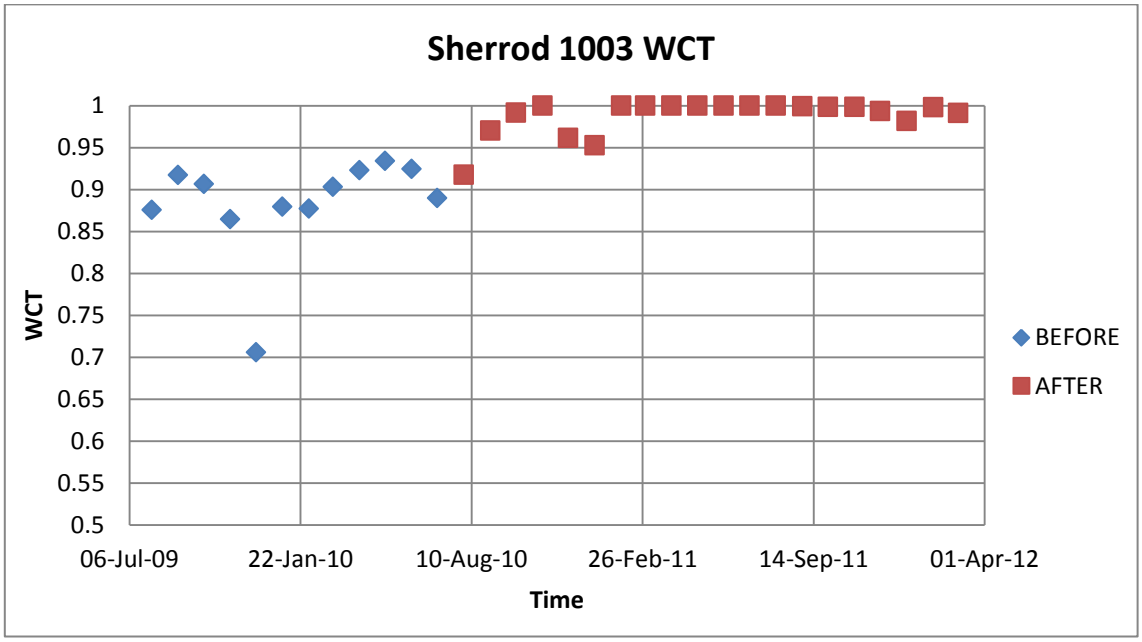

Fig. 12: Well Water Cut For Sherrod 1003

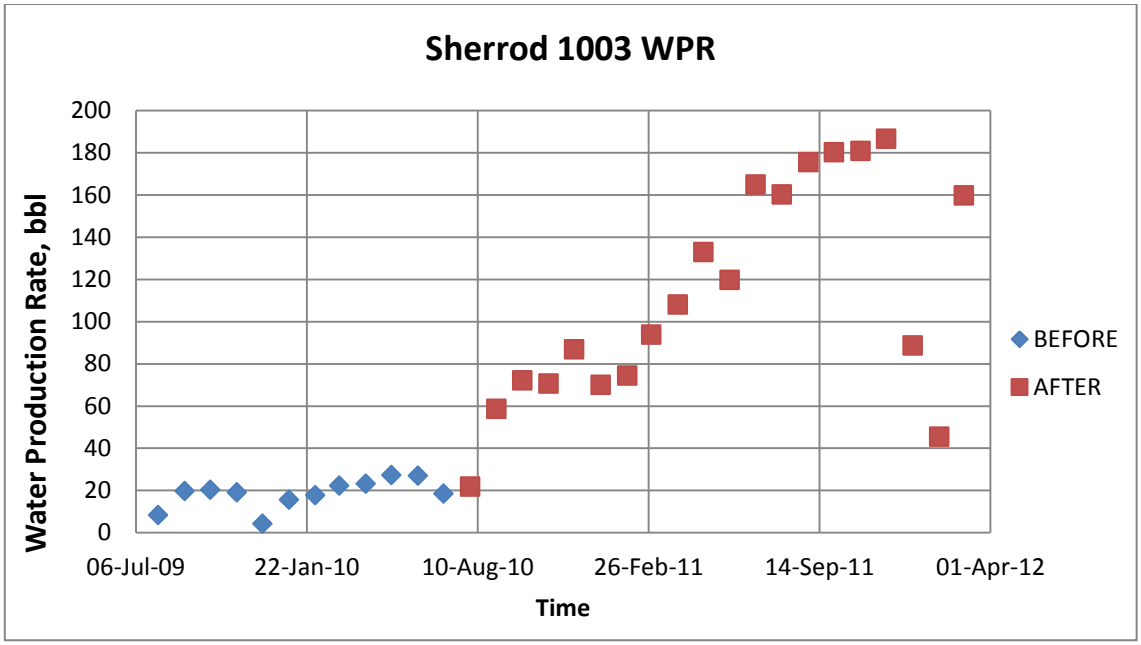

Fig. 13: Well Water Production Rate For Sherrod 1003 In STB/Day

3.4. Breakthrough Time

Breakthrough time of tracers could provide valuable information about conductivity of fracture systems. Also, analyzing it under categories based on tracer recovery may show some unique behaviors or trends, which helps in further classification. The general histogram of breakthrough time of tracer for the full field is demonstrated by Fig. 14. More than 60% of wells got breakthrough within the first 2 weeks, while the injected tracer didn't reach to almost 14% of wells. Also, after the first 2 weeks, there are local maximums with a 1-week gap before and after them. Possible

explanations for this cyclic behavior include having another set of fracture systems that are less conductive or reinjection of produced water.

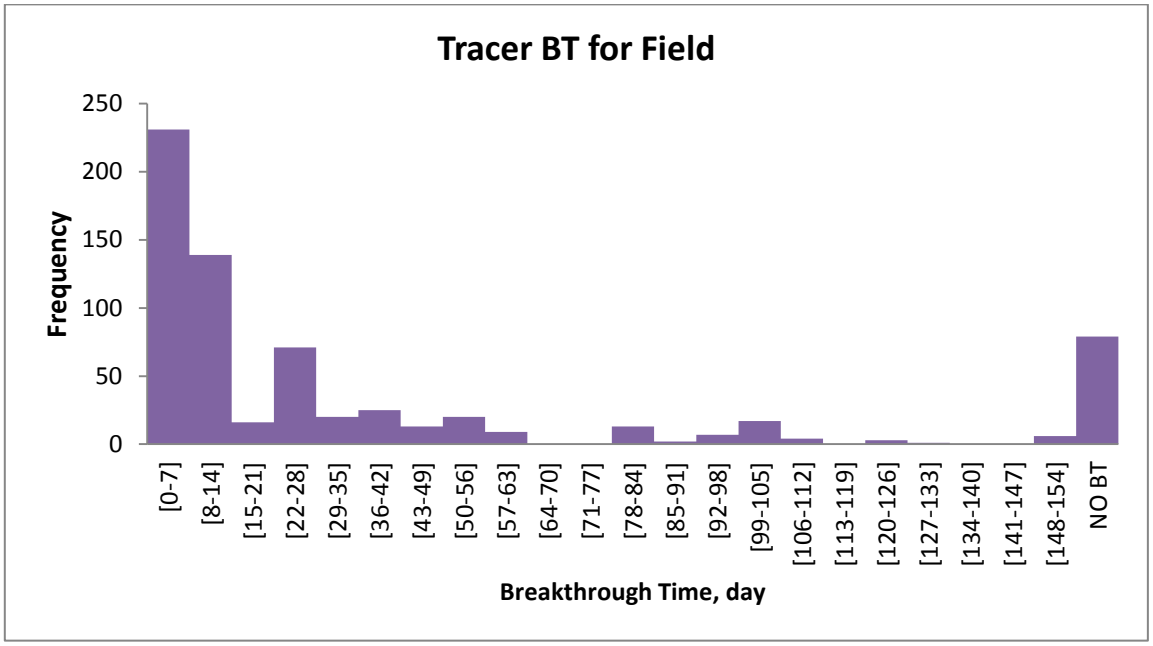

Fig. 14: Full Field Tracer's Breakthrough Time Distribution

In order to understand this cyclic trend, histograms of breakthrough time were generated for each recovery group separately, as shown in Fig. 15, Fig. 16, and Fig. 17, respectively. The low-recovery tracers exhibit almost the same trends seen in Fig. 14. This increases the possibility of the water recycling effect on late time responses rather than poorly conductive fractures because it is hard to say it is a reservoir response from this kind of low tracer recovery. On the contrary, there are no local peaks for high tracer recoveries. As can be seen from Fig. 16 and Fig. 17, breakthrough occurred even within

the first week for more than 93% of them. This proves that reinjection of water has no impact on high-tracer-recovery wells for their early time response, especially in the first 2 weeks. Thus, for accurately assessing the dominating fracture system in the Sherrod Unit, only early time response of high-tracer-recovery wells should be used.

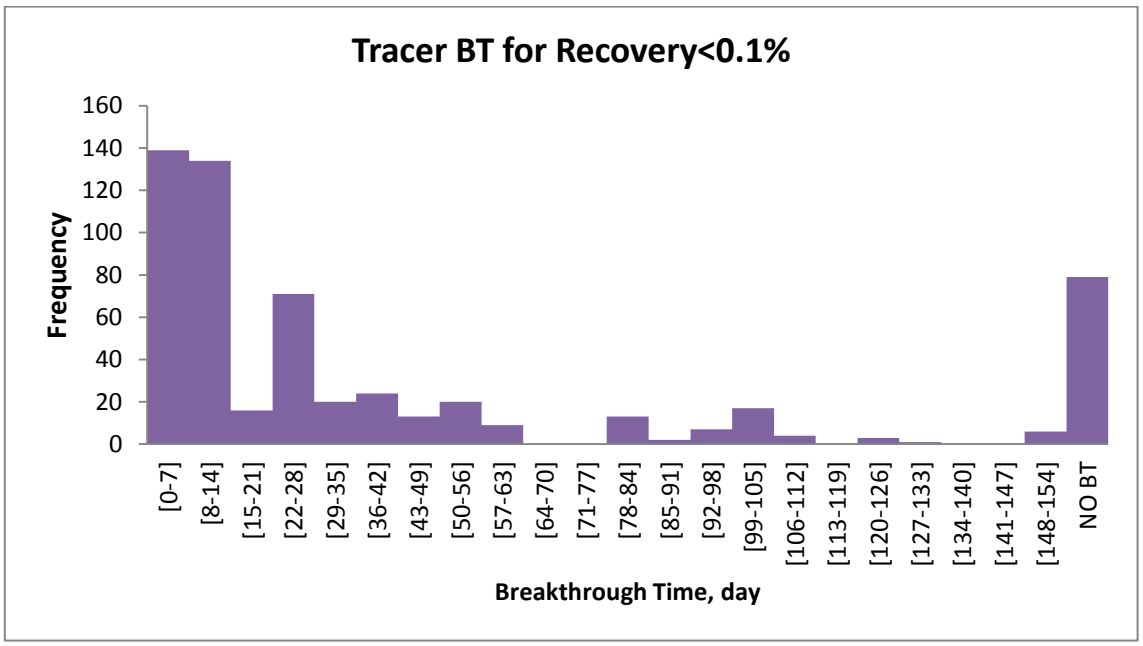

Fig. 15: Breakthrough Time Distribution For Tracer Recovery <0.1%

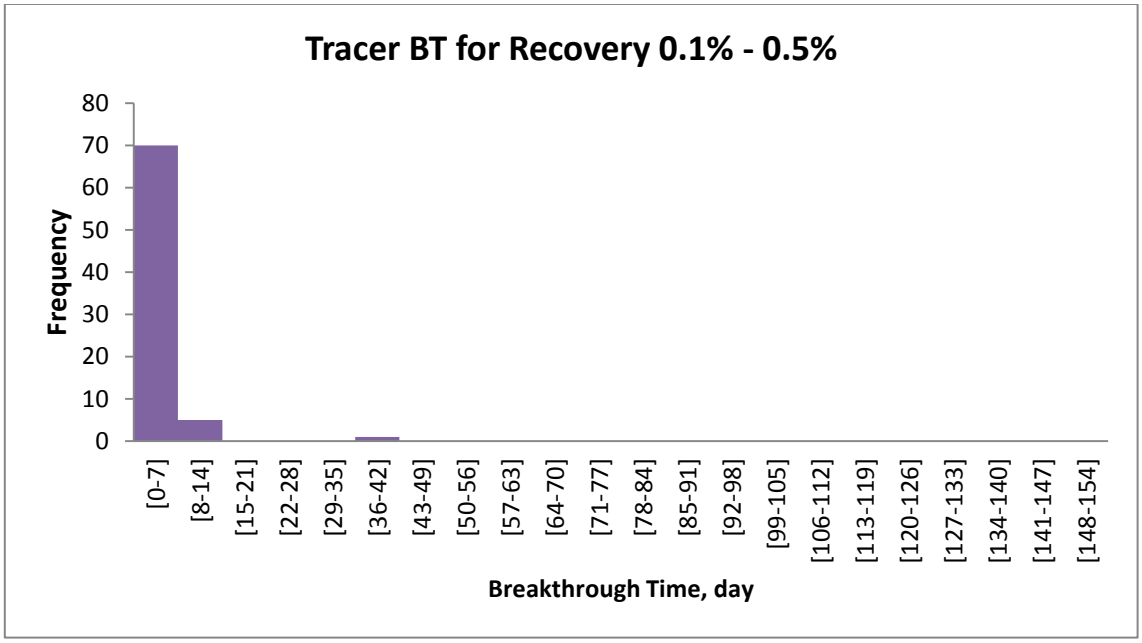

Fig. 16: Breakthrough Time Distribution For Tracer Recovery 0.1%-0.5%

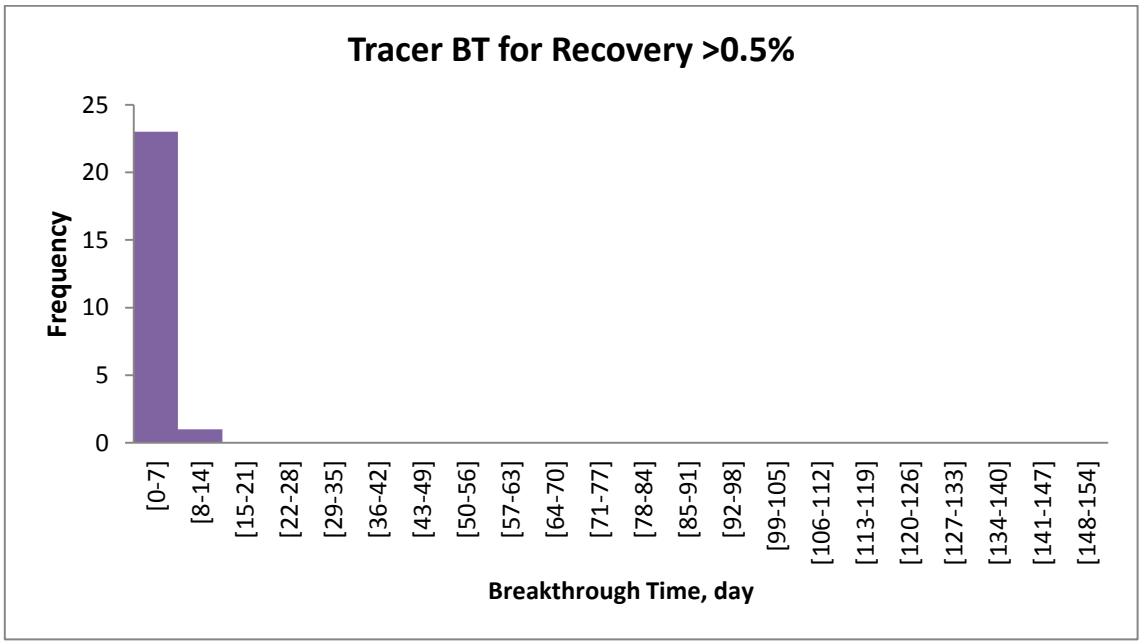

Fig. 17: Breakthrough Time Distribution For Tracer Recovery >0.5%

3.5. Tracer Velocity

Similar to breakthrough time analysis, analyzing tracer velocity can offer significant information about conductivity of fracture systems, especially their pore volume. The general distribution of tracer velocities in the Sherrod is demonstrated in Fig. 18, including zero tracer velocity, which means that the tracer didn't reach the production well. The highest tracer velocity is 11,334 ft/day, while the slowest one is 14 ft/day after eliminating zero tracer velocities. As seen from Fig. 18, smooth declining trends exist with different slopes, and almost no peak is observed for increasing velocity. However, velocity distribution for high-tracer-recovery responses, which are our main focus for fracture characterization, has many inconsistent trends with multiple peaks, shown by Fig. 19 and. Fig. 20. Based on these trends, no conclusion can be drawn with respect to highly conductive fractures. Therefore, tracer velocity analysis didn't make any contribution to characterization of the main fracture system in the Sherrod Unit.

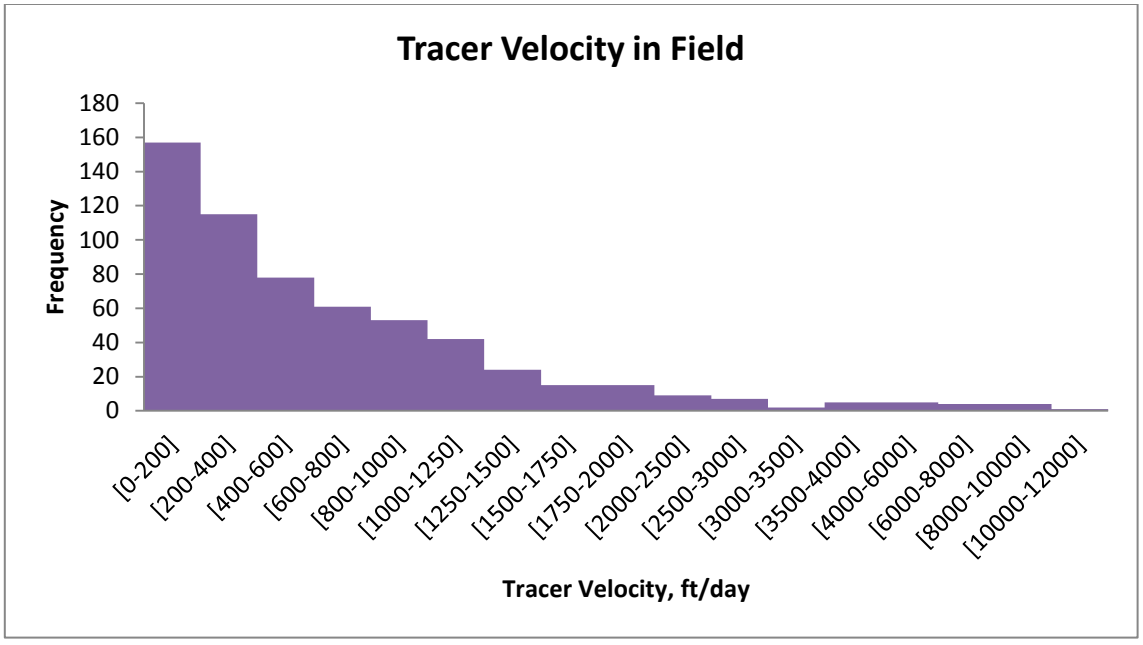

Fig. 18: Tracer Velocity Distribution For Full Field

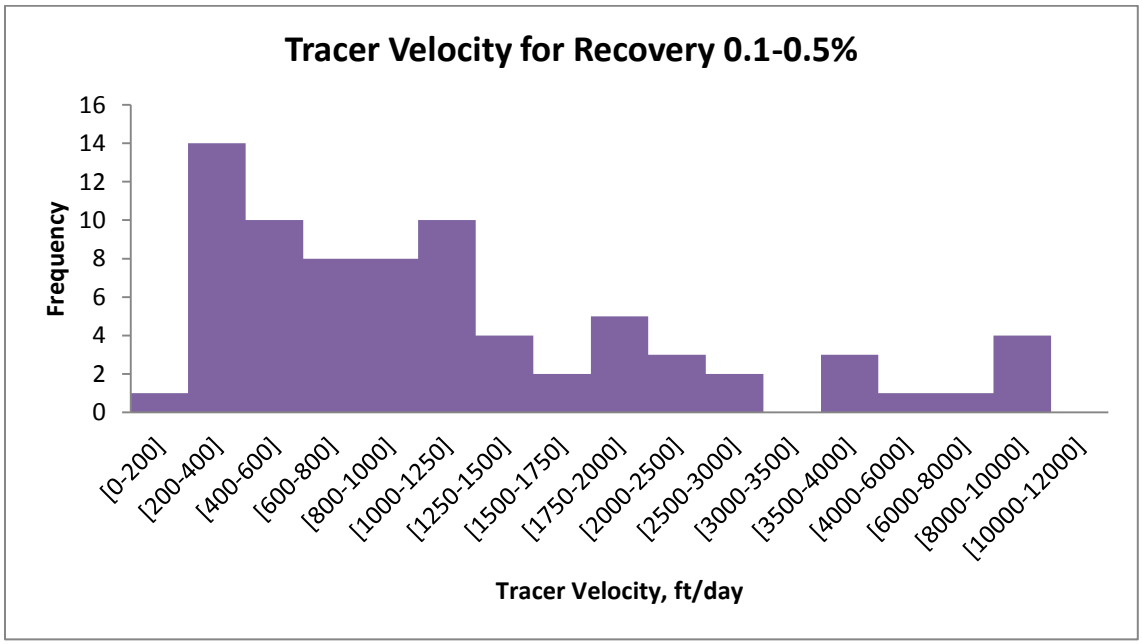

Fig. 19: Tracer Velocity Distribution For Tracer Recovery Of 0.1%-0.5%

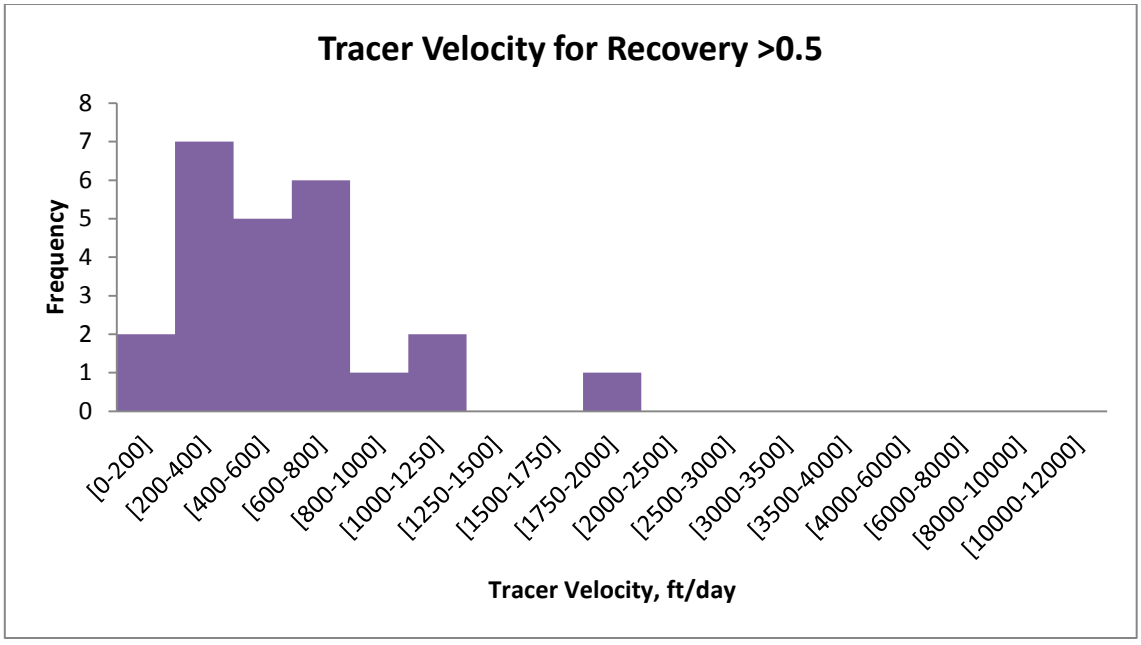

Fig. 20: Tracer Velocity Distribution For Tracer Recovery > 0.5%

3.6. Field Production Performance

Field production of the Sherrod Unit of the Spraberry Trend Area started in July 1951. Oil production was dried for almost 22 years and then water production started. As illustrated by Fig. 21, complex water-cut behavior could be associated with an external water source flowing to the Sherrod Unit. After deciding on field redevelopment in 2010, six new injectors were drilled and five old production wells were converted to injector wells. From that time, water production inclined rapidly, while the increase in oil production was not as sharp as water production, as shown in Fig. 22 and Fig. 23 with red dashed lines. Furthermore, Fig. 23 illustrates that cumulative water production

and cumulative water injection have similar trends throughout the production period. It means that most of the injected water is recycled by producers. Therefore, sweep efficiency is very low at the field scale.

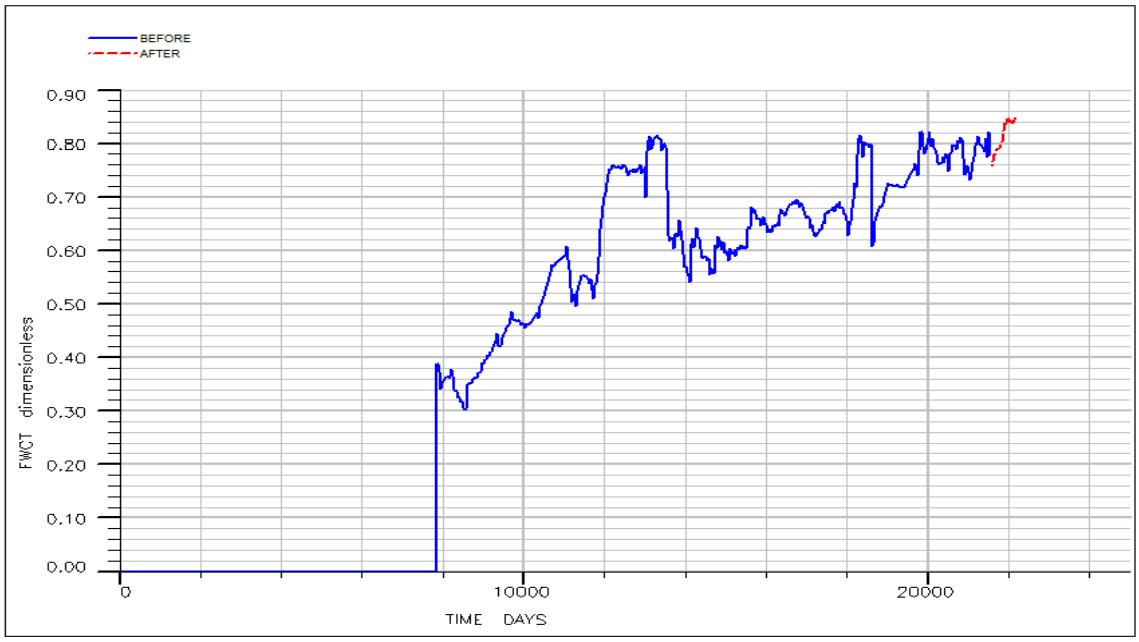

Fig. 21: Full Field Historical Water Cut

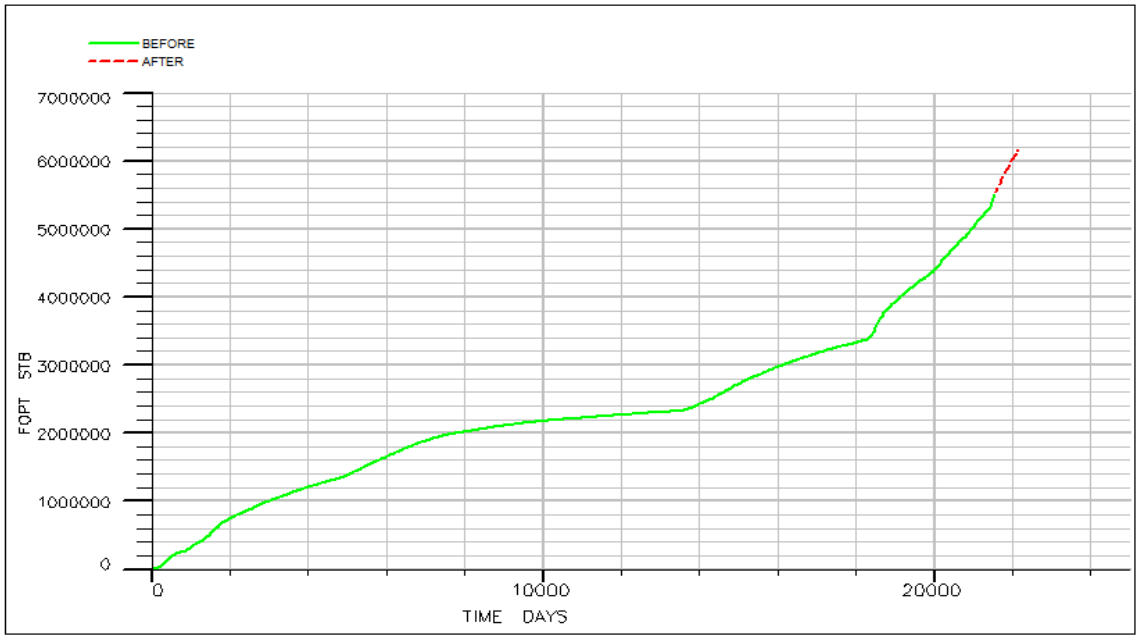

Fig. 22: Full Field Historical Oil Production, In STB

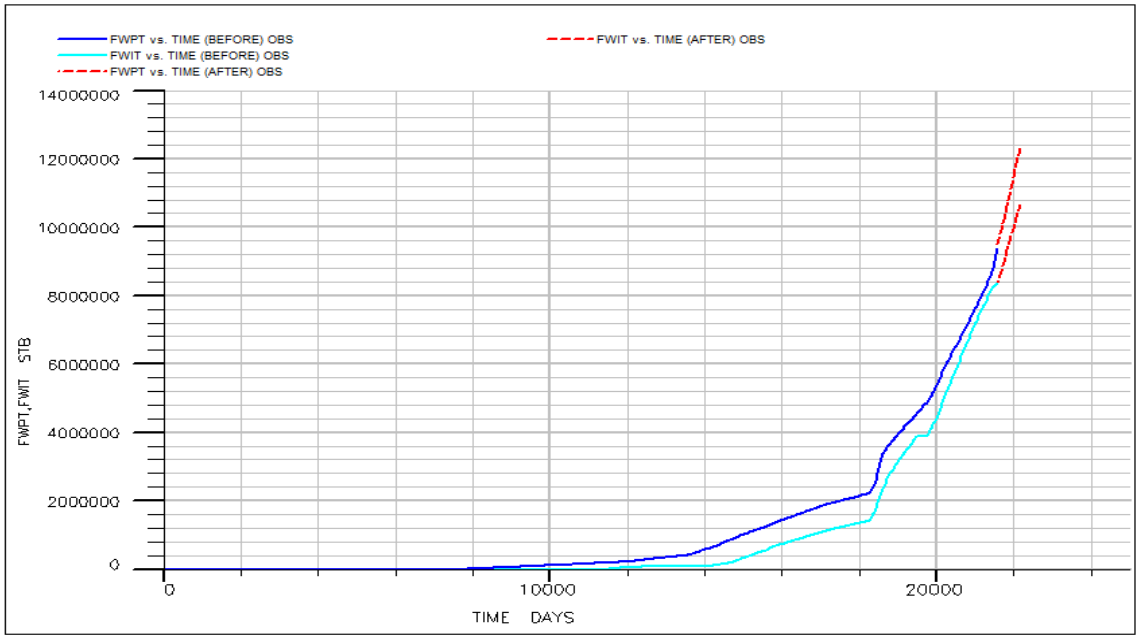

Fig. 23: Full Field Historical Water Production And Water Injection, In STB

3.7. Summary of Analytical Interpretation Techniques for the Tracer Test

A general summary of main conclusions is presented from analytical interpretation techniques:

1. Although swept pore volume is calculated for each well pair, results are not conclusive for characterization of fracture sets due to its injector-based volumetric formulation. There is no big difference between wells that show high tracer response, early breakthrough, high production rate, etc. and wells that do not. As a result, results of MOM were not taken into account for identification of fracture systems.
2. Field-wide tracer recovery is less than 10% for any injected tracer, which is too low for highly conductive fractures commonly seen in the Spraberry Trend Area. Because neither extremely low-permeability fractures, which hold water inside, nor a good matrix-fracture interaction that allows water imbibition exists, the injected tracer was not confined within the reservoir. It flowed either outside the Sherrod Unit, which is most likely, or it was produced by non-sampled wells within the Sherrod Unit. Another reason could be excessive dilution of the tracer, which was shown for the Sherrod 1003-1012W well pair.
3. Mapping of categorized tracer recovery based on its distribution is helpful to assess direction of the dominating fracture system. Even though a map of tracer recovery in the range of 0.1–0.5% shows a very complex fracture

system, it vanished, and the presence of an E-W fracture trend becomes obvious by mapping tracer recovery higher than 0.5%. Furthermore, detection of a NE-SW fracture system has been enhanced confidently by mapping those two categories in a pattern base.

4. Calculated water production due to injector based on tracer response is much lower than actual because the injected tracer was excessively diluted, which was proved for the Sherrod 1003-1012W well pair. For accurate estimation of water contribution from the injector, water production of the well should be monitored before and after the injection period, if it is present.
5. In spite of the recognition of underestimated water production based on tracer response, water influx to the Sherrod can be still a reason for abnormally high water cuts observed in the field for many wells.
6. Breakthrough time analysis showed that water recycling has an influence on low-recovery wells' response after the first 2 weeks, while its effect does not exist for high-tracer-recovery wells, at least during the first 2 weeks. To be confident, it is recommended to use only tracer responses during the first 2 weeks for interpretation of fracture sets.
7. Neither distribution of overall tracer velocities nor distribution of high-recovery tracer velocities provides any useful information that could be used for fracture characterization because of inconsistent trends.

8. Cumulative field production shows that a large amount of injected water is mostly produced by producers without a significant contribution in oil production.

CHAPTER IV

DUAL-POROSITY STREAMLINE SIMULATION

The Spraberry Trend Area consists of a tight matrix and highly conductive fracture system. The main fluid flow occurs through these fractures, while the matrix is believed to provide fluid storage. A dual-porosity model is the best candidate to reflect this kind of production performance. As a simulator, FrontSim was used to run simulations, which is the only available dual-porosity streamline simulator currently in our department. However, the only drawback of it is a lack of tracer solution for dual-porosity models.

4.1. Base Model Construction

A base three-phase, 3D, dual-porosity model was created for a selected pattern in order to conduct sensitivity analysis and manual history matching. A structural model of the study area, rock and fluid properties, matrix and fracture properties, and rock-fluid and matrix-fracture interaction properties are required in order to construct a dual-porosity model.

Initially, the general structure of the base model was constructed according to Fig. 4, in which 1U and 5U are separated by a shale formation with a thickness of 140 ft. The matrix is known as a tight matrix; however, there is no definitive information about fracture properties. Similarly, no information is available for matrix-fracture interaction

coefficient. These properties were assigned after a couple of runs, providing oil rate constraint.

Pressure, volume, and temperature (PVT) for the Sherrod was taken from differential liberation and a flash test of one of the wells located in the Spraberry Trend Area. The PVT data set used in the simulation for both oil and gas is demonstrated in Table 8 and Table 9.

Table 8: PVT Table For Oil

PVTO			
RS	**PBUB**	**Bo**	**Viscosity**
0.176	118	1.1740	1.3429
0.26	300	1.2160	1.2268
0.36	600	1.2580	1.0594
0.45	900	1.2960	0.9219
0.535	1200	1.3330	0.8143
0.621	1500	1.3690	0.7366
0.689	1750	1.3990	0.6946
0.735	1920	1.4230	0.6680
0.735	2100	1.4202	0.6700
0.735	2400	1.4152	0.6800
0.735	2700	1.4105	0.6900
0.735	3000	1.4059	0.7100

Table 9: PVT Table For Gas

PVDG		
PBUB	**Bg**	**Viscosity**
14.7	204.631	0.011
141.7	20.725	0.011
268.7	10.667	0.011
395.8	7.065	0.012
522.8	5.214	0.012
649.8	4.088	0.012
776.8	3.332	0.013
903.8	2.790	0.013
1030.9	2.385	0.014
1157.9	2.072	0.014
1284.9	1.824	0.015
1411.9	1.626	0.016
1538.9	1.464	0.017
1666.0	1.332	0.018
1793.0	1.224	0.019
1920.0	1.133	0.020
2136.0	1.012	0.022
2352.0	0.922	0.023
2568.0	0.853	0.025
2784.0	0.799	0.027
3000.0	0.756	0.029

For matrix capillary pressure, measurements done by the static equilibrium method were taken from the paper written by Guo et al. (1998). Details are presented in Fig. 24 below.

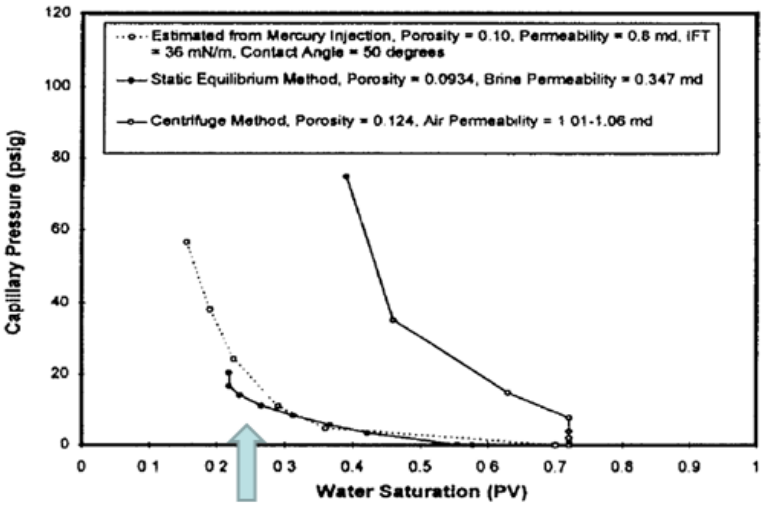

Fig. 6 - Comparison of imbibition capillary pressure curves obtained using various method for core samples from the Spraberry Trend Area.

Sw	Pc (psia)
0.22	20
0.24	14
0.27	11
0.31	9
0.37	6
0.42	4
0.495	2
0.57	0

Fig. 24: Measured Matrix Capillary Pressure For Spraberry, Guo et al. (1998)

Based on end points of residuals from capillary pressure data, which are 0.22 for water and 0.57 for oil, relative permeability for the matrix was constructed by using correlations. In the equations shown below, S_w is water saturation, S_{wr} is connate water saturation, S_{or} is residual oil saturation, S_n is normalized water saturation, k_{rwe} is relative permeability of water at residual oil saturation, which is taken as 0.8, k_{rw} is relative permeability of water, k_{ro} is relative permeability of oil, "no" represents the oil coefficient of 2.5, and "nw" represents the water coefficient of 2.5. Calculated relative

permeability of individual liquids is shown by Fig. 25. Contrary to the matrix, relative permeability of both oil and water is a straight line for fractures with zero capillary pressure, which is the most common way of modeling fractures.

$$S_n = \frac{S_w - S_{wr}}{1 - S_{or} - S_{wr}} \tag{4.1}$$

$$k_{rw} = k_{rwe} S_n^{nw} \tag{4.2}$$

$$k_{ro} = (1 - S_n)^{no} \tag{4.3}$$

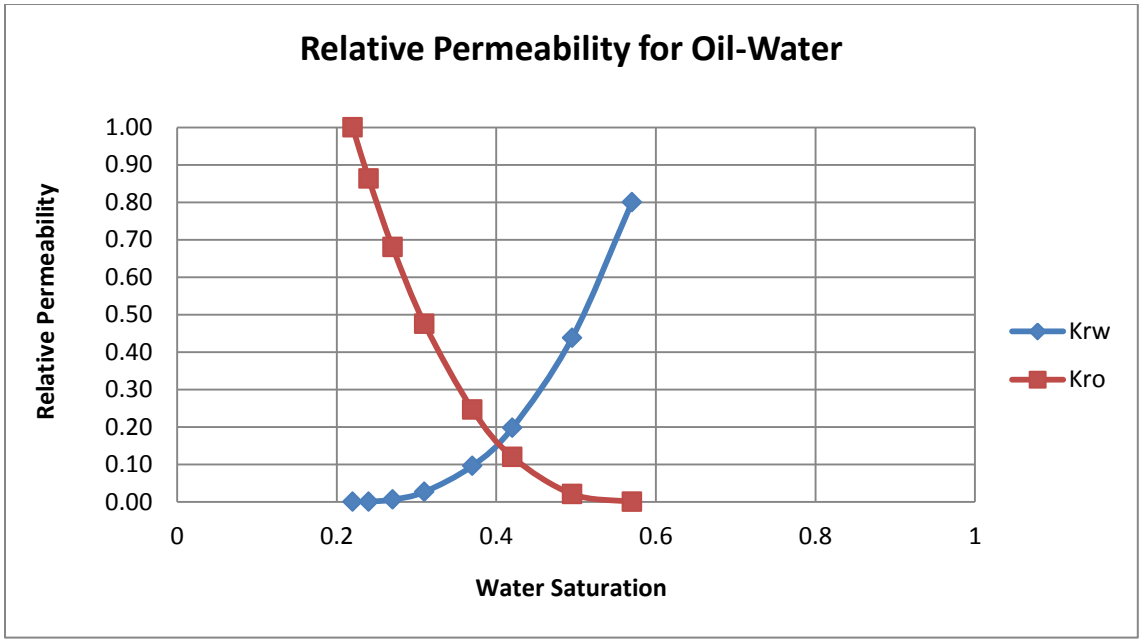

Fig. 25: Oil-Water Relative Permeability Curves

4.2. Sensitivity Analysis

Because FrontSim doesn't calculate tracer concentration in a dual-porosity model, the main objective was to observe water production response for changes in reservoir properties. As a result, simulations were compared with respect to field water cut after each sensitivity case.

A three-phase, dual-porosity model was built with available data stated previously. The constructed model consists of three layers: 1U, shale, and 5U. For unknown properties, the average value was assigned initially and changed if it was required. Main properties are listed in Table 10, including top depth of the structure,

thickness of the layers, matrix porosity, fracture porosity, matrix permeability, fracture porosity, and matrix-fracture interaction coefficient. For simulation, an inverted nine-spot of Sherrod 1012W was selected because four of the wells located there were newly drilled and four of them showed very high tracer response in both E-W and NE-SW directions. This pattern was simulated from the start of injection under the oil constraint operation limit. Sensitivities were conducted on 38×38×6 grid system with a grid dimension of 100 ft. A sample is illustrated by Fig. 26. Due to grid block size, time step is limited to 0.1 days by the MAXSTEP keyword for accuracy.

Table 10: Initial Model Properties For Sensitivity Analysis

INITIAL PROPERTIES	
Top Depth	6930 ft
h_{1U}	10 ft
h_{SHALE}	140 ft
h_{5U}	15 ft
$\emptyset_m$	0.1
$\emptyset_f$	0.005
k_m	0.5 md
k_f	1000 md
σ	0.0001

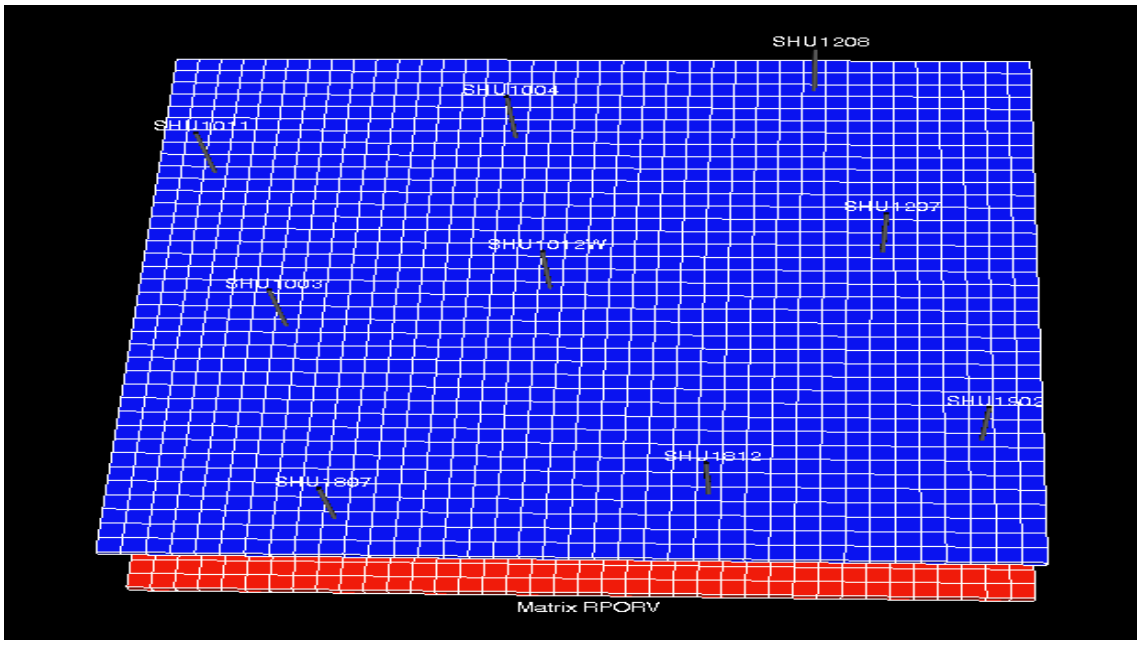

Fig. 26: Grid system And Well Locations Of Sample File For Sensitivity Analysis

Sensitivity analysis was done for sigma, water saturation, pressure, matrix porosity, fracture porosity, fracture permeability, matrix capillary pressure, matrix relative permeability, and matrix residual oil saturation. After being sure of the producing historical oil rate, field water-cut responses were compared with each other to figure out which parameter was more effective on water production.

Sigma was used for defining matrix-fracture flow interaction. It was calculated based on fracture spacing shown previously. Generally, it is a history-matching parameter for field studies. Because our model was started by capillary-gravity equilibration, both fracture and matrix are at irreducible water saturation. Hence, water production occurs once injected water reaches production wells. As seen in Fig. 27, which is plotted by increasing order, the highest field water cut belongs to the smallest sigma; however, it decreases by increasing sigma because lower sigma means less

communication between matrix and fracture. Therefore, injected water flows directly to production wells rather than imbibing into the matrix. Moreover, a sigma of 0.01 is the limit for water production. There is no water production for a sigma of 0.01 or higher because injected water does not reach production wells. This kind of low sigma is unexpected for the Spraberry, where a large amount of water production is believed to be due to a highly dense fracture system. Another unexpected observation is that water didn't break through, even for more than 600 days; however, injected tracer was produced from Sherrod 1003 within 1 day. These are highlighted in the history-matching section.

CASE	SIGMA
A1	0.0000001
A2	0.000001
A3	0.00001
A4	0.0001
A5	0.001
A6	0.01
A7	0.1
A8	1
A9	10

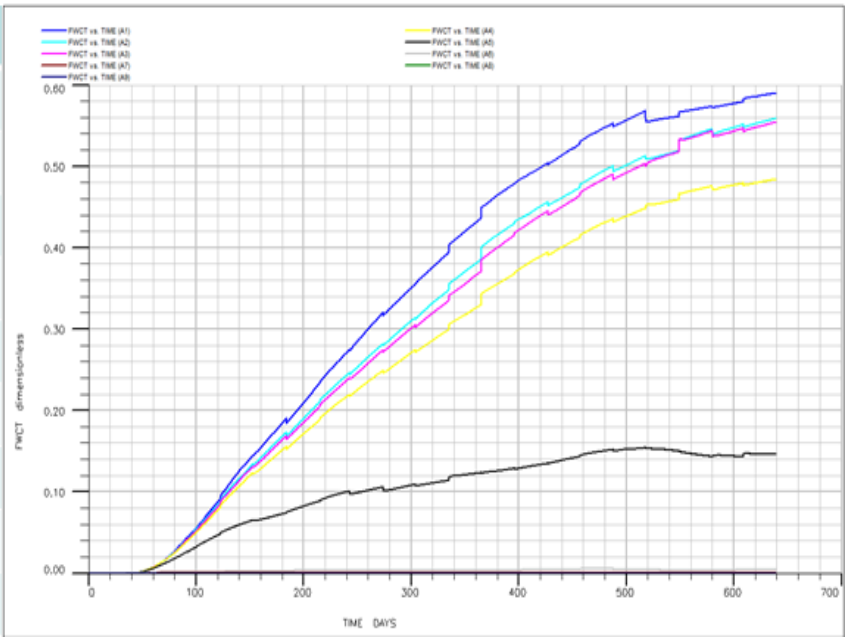

Fig. 27: Field Water Cut Responses For Increasing Sigma

As mentioned earlier, the base model was initialized by gravity-capillary forces. To test water saturation effect on water-cut responses, it was defined explicitly. Fig. 28 shows that higher water saturation corresponds to higher field water cut, as expected. Also, there is no difference in terms of trend or slope between cases, the only difference exists in magnitude. Unlike water saturation, initial pressure has very little effect on water production. As seen in Fig. 29, water-cut profile is almost unchanging for a wide range of initial pressures. Therefore, pressure can be neglected during the history-matching procedure.

CASE	Sw
A1	0.22
A2	0.24
A3	0.27
A4	0.31
A5	0.37
A6	0.42
A7	0.57
A8	0.65
A9	0.75
A10	0.85

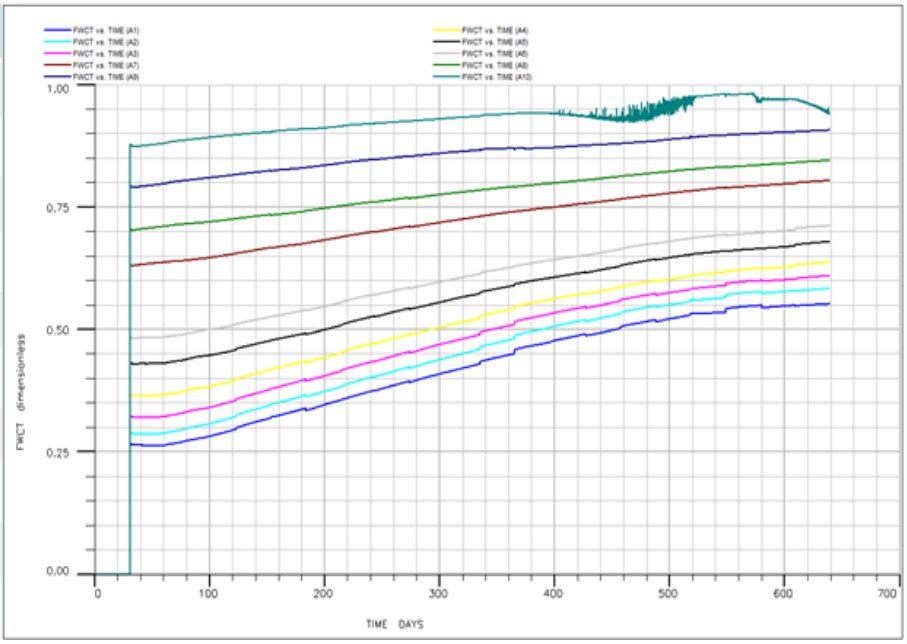

Fig. 28: Field Water Cut Responses For Increasing Water Saturation

CASE	P(psi)
A1	650
A2	900
A3	1200
A4	1500
A5	1750
A6	1920
A7	2100

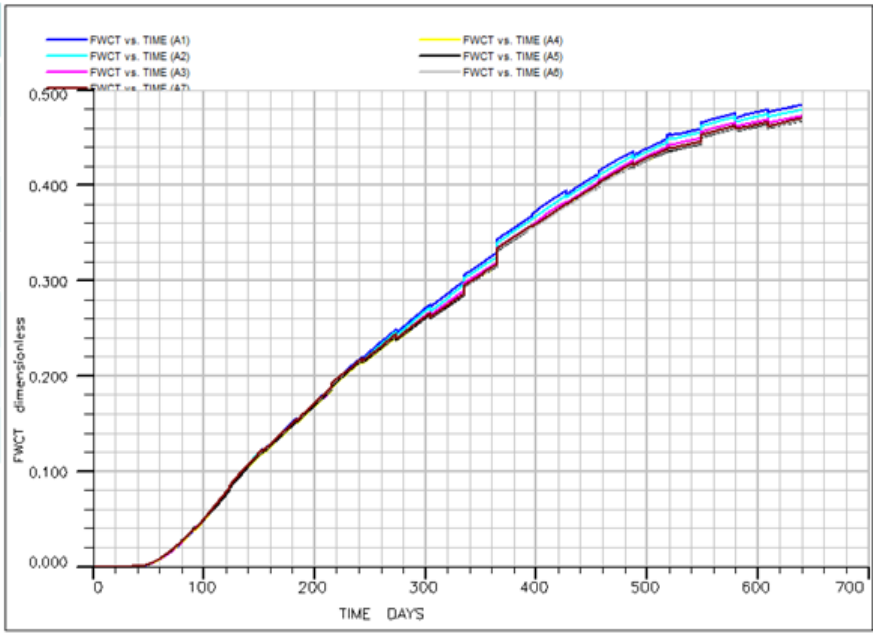

Fig. 29: Field Water Cut Responses For Increasing Initial Pressure

Although the low sigma used in our model limits effectiveness of matrix porosity in water production, it still has an impact on water-cut responses to a certain extent. More porous rocks require more volume and more time to be filled; therefore, it reduces the amount of received water and delays the time for the same amount of water production compared with less porous rocks. However, the maximum difference is 0.08 for the Spraberry-type porosity range, illustrated by Fig. 30. So matrix porosity will not be considered for history matching.

CASE	Øm
A1	0.01
A2	0.02
A3	0.04
A4	0.06
A5	0.08
A6	0.1
A7	0.12
A8	0.15

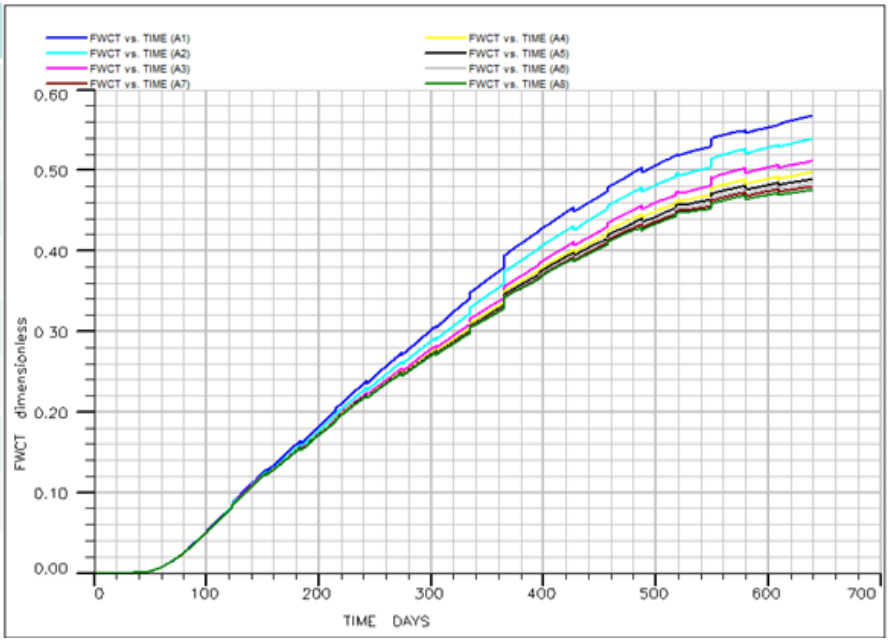

Fig. 30: Field Water Cut Responses For Increasing Matrix Porosity

On the other hand, significant differences exist in both magnitude and trend of water cut. It can be easily seen from Fig. 31 that a smaller fracture porosity results in faster breakthrough and generally higher water-cut responses compared with more porous media, where only a small amount of injected water can reach producers because of filling up the pores. However, some porosity values have caused more water production than the smallest case at the end of the simulation in spite of the fact that those do not have as sharp a water-cut profile as it does. Thus, not only breakthrough time, but also amount of water production should be evaluated carefully in history matching.

CASE	Ø
A1	0.00005
A2	0.0001
A3	0.0005
A4	0.001
A5	0.005
A6	0.01
A7	0.05
A8	0.1

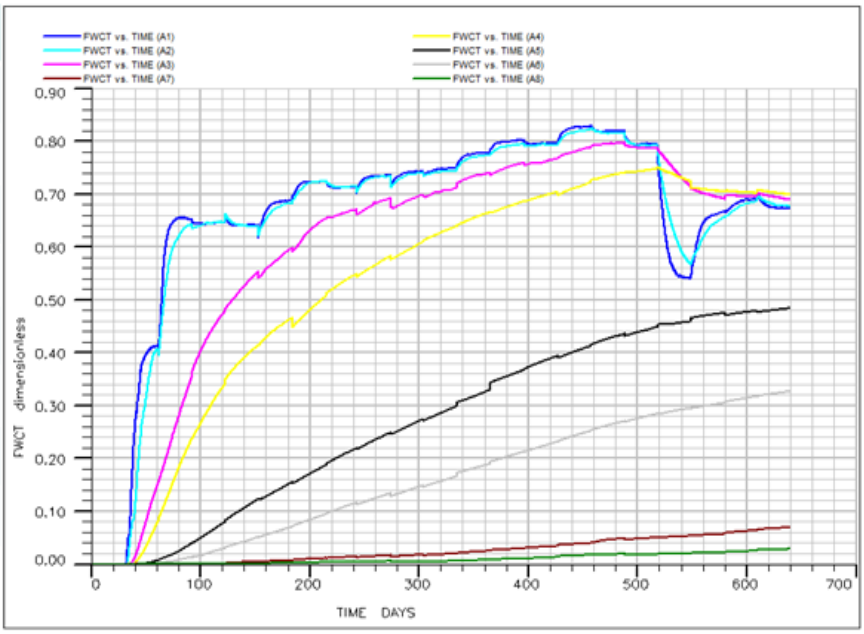

Fig. 31: Field Water Cut Responses For Increasing Fracture Porosity

Because flow rate is directly proportional to permeability, an increase in fracture permeability leads to a large amount of water production. Besides that, a sudden rise in water-cut profile is observed for more conductive fractures, shown by Fig. 32. For history matching, the impact of the fracture permeability on water production will be considered. The only problem observed about fracture permeability is stability of simulation for dual-porosity models in the case of fracture permeabilities exceeding 10,000 mD.

CASE	Kf(md)
A1	100
A2	1000
A3	2000
A4	5000
A5	10000
A6	50000
A7	100000
A8	500000

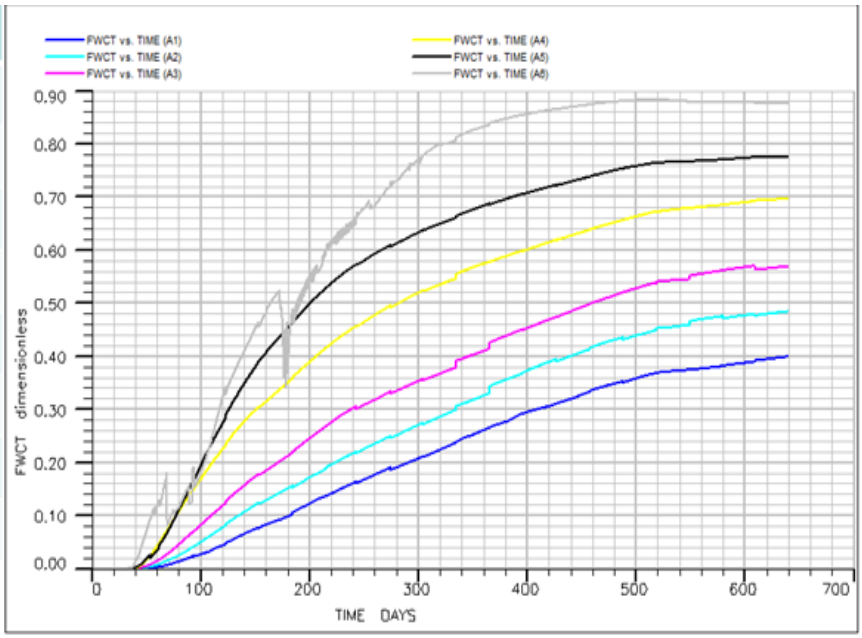

Fig. 32: Field Water Cut Responses For Increasing Fracture Permeability

Sensitivity analysis has also been done for capillary pressure of the matrix. The data for sensitivity is obtained by both multiplying and dividing capillary pressure in the base case. According to Fig. 33, more capillary pressure means less water production because higher capillary pressure is one the characteristics of strongly water-wet rock, in which the imbibition mechanism works efficiently. Therefore, a large amount of water enters the matrix pores instead of flowing directly through fractures. Because of the lack of measured capillary pressure for the Sherrod, the same capillary pressure data set was used for the history-matching case.

Sw	1	2	3	4	5
0.22	5	10	20	40	80
0.24	3.5	7	14	28	56
0.27	2.75	5.5	11	22	44
0.31	2.25	4.5	9	18	36
0.37	1.5	3	6	12	24
0.42	1	2	4	8	16
0.50	0.5	1	2	4	8
0.57	0	0	0	0	0

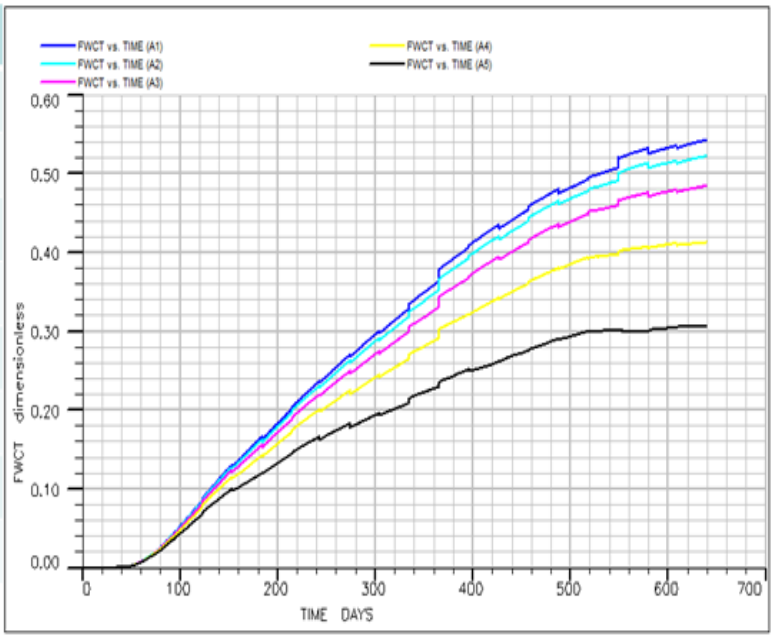

Fig. 33: Field Water Cut Responses For Increasing Matrix Capillary Pressure

Unlike capillary pressure of the matrix, Fig. 34 shows that relative permeability difference formed by a different water-oil exponent doesn't change the production performance of this particular dual-porosity model. The underlying reason is most probably both low sigma and low matrix permeabilities that prevent or reduce imbibition of water. Similarly, a decrease in residual oil saturation doesn't make any difference in water-cut profile due to the reasons stated above. All end points show identical field water production, as illustrated by Fig. 35. As a result, both relative permeability and residual oil saturation of the matrix were not considered and were used as they are.

CASE	no & nw
A1	1.5
A2	2
A3	2.5
A4	3

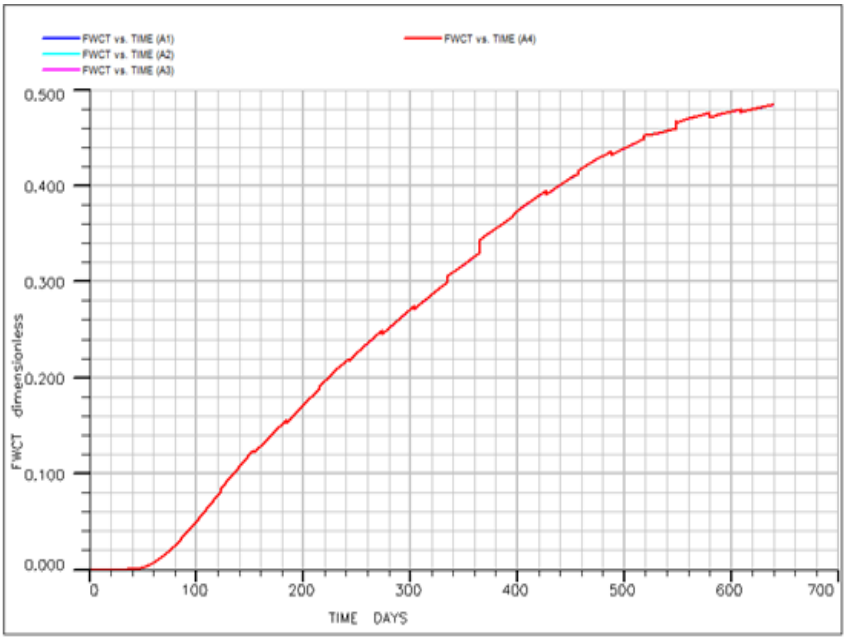

Fig. 34: Field Water Cut Responses For Increasing Oil and Water Exponent

CASE	1 - Sor
A1	0.52
A2	0.57
A3	0.65
A4	0.7
A5	0.75
A6	0.8

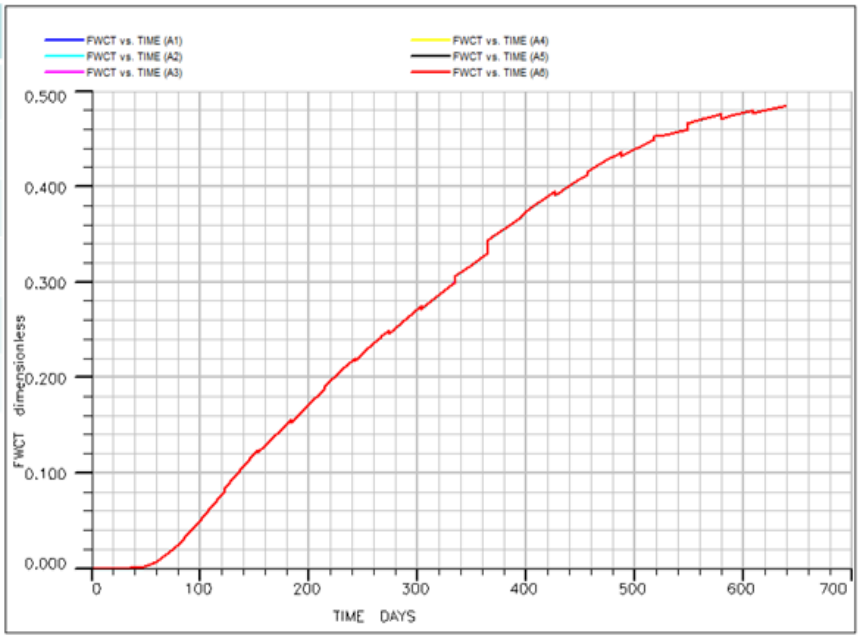

Fig. 35: Field Water Cut Responses For Decreasing Residual Oil Saturation

4.3. History Matching

From sensitivity analysis, important reservoir parameters that mainly control water production were determined as sigma, water saturation, fracture porosity, and fracture permeability. Once those were identified, manual history matching began to replicate both observed field and individual well production performance. For accuracy and visualization, the grid system was changed to 76×76×6, including fractures with the same areal resolution. Also, the thickness of 5U was reduced to 10 ft based on perforations from the injection profile log of 1012W. Another important change was controlling criteria switched from oil rate constraint to total liquid rate constraint. This constraint is more suitable for streamline simulation because streamlines are calculated from total fluid velocity rather than individual oil or water velocity.

4.3.1. History Matching for Cumulative Field Production

In manual history matching, early efforts are put into matching cumulative liquid production. Because it is a volumetric issue, actual production for the individual liquid was matched by adjusting its saturation. However, the initial focus was assigning a sigma coefficient for our case. According to the fracture system in Fig. 4, sigma was calculated as 1.84 from Kazemi's shape factor formula provided before. In this case, water saturation was assumed to be the main reason for high-water-cut observations, so fracture water saturation was determined as 0.95. Even for this kind of high water

saturation, sigma based on fracture spacing produces much more oil than observed data, shown by Fig. 36. To ensure sigma effect on oil production, water saturation was increased to 0.995, and then each case was simulated for that. Fig. 37 demonstrates that even a sigma of 0.01 has more oil production than observed for such extreme water saturation. This highlights that the actual matrix-fracture interaction in the field is much lower than calculated. There should be some other mechanisms that inhibit counter-current flow between the matrix and fracture in spite of the closely spaced fracture system. The primary reason seems to be fracture mineralization. As illustrated by Fig. 38, excessive mineralization on the fracture surface causes very poor matrix-fracture interaction. Therefore, most injected water didn't sweep oil from the matrix because it couldn't imbibe into the matrix. On the other hand, a sigma of only 0.001 produces less oil than the observed cumulative oil production in Fig. 36. However, before water injection started, water cut for wells was less than 0.95. Thus, initial water saturation in the simulation should be less than 0.95 because injected water is the main reason for high water cut, especially for high-tracer-recovery wells. As a result, a sigma of 0.001 was assigned to represent the field-wide matrix-fracture interaction for the next stages of history matching.

CASE	SIGMA
A1	1.84
A2	0.1
A3	0.01
A4	0.001

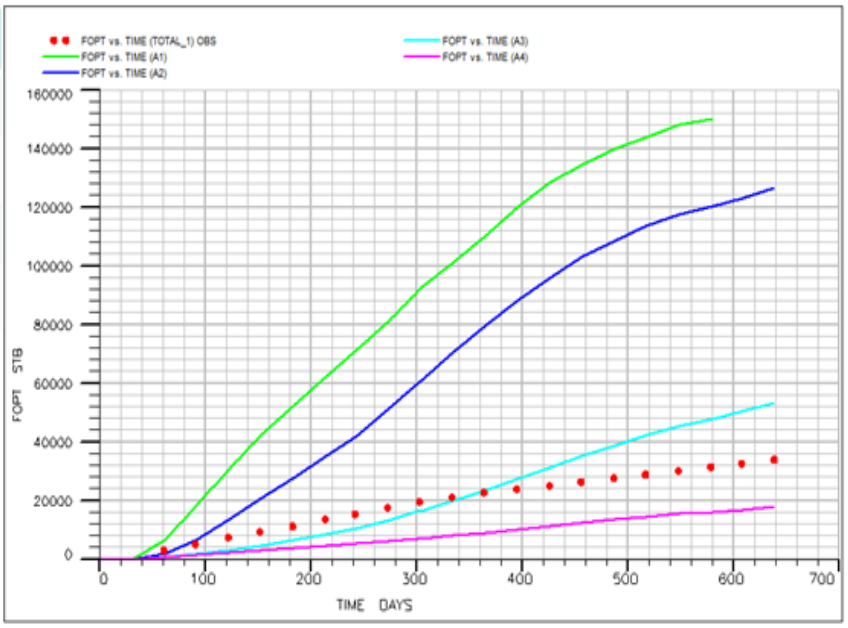

Fig. 36: Cumulative Production Of Field At Sw = 0.95 For Increasing Sigma

CASE	SIGMA
A1	1.84
A2	0.1
A3	0.01

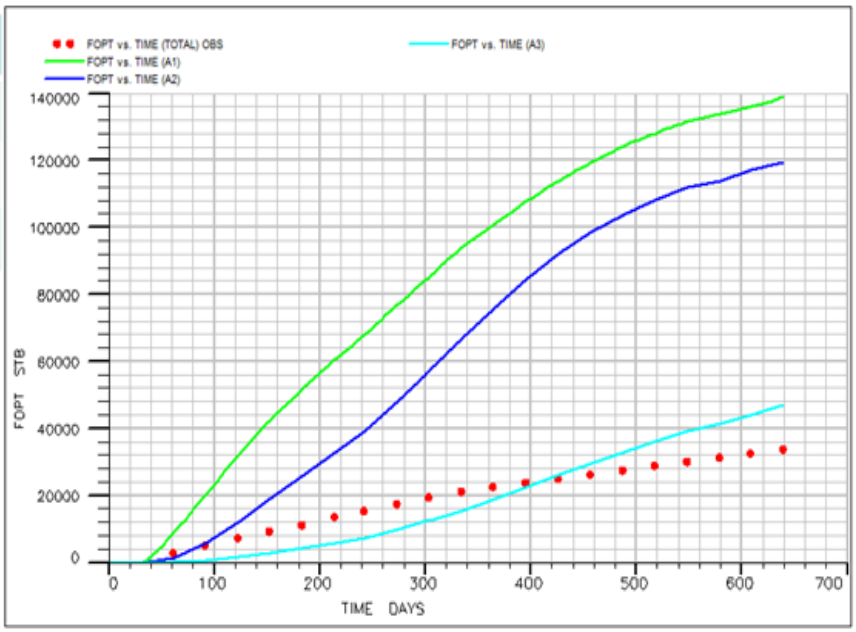

Fig. 37: Cumulative Production Of Field At Sw = 0.995 For Increasing Sigma

Fig. 38: Observed Mineralization On Fracture Surface From Spraberry Core

Once sigma was kept constant at 0.001, only initial water saturation and fracture porosity remained as key parameters in order to get a match for the cumulative field because initial water saturation determines amount of oil in place and the latter controls not only amount of oil in place, but also amount of water production due to injected water. Estimating the amount of water in the matrix and in the fracture is critical for initial water saturation distribution. To understand the impact of water distribution in the matrix and fracture, sensitivity analysis was done for increasing water saturation in the fracture while at the same time decreasing it in the matrix. It can be seen from Fig. 39 that higher oil production during the early time is due to lower water saturation in the fracture, while lower matrix water saturation causes large oil production during the late time, as expected. However, actual field performance is closer to the simulated case, in which the saturation difference between the matrix and fracture is low for this particular

simulation model. This observation is vital to evaluate actual field performance based on this model. First of all, the discrepancy between the matrix and fracture in terms of initial water saturation should be low according to this model, which means that water saturation in the matrix is higher than expected. This could be achieved under two circumstances—either initial fluid distribution in the reservoir or an external water source flowing to the field. The first one is related to migration of oil or water during the primary reservoir process. In other words, the matrix was already saturated by a large amount of water before any field production started. The other reason could be that the matrix was watered by water influx coming from an external source. Both initial water saturation measurements during primary production and the external water source hypothesis in the Spraberry support having high initial water saturation in the matrix. Secondly, a large discrepancy in saturation between the two media reveals the importance of sigma on oil production. Although its value is in the order of 10^{-3}, the discrepancy in oil production becomes larger with an increase in saturation difference between the matrix and fracture system for this particular model. Even this small sigma could be bigger than the actual sigma of the field. However, it was not changed for history matching because further reduction of sigma might prevent assessing the effect of reservoir properties on field performance. After several runs with that model, an initial matrix water saturation of 0.53 and initial fracture saturation of 0.76 provided the final match obtained for cumulative oil production and cumulative water production, as shown in Fig. 40 and Fig. 41, respectively. Well-by-well cumulative oil production corresponding to this match is demonstrated in Fig. 42 to Fig. 49.

CASE	Sw_m	Sw_f
A1	0.515	0.74
A2	0.48	0.78
A3	0.45	0.84
A4	0.40	0.90

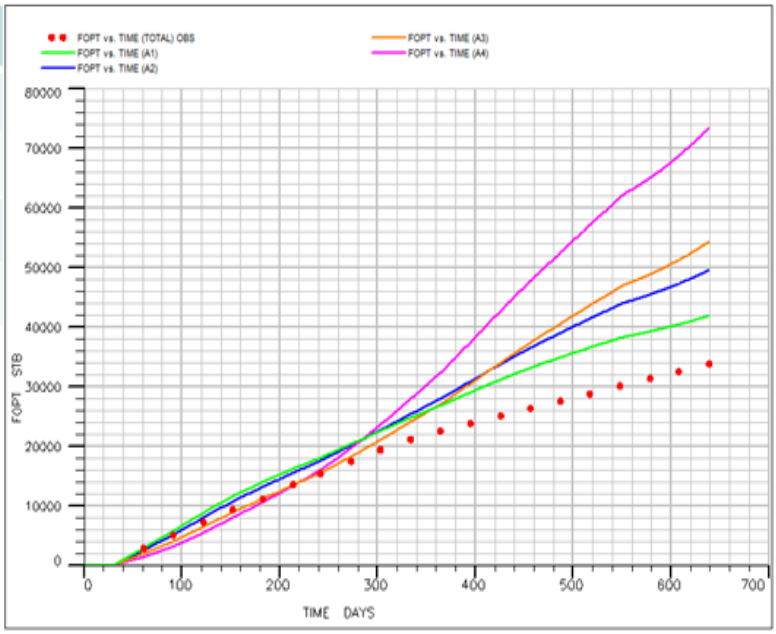

Fig. 39: Effect Of Initial Water Saturation On Cumulative Oil Production

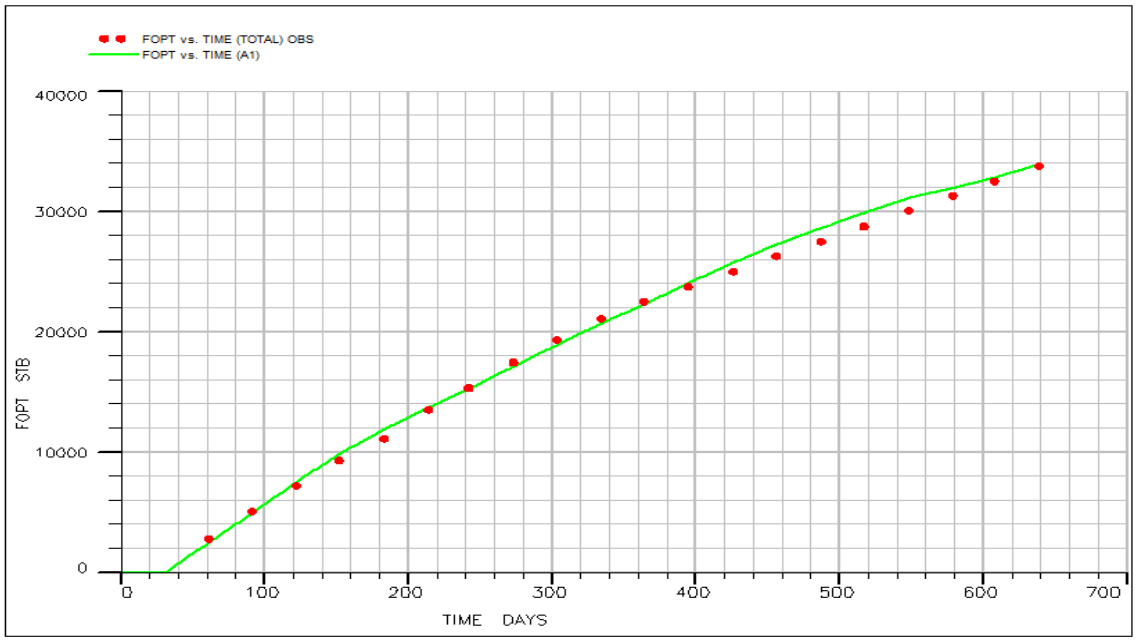

Fig. 40: Observed And Simulated Cumulative Oil Production In Field

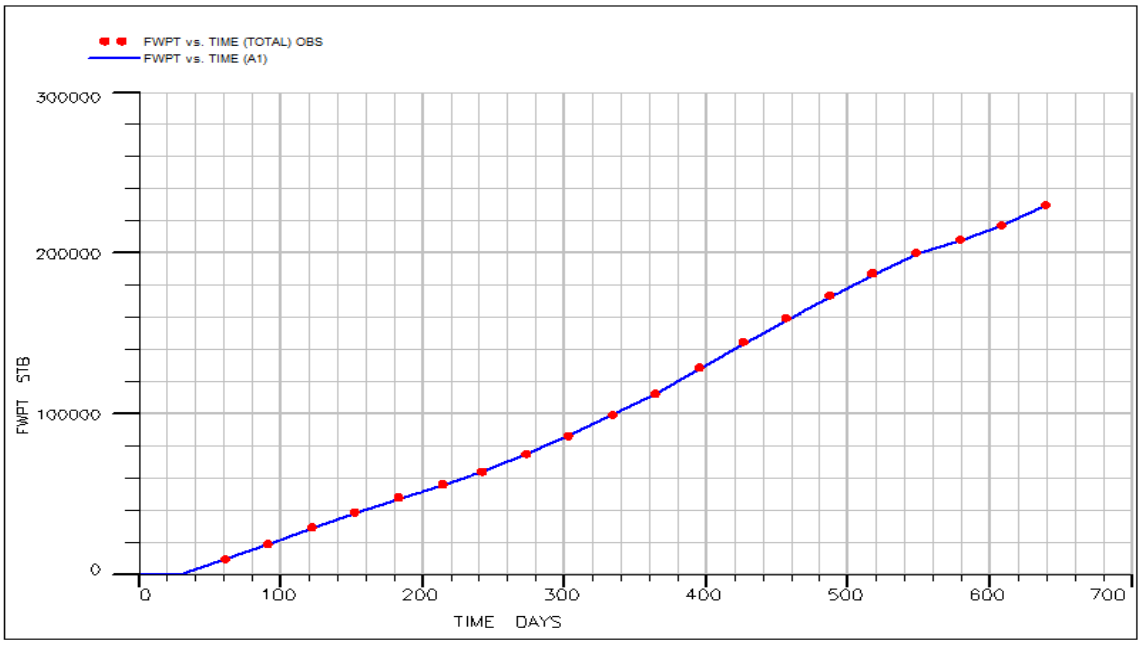

Fig. 41: Observed And Simulated Cumulative Water Production In Field

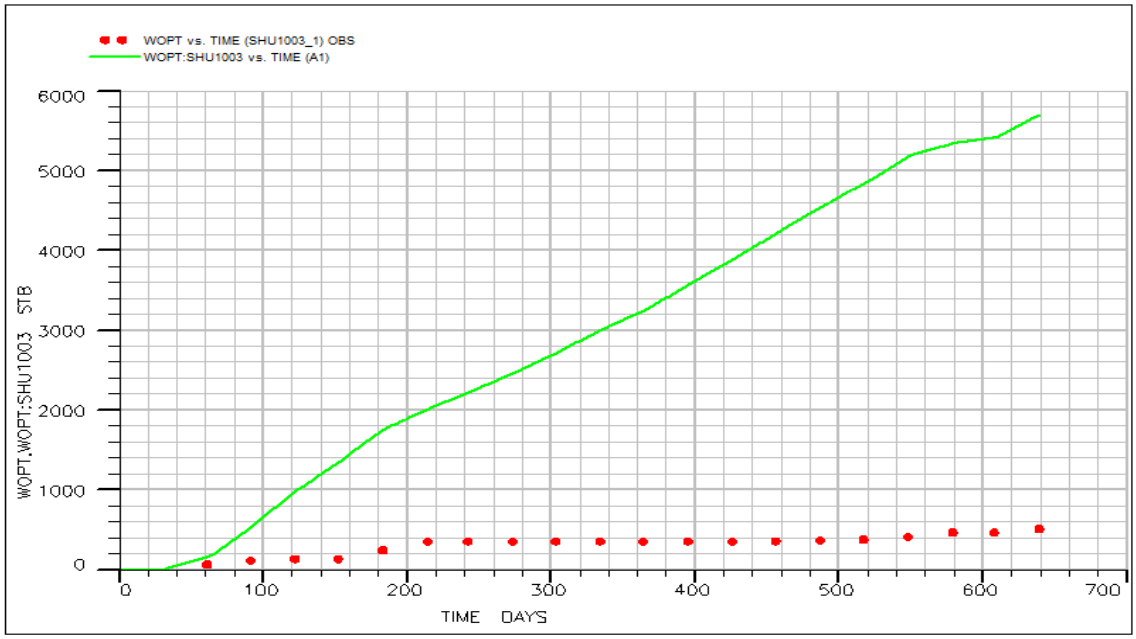

Fig. 42: Cumulative Oil Production For Sherrod 1003

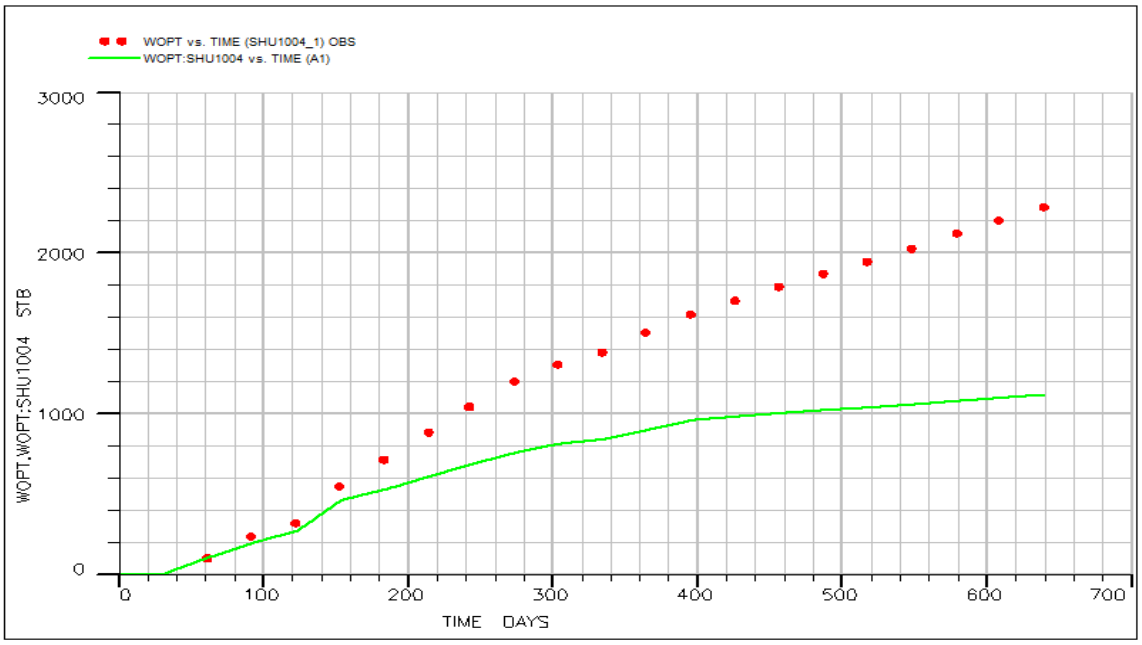

Fig. 43: Cumulative Oil Production For Sherrod 1004

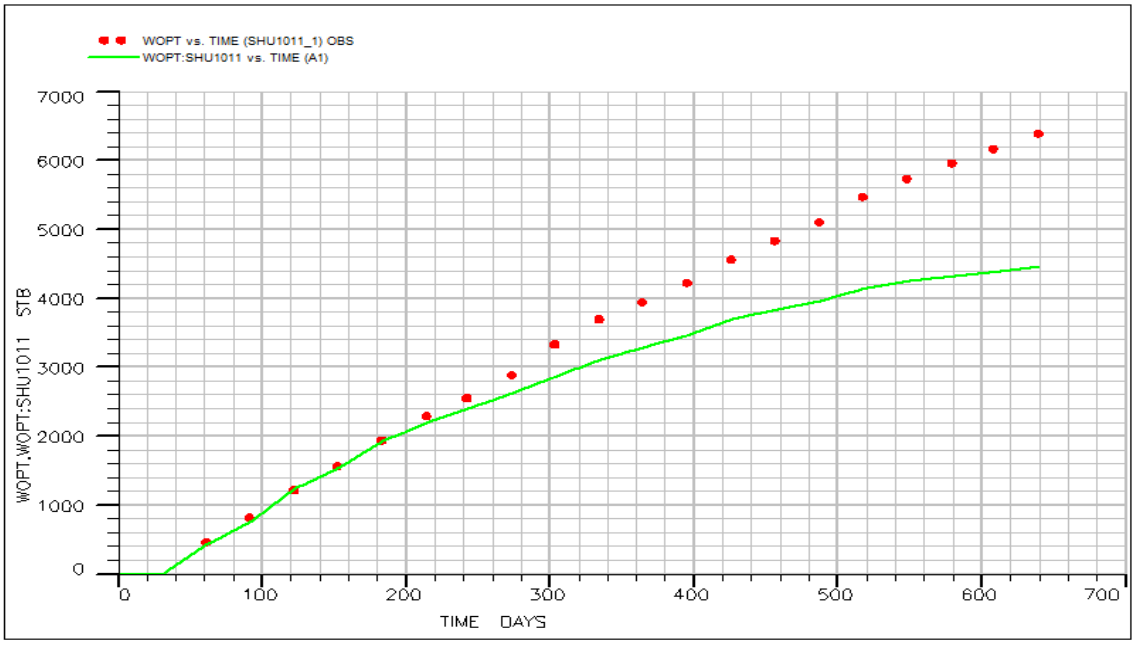

Fig. 44: Cumulative Oil Production For Sherrod 1011

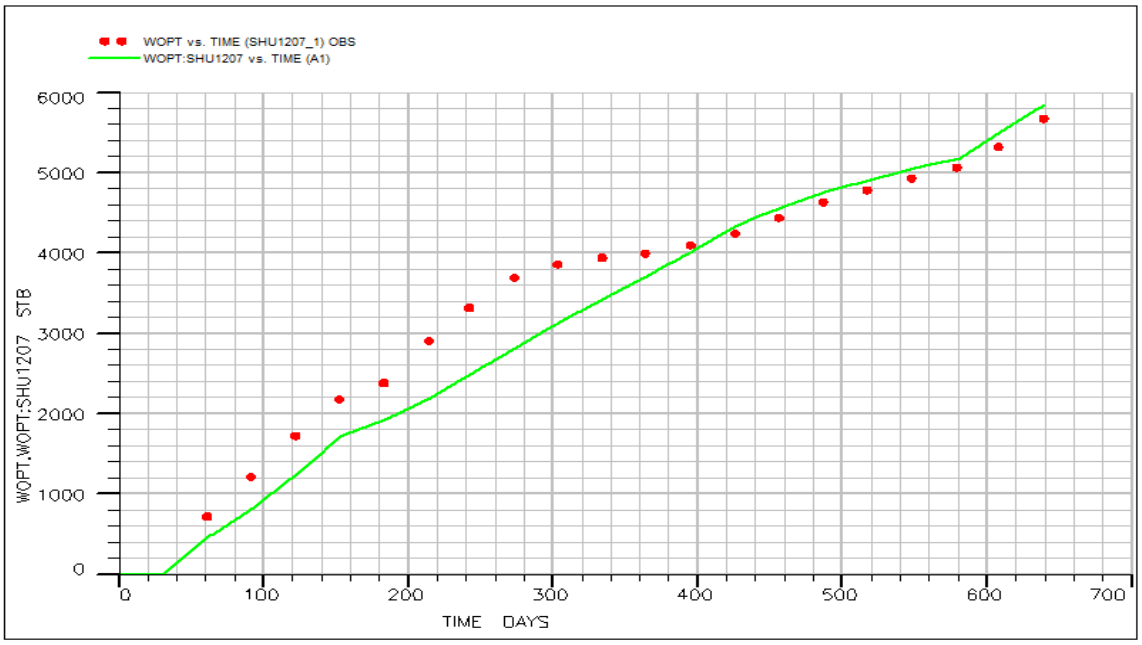

Fig. 45: Cumulative Oil Production For Sherrod 1207

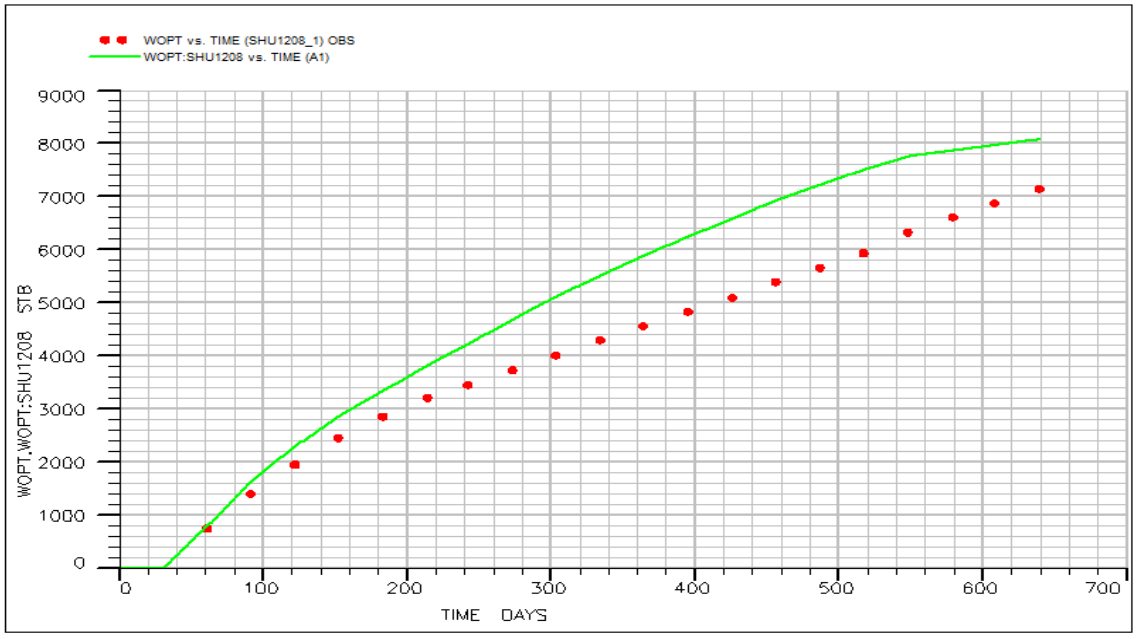

Fig. 46: Cumulative Oil Production For Sherrod 1208

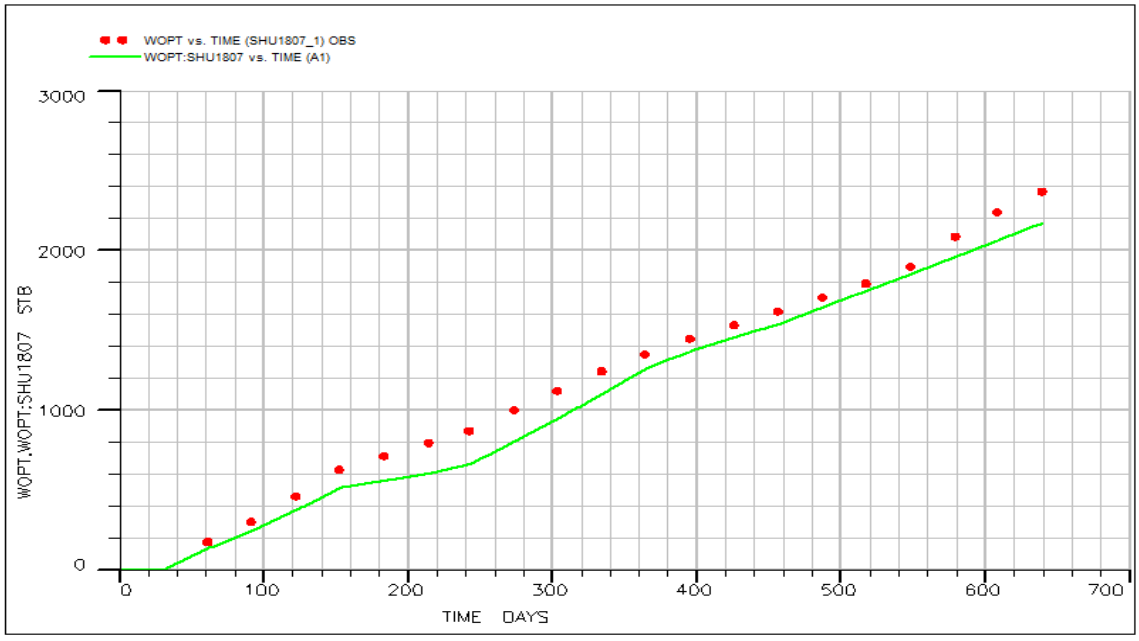

Fig. 47: Cumulative Oil Production For Sherrod 1807

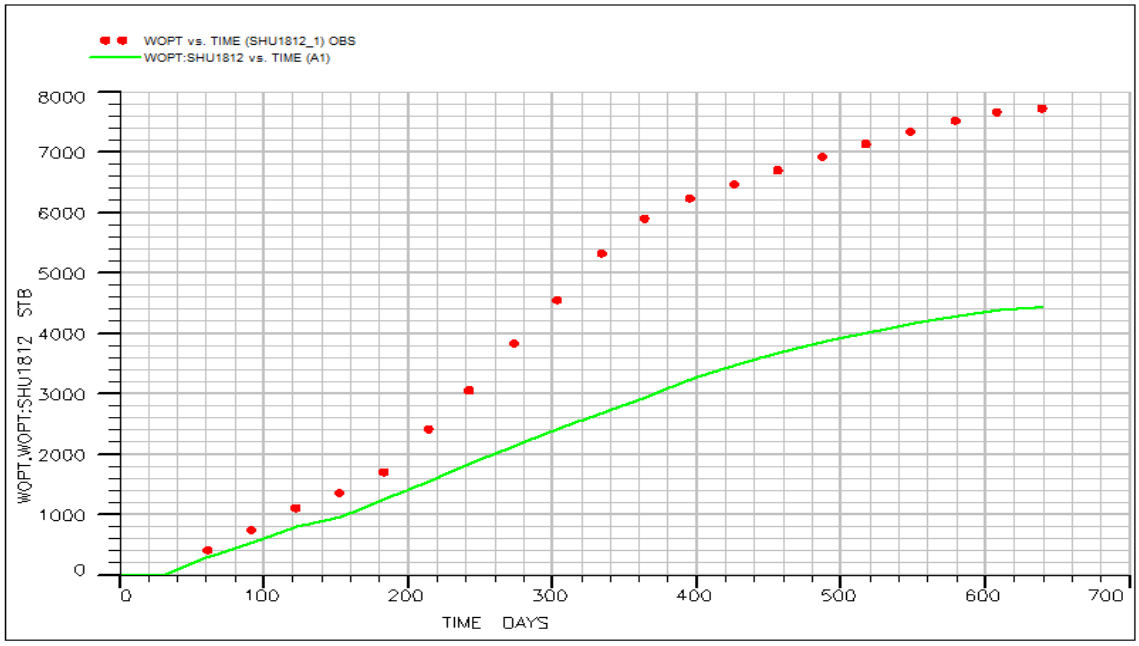

Fig. 48: Cumulative Oil Production For Sherrod 1812

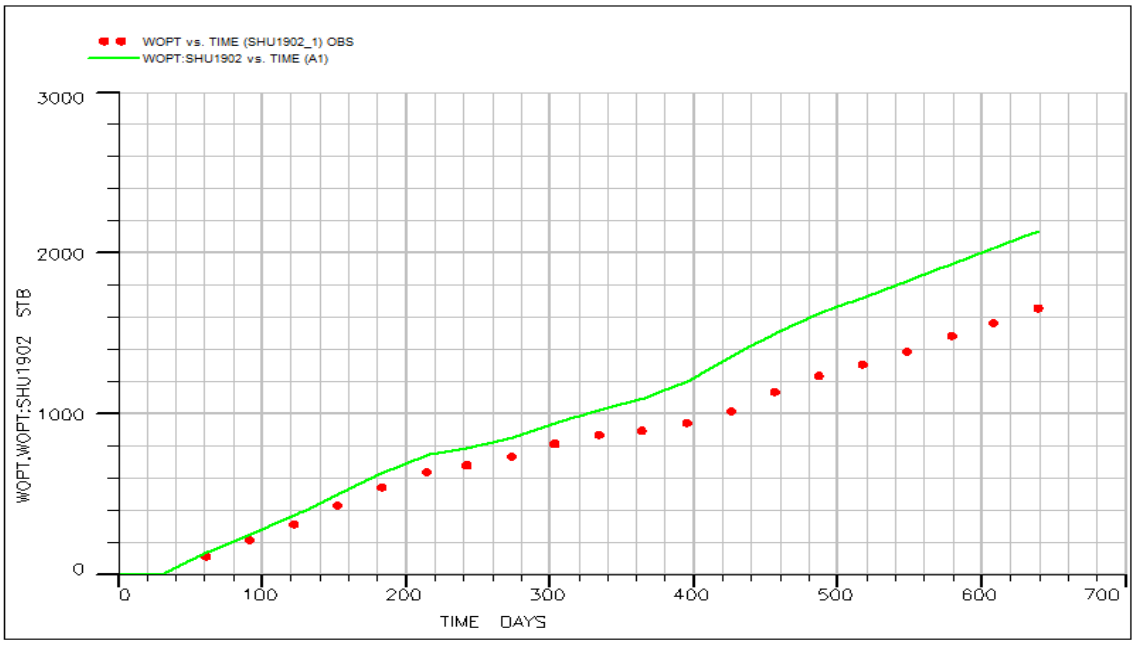

Fig. 49: Cumulative Oil Production For Sherrod 1902

4.3.2. Well-by-Well History Matching

Although cumulative field production closely agrees with observed data, individual well performance is far from actual for many of them. The main reason for this is incorrect distribution of injected water. In other words, actual water allocation from the injector for each well is different from the simulation case. Geometric allocation factors are too poor to identify the dynamic relationship between injector and producer. To quantify actual allocated water for each well, there should be some dynamic data that provide information about the relationship of the injector-producer well pair. The novelty of the inter-well tracer test emerges at this point, where it directly

assesses this relationship. Before moving to well-by-well history matching, tracer results should be evaluated for a better description of fluid flow and should be used for adjusting reservoir parameters. Both cumulative liquid production (represented by dark blue) and tracer response (represented by red) were delineated, as shown in Fig. 50. The total weight of each well in the pattern is demonstrated as a percentage for both cumulative liquid and tracer production. Also, a small portion in the dark blue circle corresponds to cumulative oil production, while the rest of it shows cumulative water production.

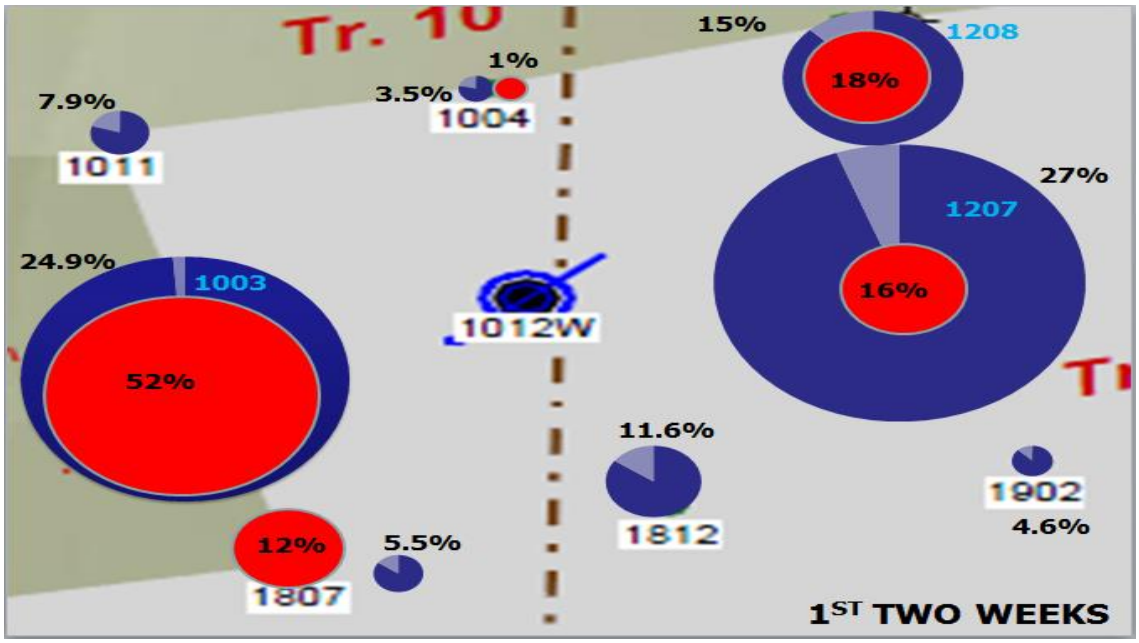

Fig. 50: Cumulative Liquid And Tracer Production For Sherrod 1012W Pattern

This composite analysis gives insightful information about reservoir characterization. First of all, both production and tracer data indicate flow domination in the E-W direction. They also show other domination in fluid flow in the NE-SW direction in spite of the smaller quantity compared with E-W. These flow trends remark on the existence of highly conductive fracture systems in these directions, as mentioned before. However, a very poor fracture system was observed in N-S direction, while almost no fracture system exists in the NW-SE direction according to tracer recovery. For further analysis, wells were categorized based on tracer presence. Sherrod 1003, 1207, 1208, and 1807 showed high tracer response, and Sherrod 1004, 1011, 1812, and 1902 showed either very low or no tracer response.

Sherrod 1003 definitely has the highest water allocation from the injector based on these data. Even though Sherrod 1207 produces the largest amount of liquid in the pattern, at least half the production comes from the nearby injector of Sherrod 1202W. This was confirmed by comparison of tracer recovery and breakthrough time for Sherrod 1012W and Sherrod 1202W injectors. Sherrod 1207 has a tracer recovery of 0.912% with 5 days breakthrough from Sherrod 1012W, while it has 1.705% tracer recovery with a breakthrough time of 2 days for Sherrod 1202W. Based on that, the proportion of Sherrod 1207 in the pattern could be lowered by half. This reduction makes water movement clear because Sherrod 1208 receives more water from the injector compared with Sherrod 1207 according to the new ratio. Tracer observation has exactly the same conclusion, in which higher recovery was observed for Sherrod 1208. The behavior of Sherrod 1807 is more complex than the others because it showed high tracer recovery;

however, total liquid production is less than 6%. This kind of poor production can be clarified by the fact that the amount of water received from the injector was actually smaller than expected based on tracer results. Hence, the allocation factor for Sherrod 1807 should be low. Furthermore, it can be concluded that injected water tends to flow in the W and N-E directions from both cumulative production and tracer recovery wells. The underlying reason could be dipping of the reservoir and pressure difference rather than due to only an oriented fracture system.

For Sherrod 1004, both cumulative production and tracer recovery is very low. Unlike the old well, Sherrod 1004, Sherrod 1011 has moderately high liquid production as a new well without any contribution from the injector. Having no tracer response could be the outcome of a sealing fault between Sherrod 1011 and Sherrod 1012W, as well as the lack of a NW-SE fracture system. Similarly, Sherrod 1812, which is also a new well, produces a significant amount of liquid, while received water due to the injector is negligible. Sherrod 1902 again shows a low production capacity with insignificant tracer response. It is clear that old wells, Sherrod 1004 and Sherrod 1902, produce much less than new wells, Sherrod 1011 and Sherrod 1812, as expected because the drainage area of the new wells hasn't swept yet and was already depleted for the old ones.

According to the conclusions from a composite interpretation of production and tracer data, some of the grid blocks were modified in order to create flow anisotropy. Any kind of cell-based modification was applied to both 1U and 5U. Initial trials for history matching were changing fracture porosity and fracture permeability of modified

grid cells. However, it was not good enough to obtain a reasonable match because certain differences were present either during the early time or late time. To compensate for these differences, initial saturation of nearby cells was adapted mostly based on being an old or new well, as well as fracture porosity. Fig. 51, Fig. 52 and Fig. 53 demonstrate fracture porosity, fracture permeability, and initial fracture water saturation for the history-matched model, respectively.

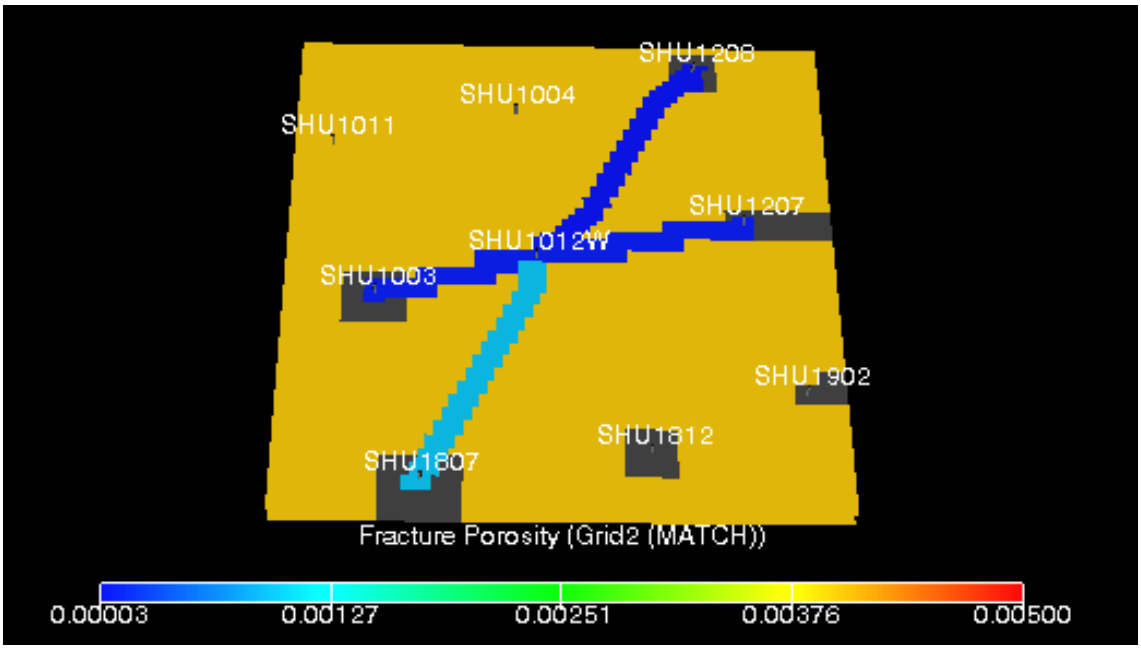

Fig. 51: Fracture Porosity Modification For History Matched Model

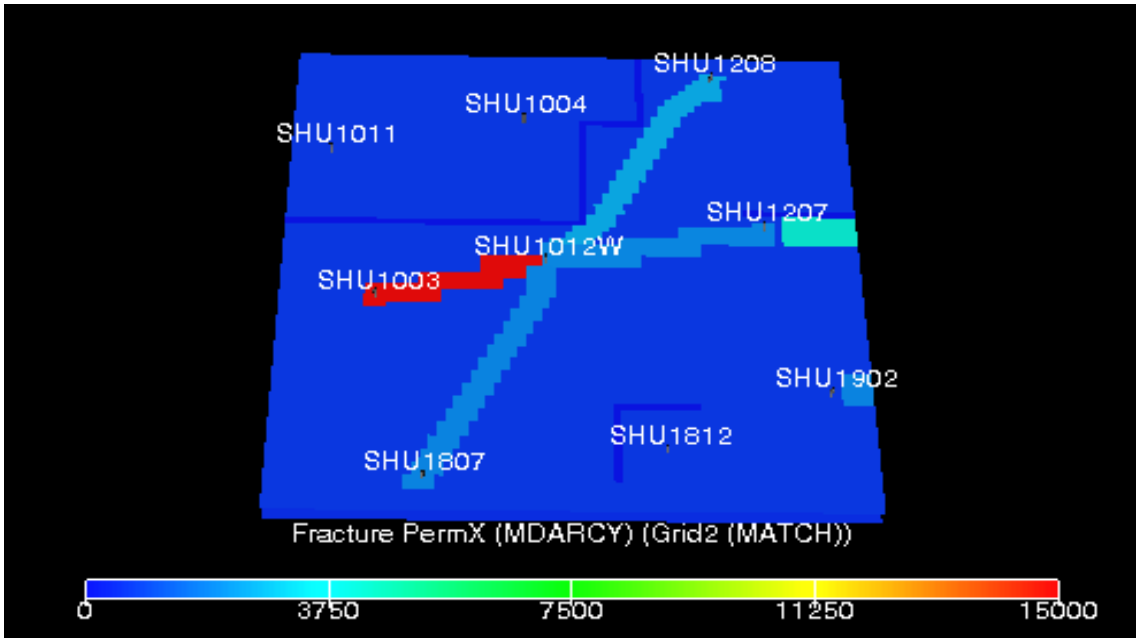

Fig. 52: Fracture Permeability Modification For History Matched Model

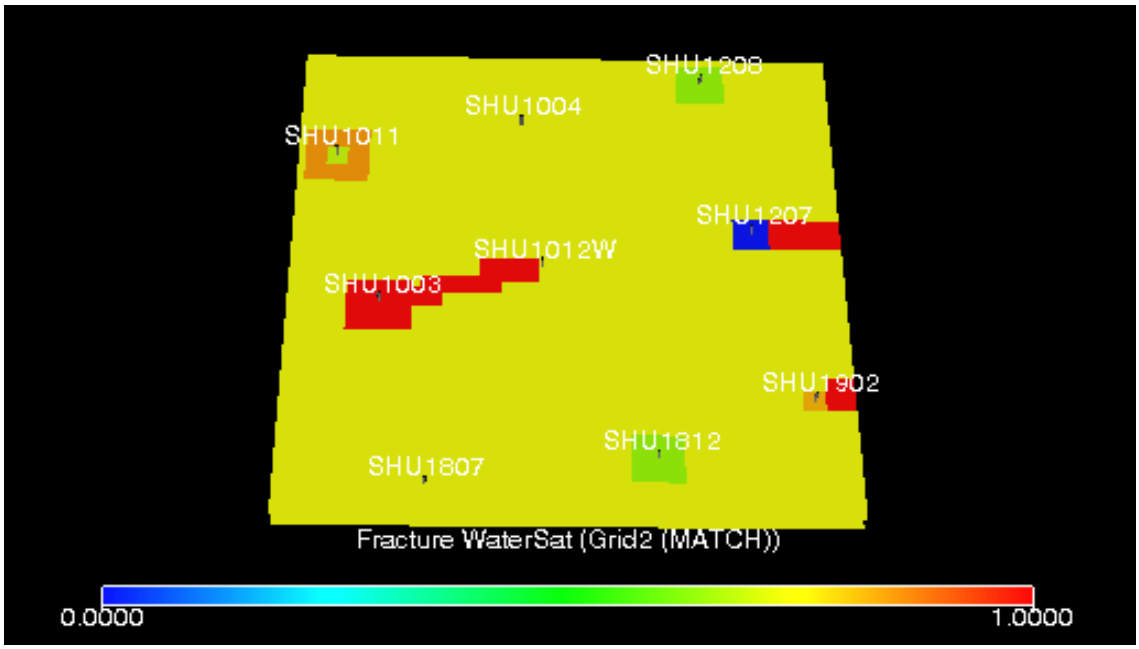

Fig. 53: Fracture Water Saturation Modification For History Matched Model

After conducting several runs to get a match for wells, cumulative field production was not as good as previously seen, especially for oil production. However, initial water saturation in the fracture and matrix were reduced to 0.74 and 0.515, respectively. The final match was very close to actual data for both the field and individual wells. Especially for water production, each well has an almost perfect match. The sample FrontSim file can be found in Appendix A. Fig. 54 to Fig. 77 present simulation results for the field and each well separately. Because gas production couldn't be matched, GOR is different than observed, as shown in Fig. 59. However, Fig. 61 demonstrates that in spite of small separation, the voidage replacement ratio follows the same trend with observed data. In addition, both of them are less than unified, which proves that the amount of fluid flow is not equal to the amount of fluid produced. As a result, gas production and its effects were not considered in further stages. In terms of oil production, only Sherrod 1003 seems different than observed. However, 500 bbl of oil difference is negligible for a cumulative water production of 70,000 bbl. Also, the model was not able to match oil production for Sherrod 1902 during the late time. Increased water saturation and fracture saturation of nearby cells to include the Sherrod 1202W effect didn't improve the match. Besides liquid production match for wells, tracer breakthrough time was matched, as illustrated by Fig. 78. Except for Sherrod 1807, they are exactly same for observed breakthrough time. Movement of injected water in the pattern was described efficiently by TOF (time-of-flight) visualization, which was run as a dry model to represent flow only due to the injector. The grid base plots for fracture water saturation, matrix water saturation, fracture reservoir pressure, and fracture gas

saturation at the beginning of simulation and at the end of history matching are found in Appendix B. Even though pressure is higher than bubblepoint pressure, gas saturation is bigger than zero for Sherrod 1807. After final checks, a request was sent to customer service of FrontSim, and they commented that a low production rate might cause an error during back-and-forth saturation updating.

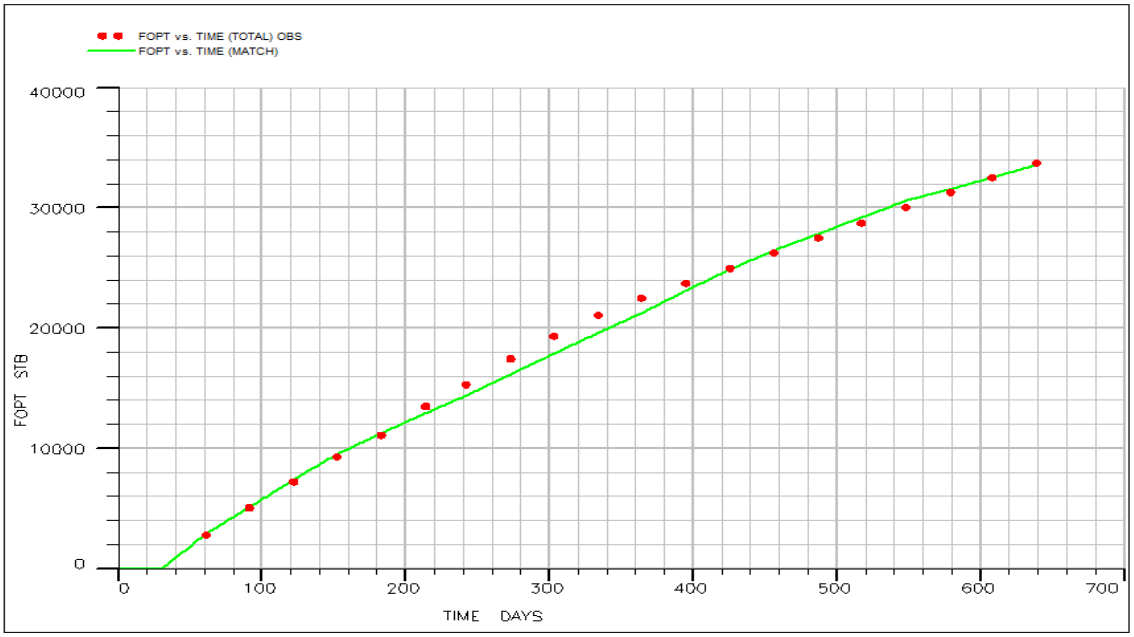

Fig. 54: Final History Match For Cumulative Oil Production

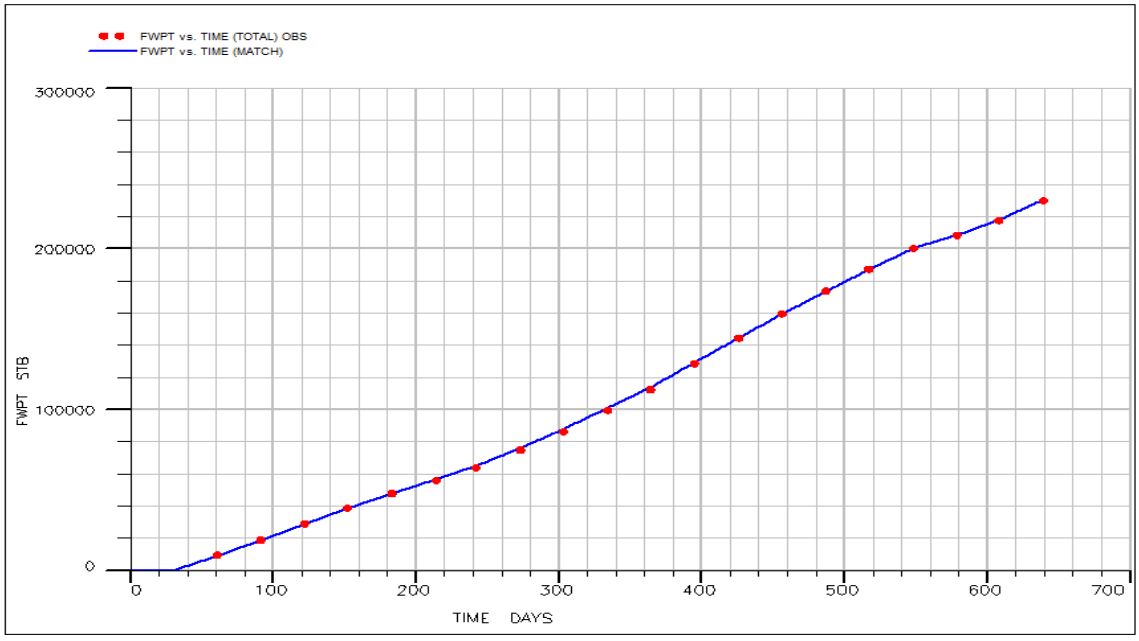

Fig. 55: Final History Match For Cumulative Water Production

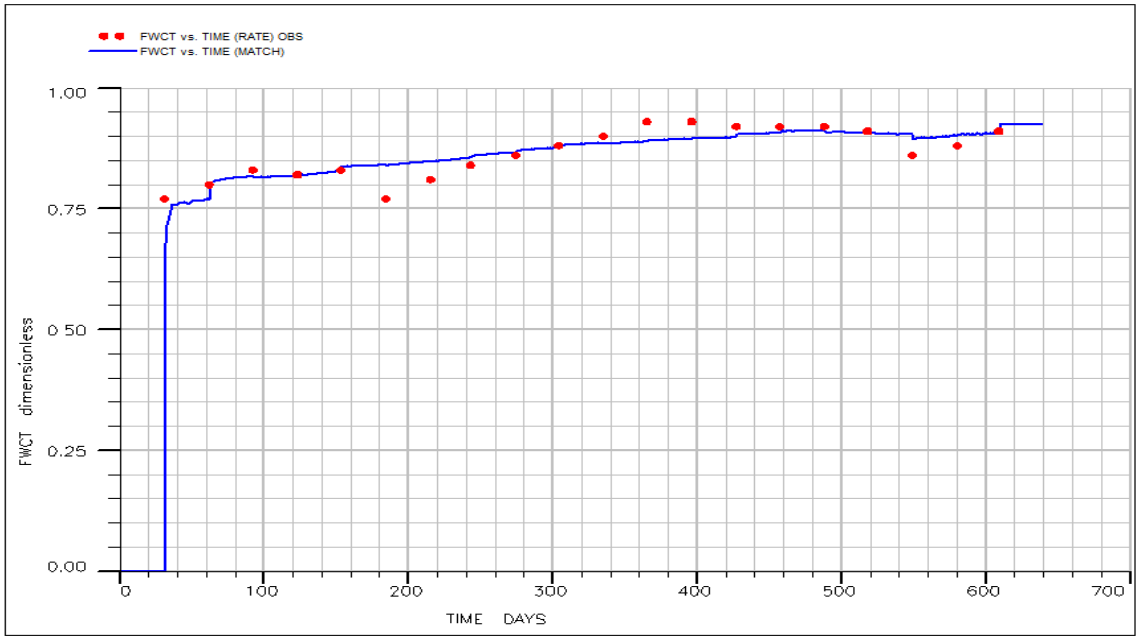

Fig. 56: Final History Match For Field Water Cut

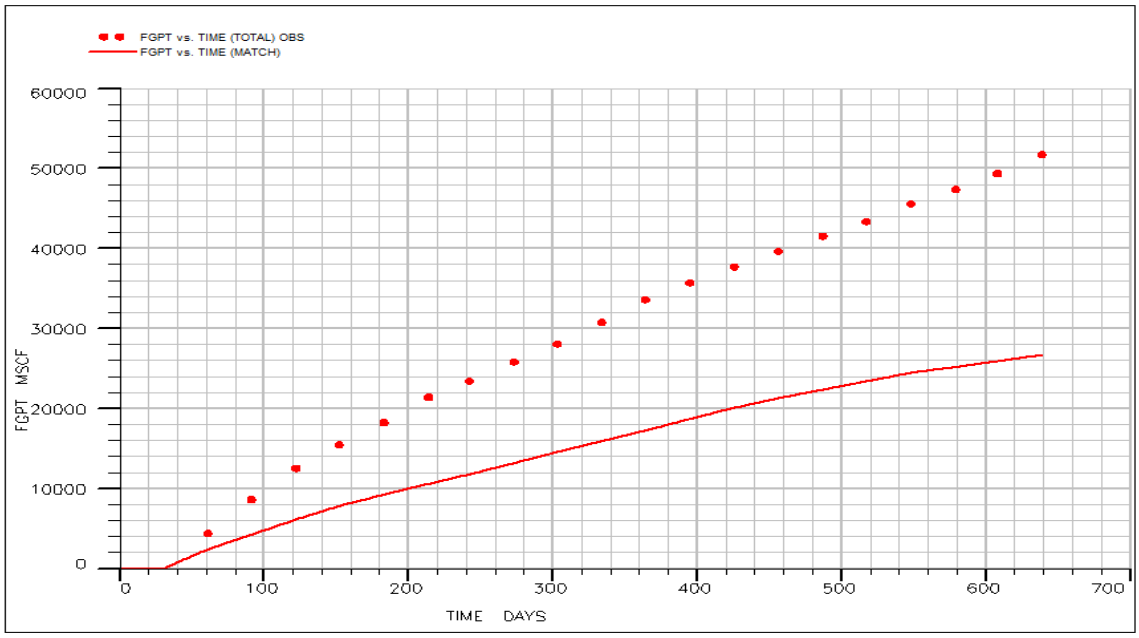

Fig. 57: Final History Match For Cumulative Gas Production

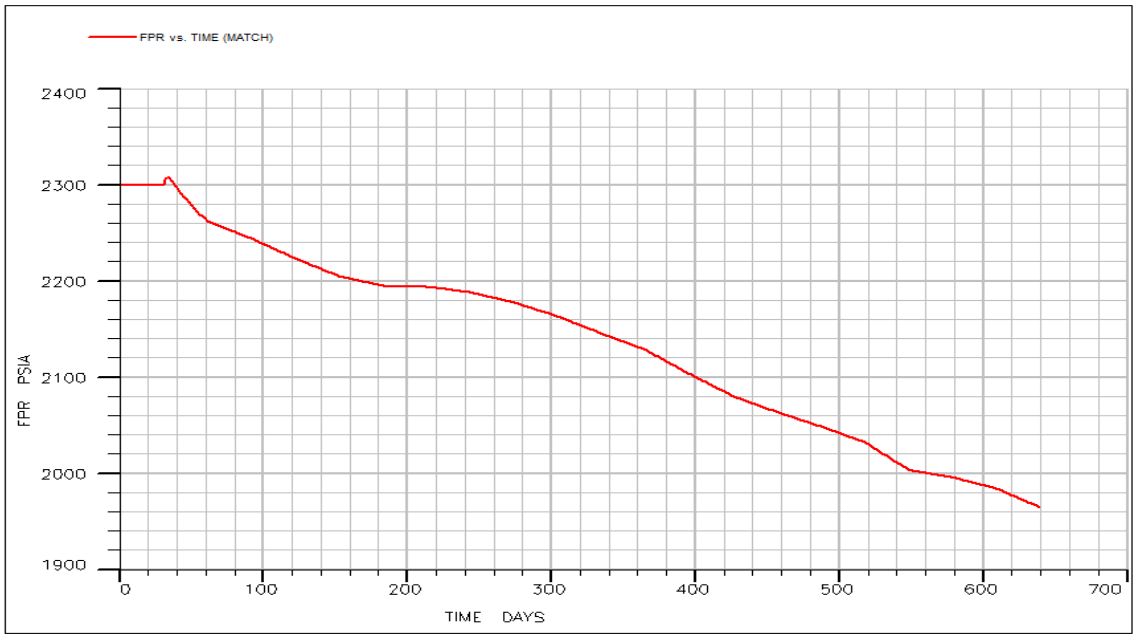

Fig. 58: Average Field Pressure For Final History Matched Model

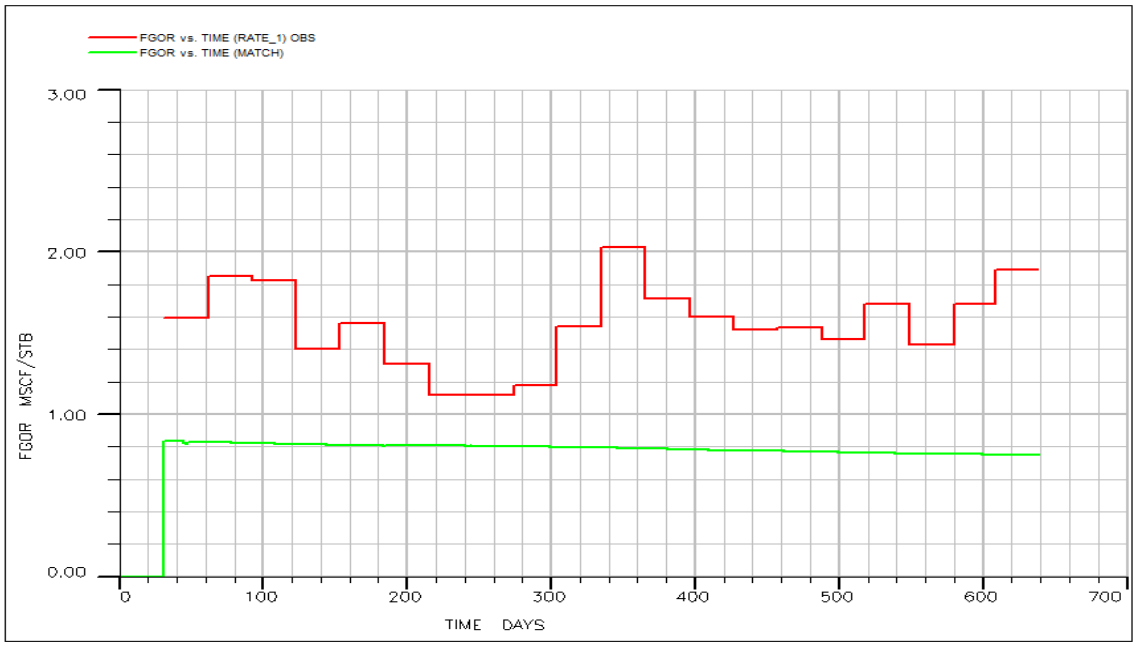

Fig. 59: Final History Match For Field Gas-Oil-Ratio

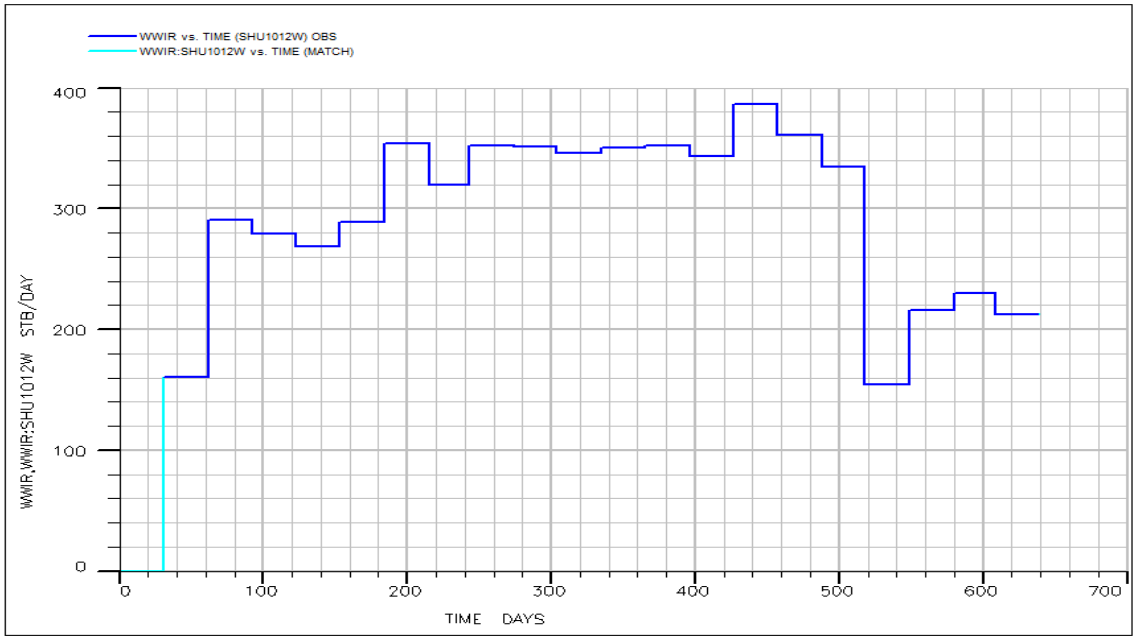

Fig. 60: Monthly Field Water Injection Rate

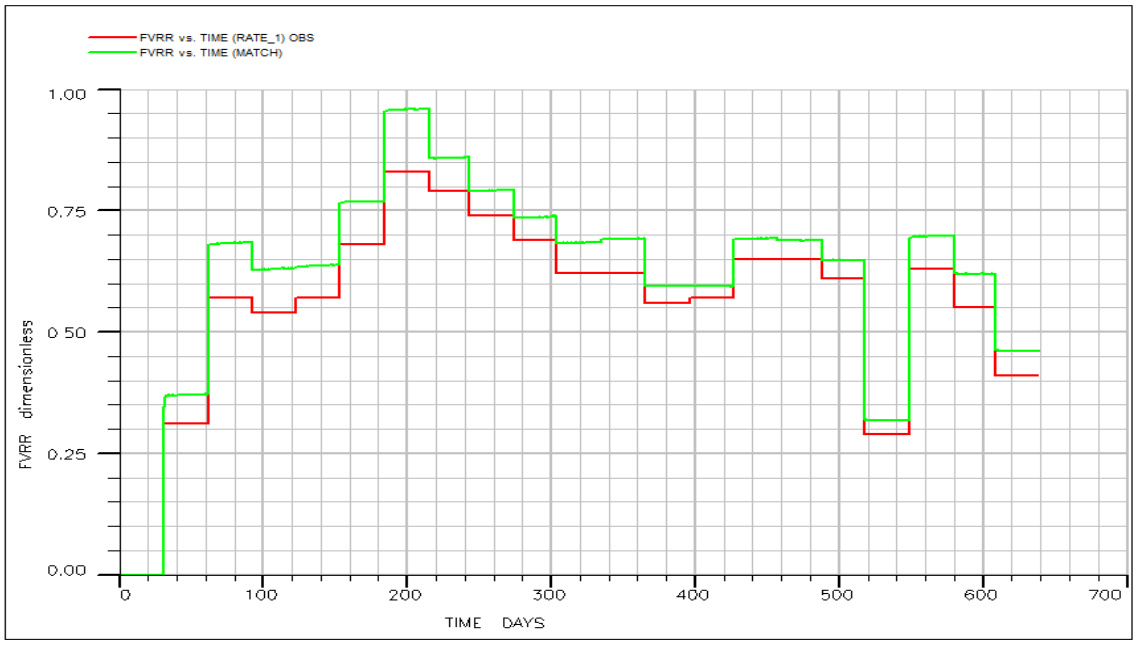

Fig. 61: Final History Match For Field Voidage Replacement Ratio

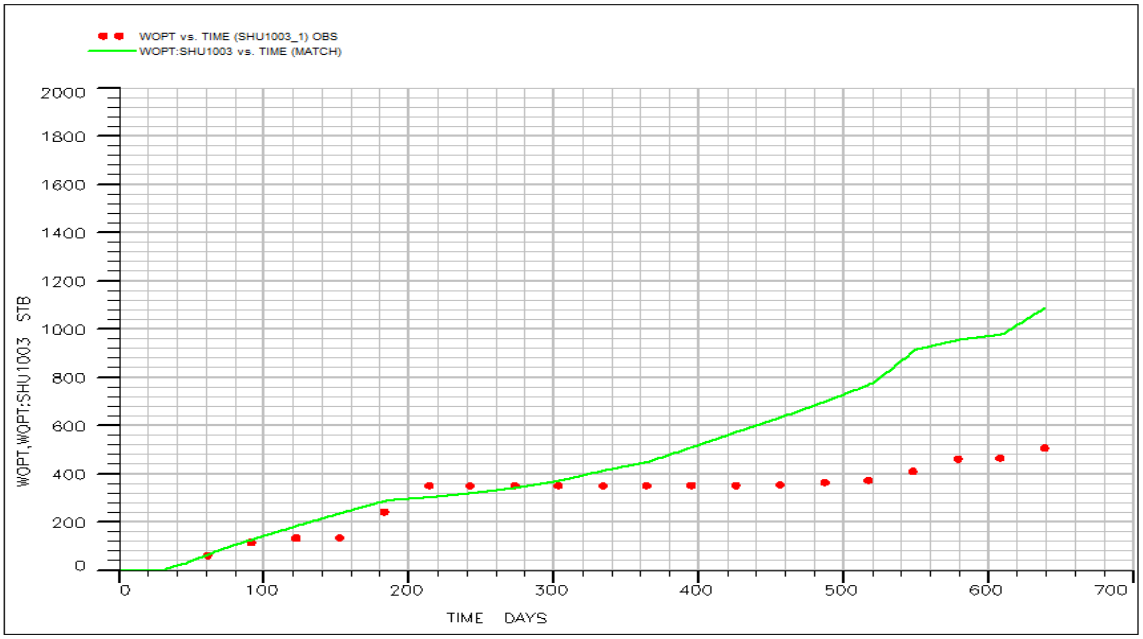

Fig. 62: Oil Production History Match For Sherrod 1003

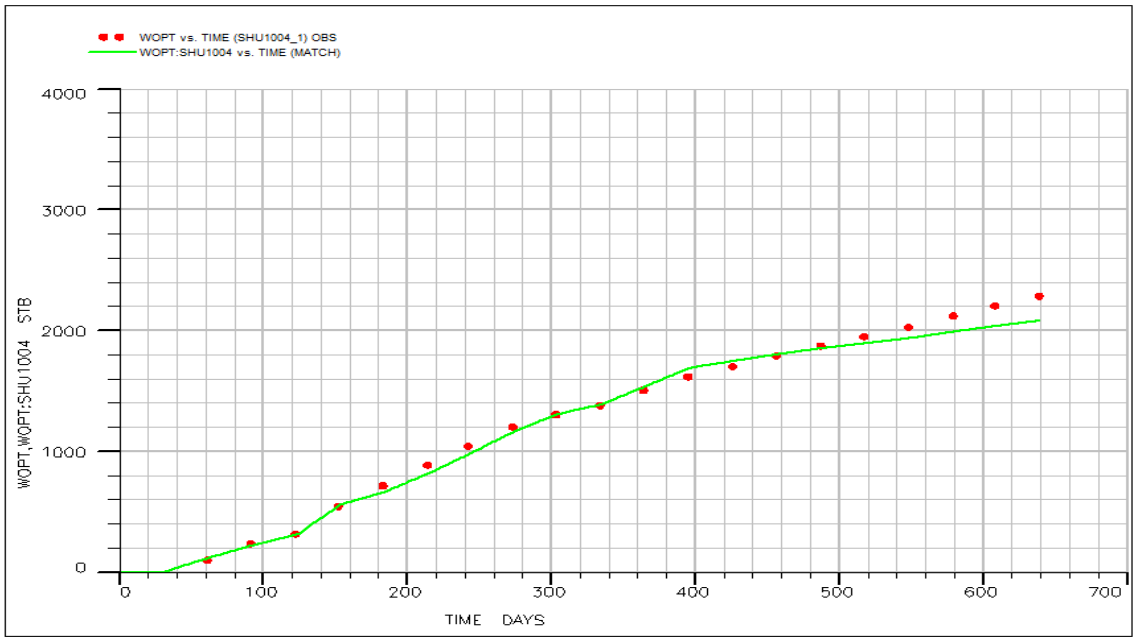

Fig. 63: Oil Production History Match For Sherrod 1004

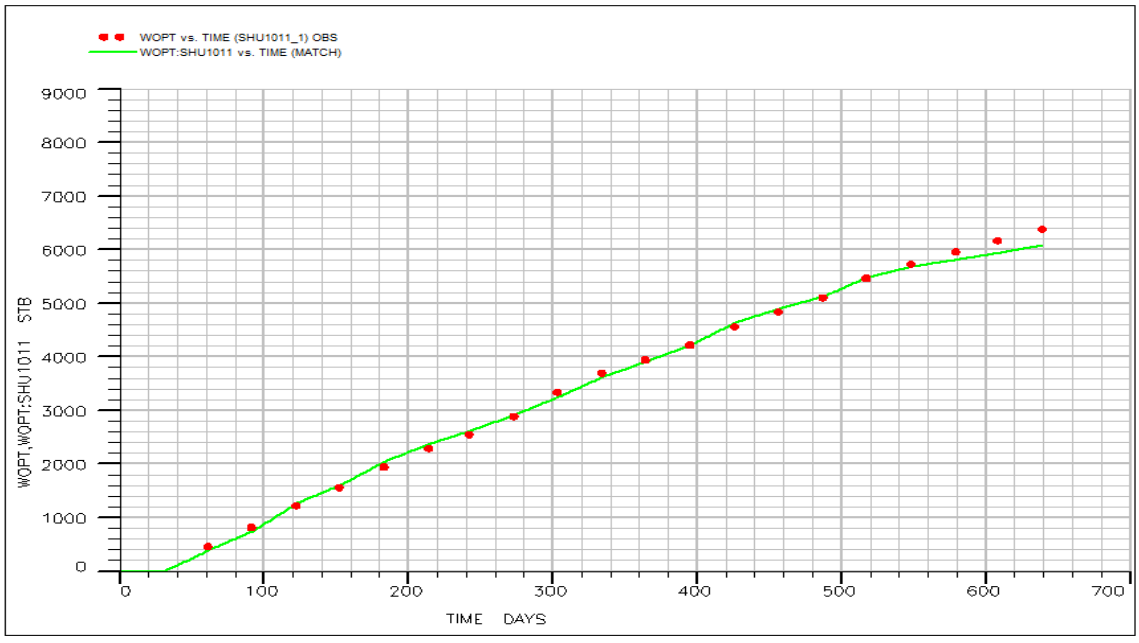

Fig. 64: Oil Production History Match For Sherrod 1011

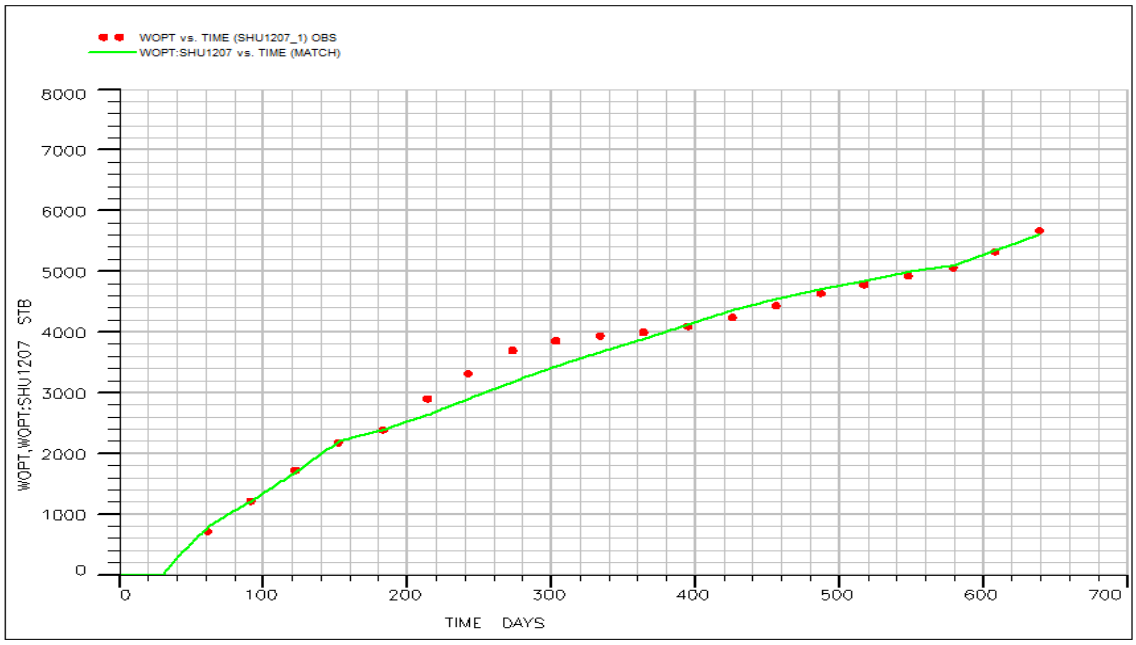

Fig. 65: Oil Production History Match For Sherrod 1207

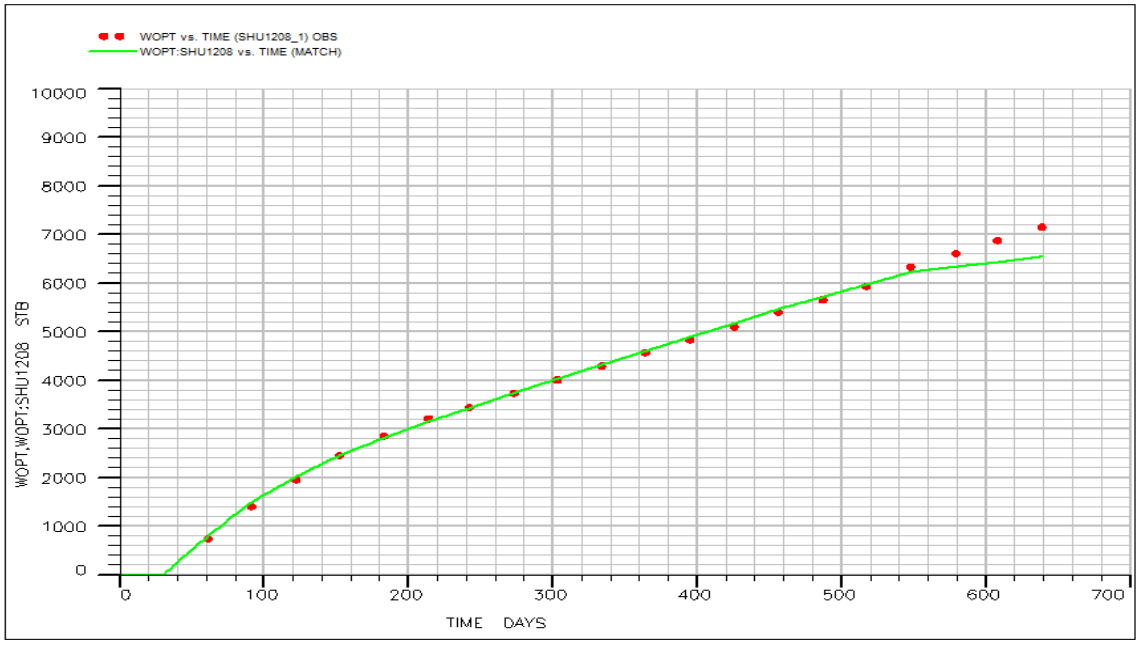

Fig. 66: Oil Production History Match For Sherrod 1208

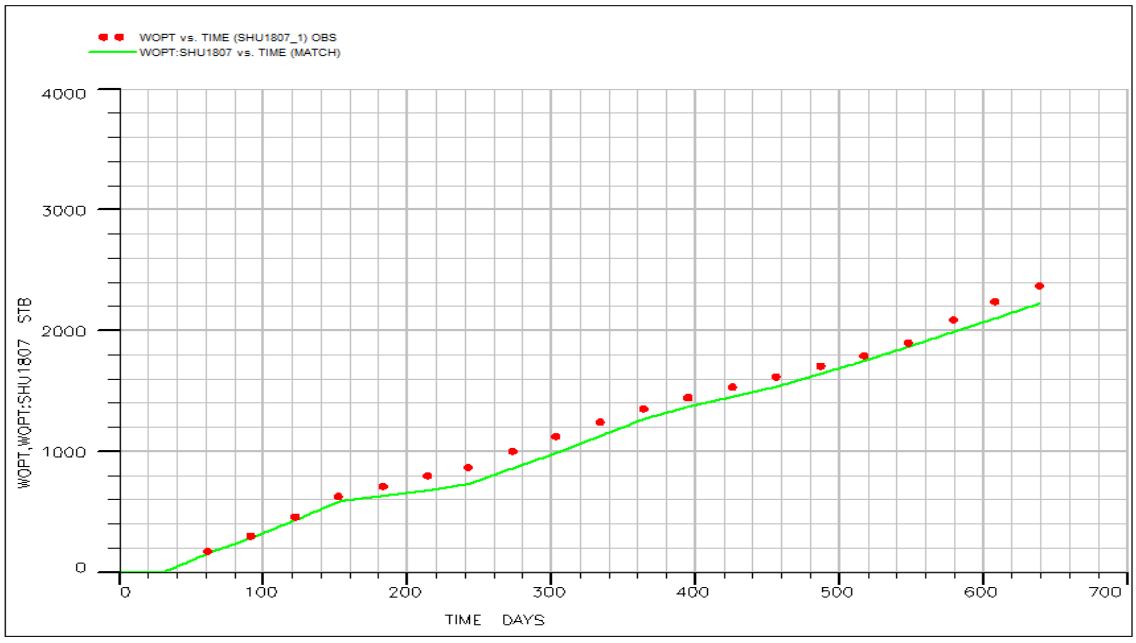

Fig. 67: Oil Production History Match For Sherrod 1807

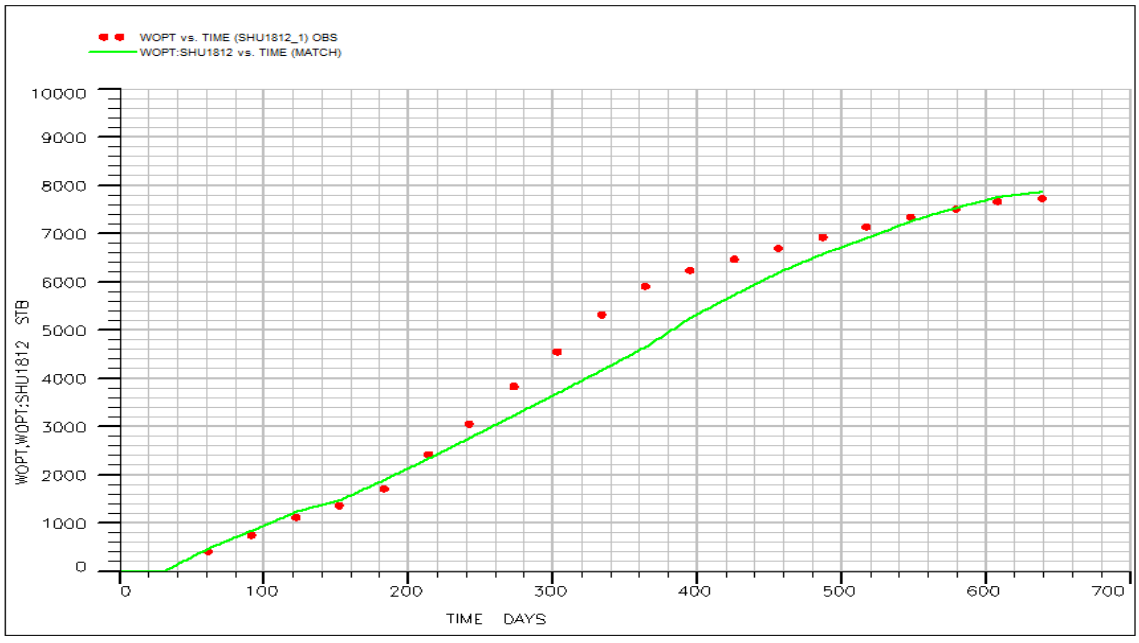

Fig. 68: Oil Production History Match For Sherrod 1812

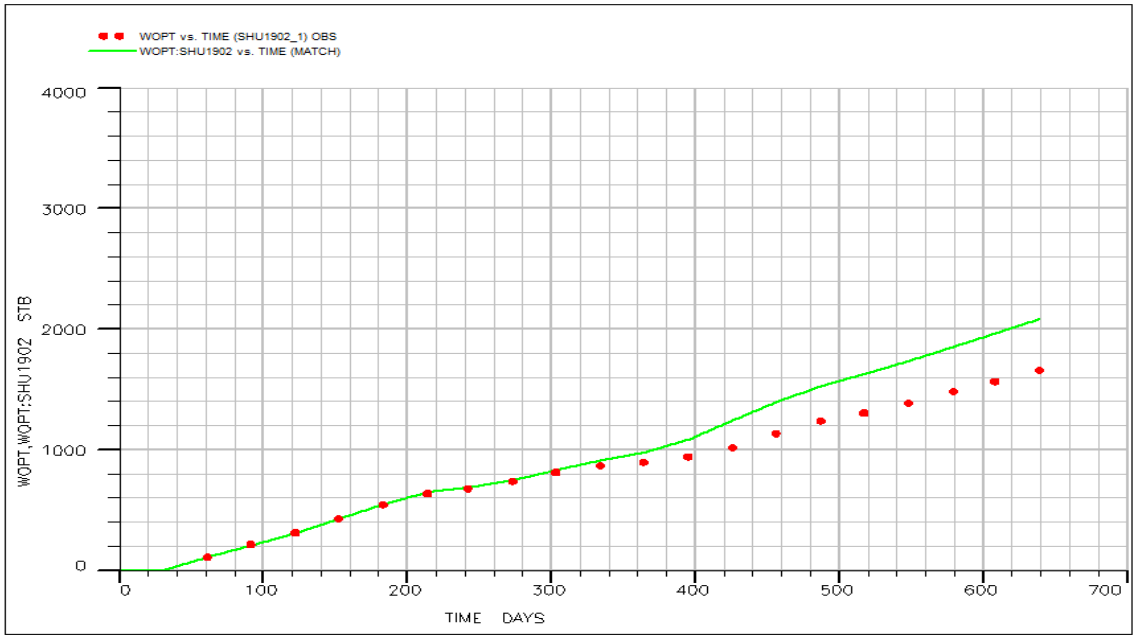

Fig. 69: Oil Production History Match For Sherrod 1902

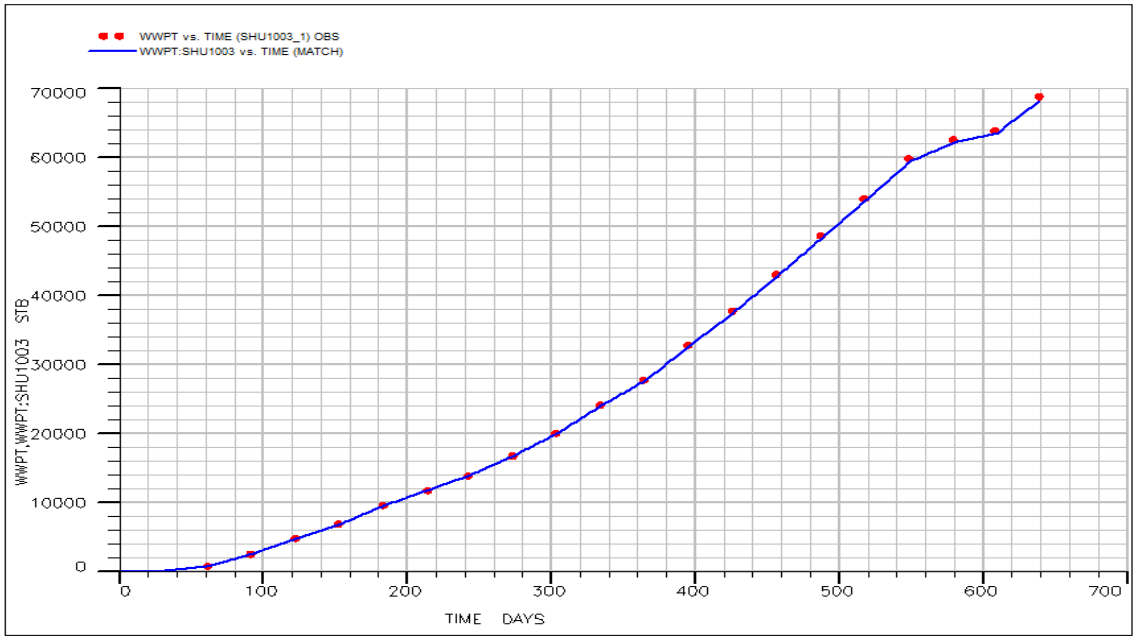

Fig. 70: Water Production History Match For Sherrod 1003

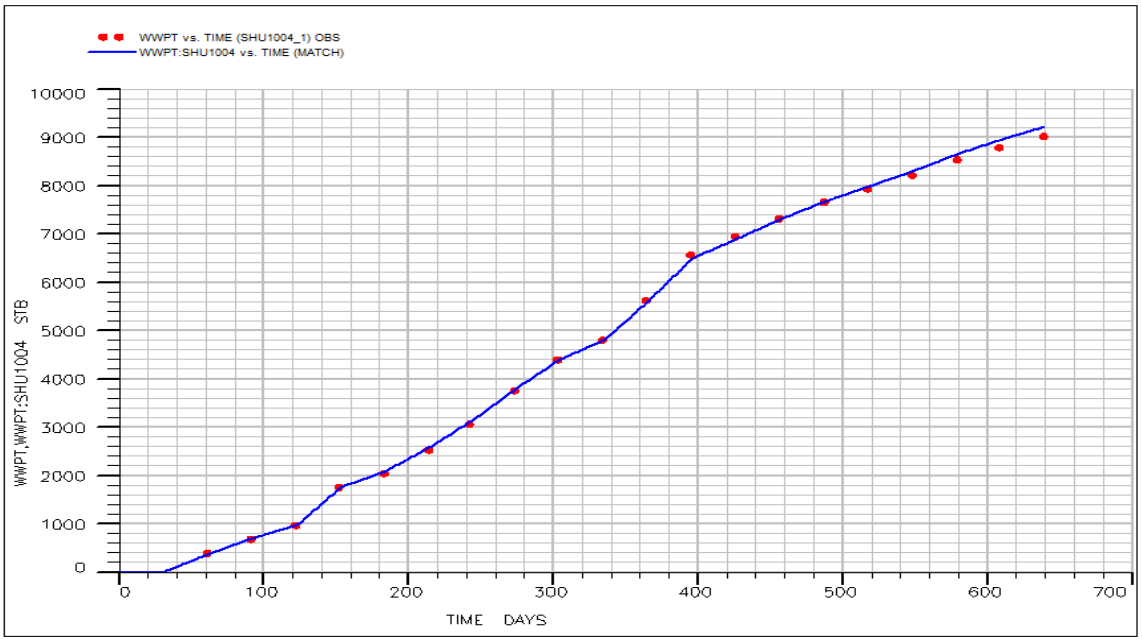

Fig. 71: Water Production History Match For Sherrod 1004

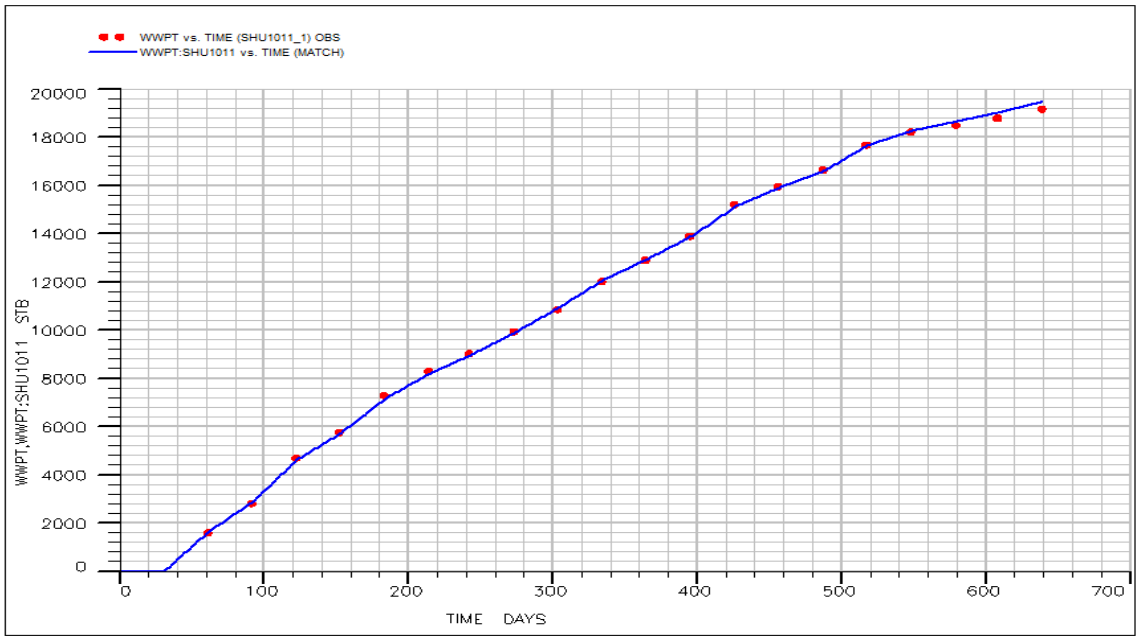

Fig. 72: Water Production History Match For Sherrod 1011

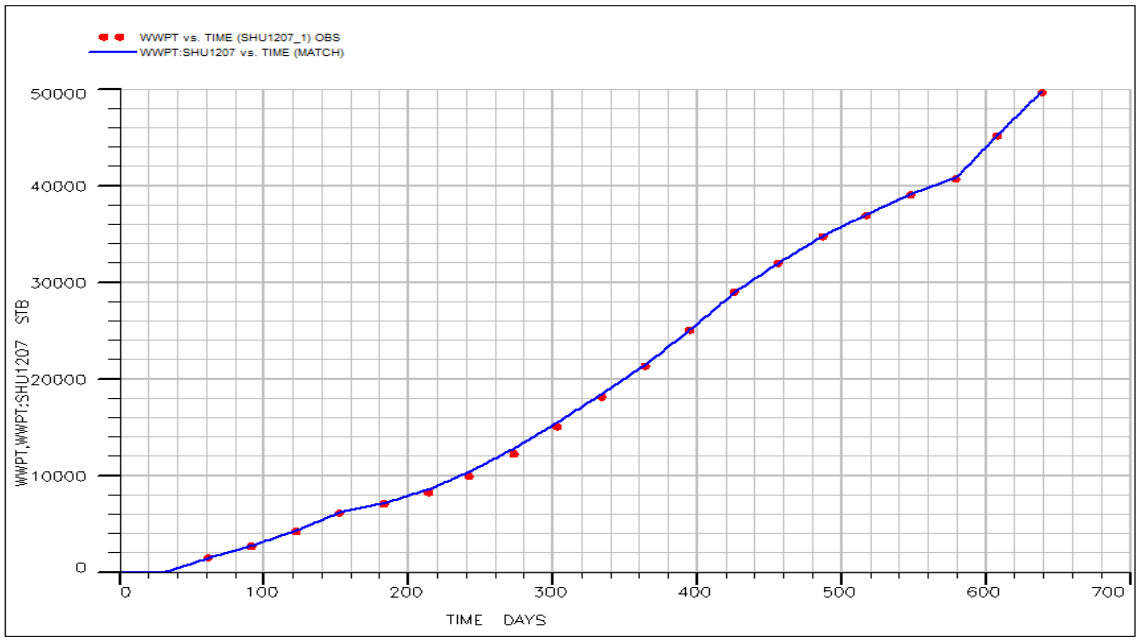

Fig. 73: Water Production History Match For Sherrod 1207

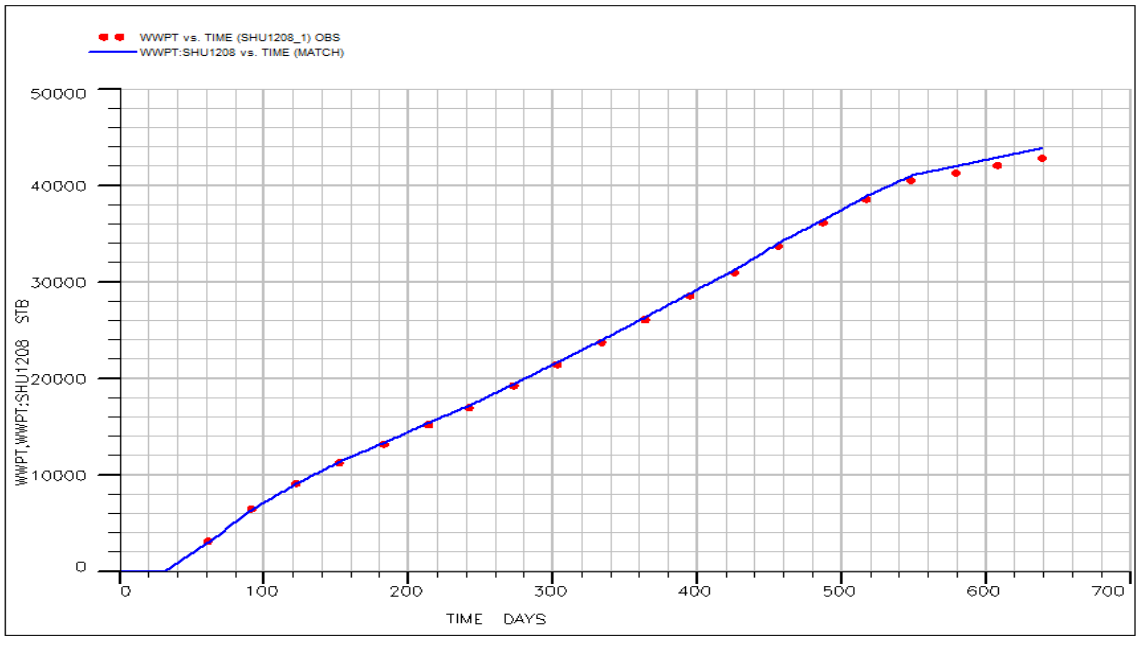

Fig. 74: Water Production History Match For Sherrod 1208

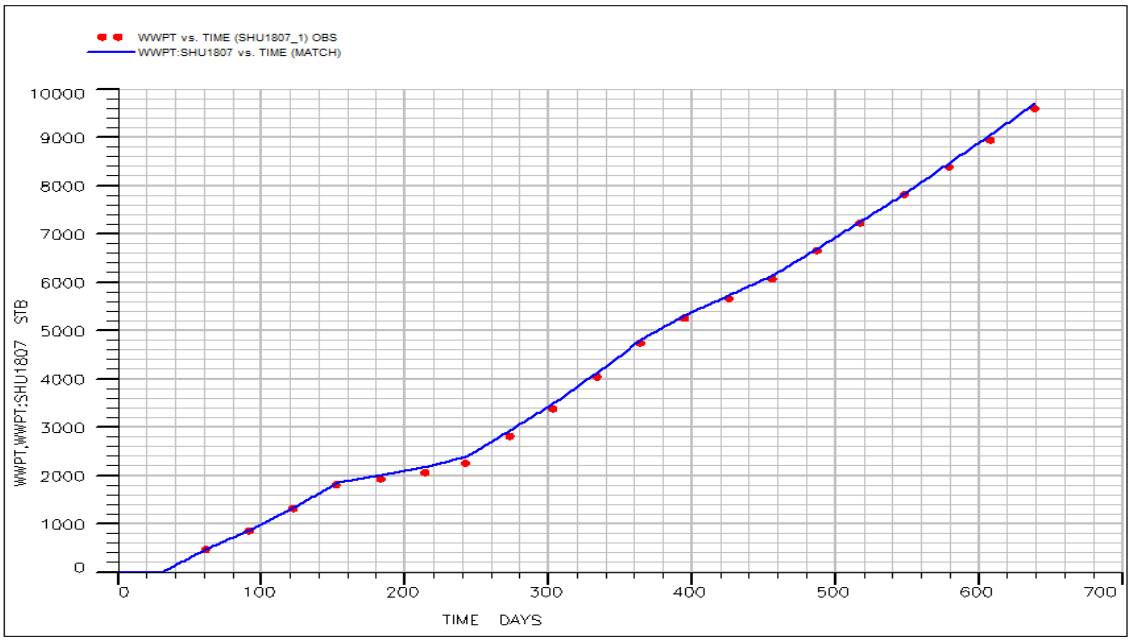

Fig. 75: Water Production History Match For Sherrod 1807

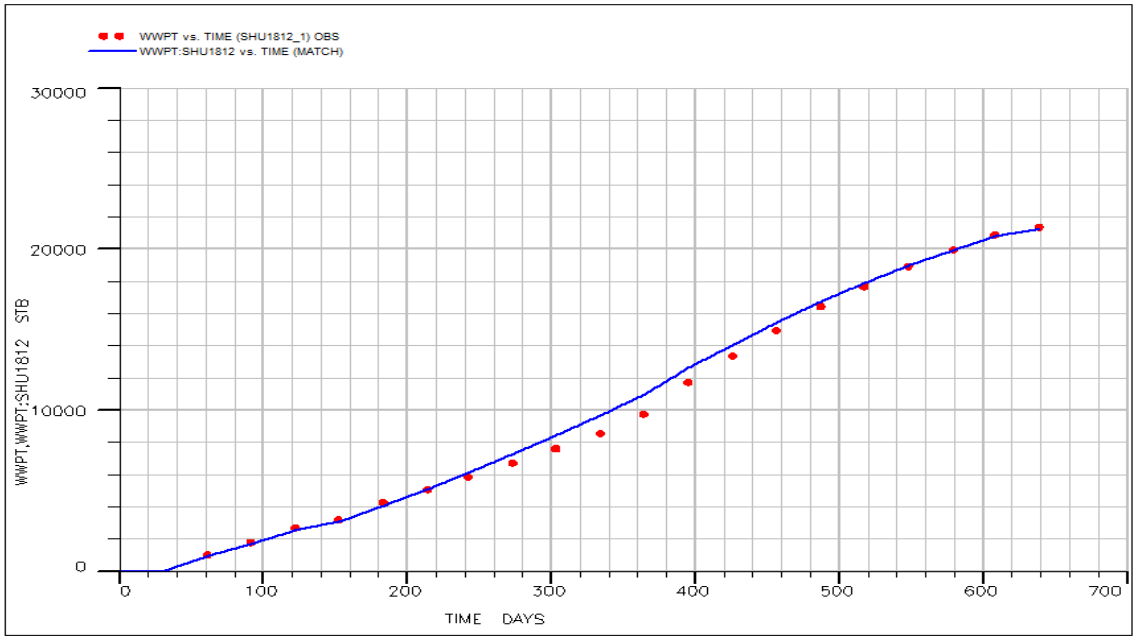

Fig. 76: Water Production History Match For Sherrod 1812

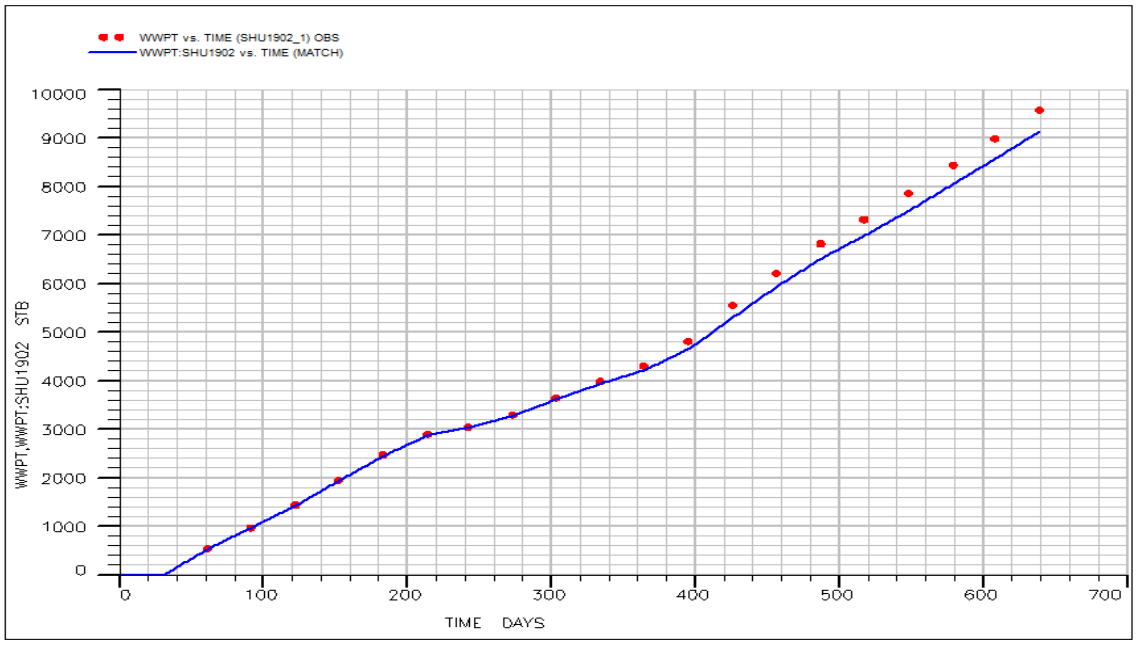

Fig. 77: Water Production History Match For Sherrod 1902

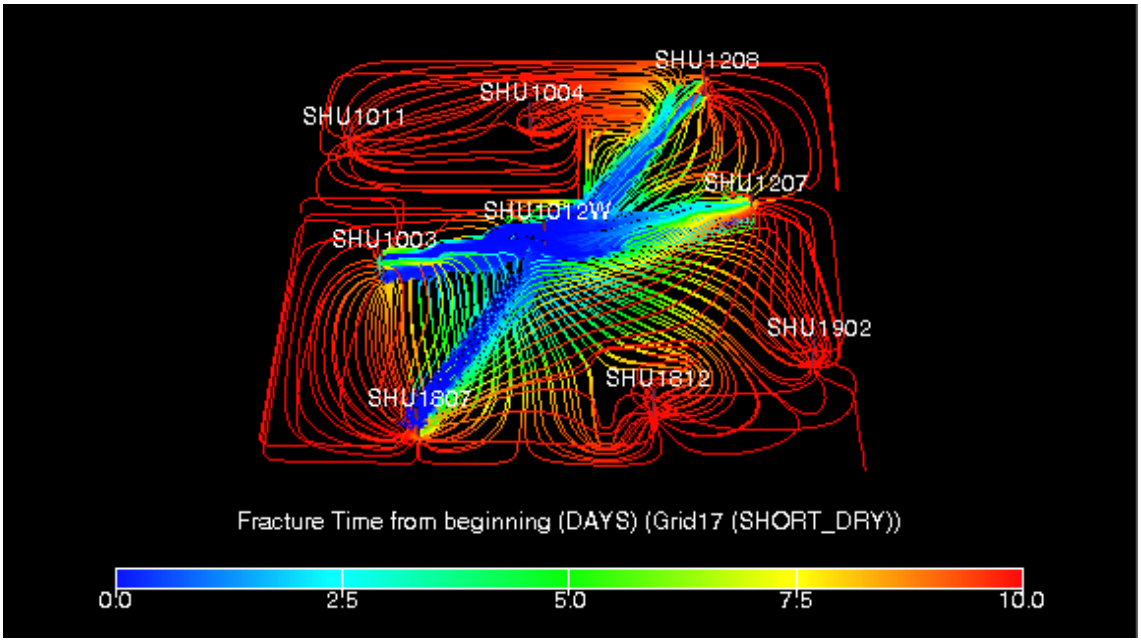

Fig. 78: Time-Of-Flight (TOF) At Tracer Injection

4.4. FrontSim and ECLIPSE Comparison

To compare the difference in solutions between finite-difference and streamline base flow simulation, the history-matched model was converted to the equivalent finite difference model. As seen in Fig. 79, where green represents the FrontSim solution and blue belongs to ECLIPSE, cumulative oil production calculated by the finite difference method is bigger. Correspondingly, less water production is observed in this particular model with the finite difference solution scheme, as shown by Fig. 80, in which the FrontSim solution is represented by light blue and dark blue corresponds to the ECLIPSE solution. The difference in phase production could be attributed to a fully implicit solution of the saturation equation in the finite difference method while it is solved explicitly in the streamline simulation. Also, three-phase formulation of streamline simulation may not be as good as finite difference in dual-porosity models because streamline simulation is generally powerful for an oil-water single-porosity model with a large number of grids. By being conscious of these small differences in calculation, streamline simulation was used in this study.

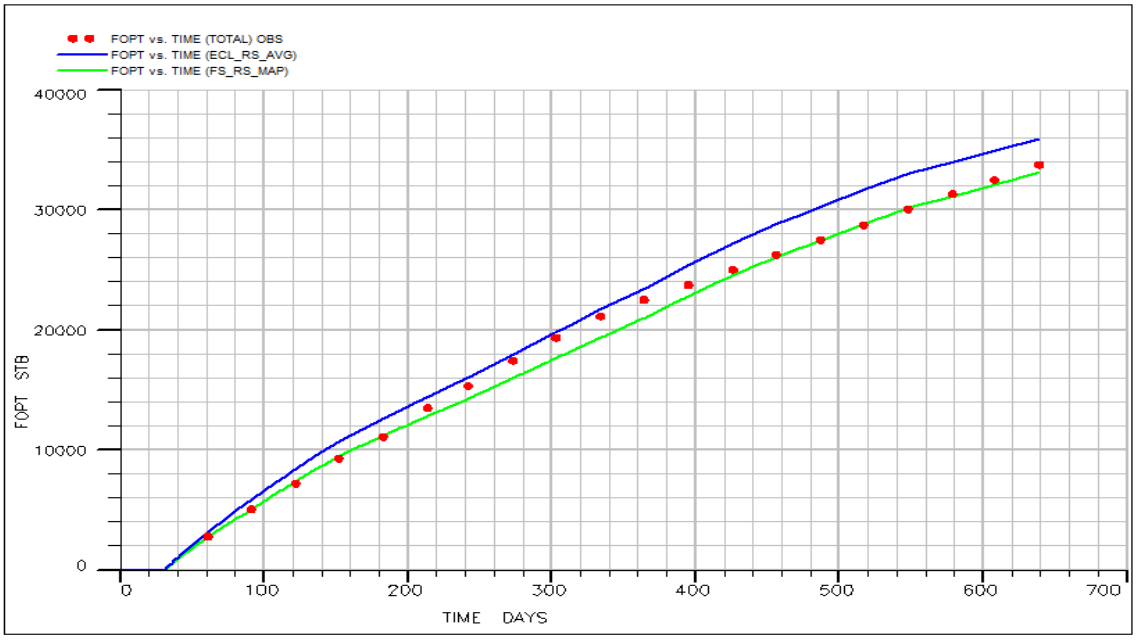

Fig. 79: Simulator Comparison For Cumulative Oil Production

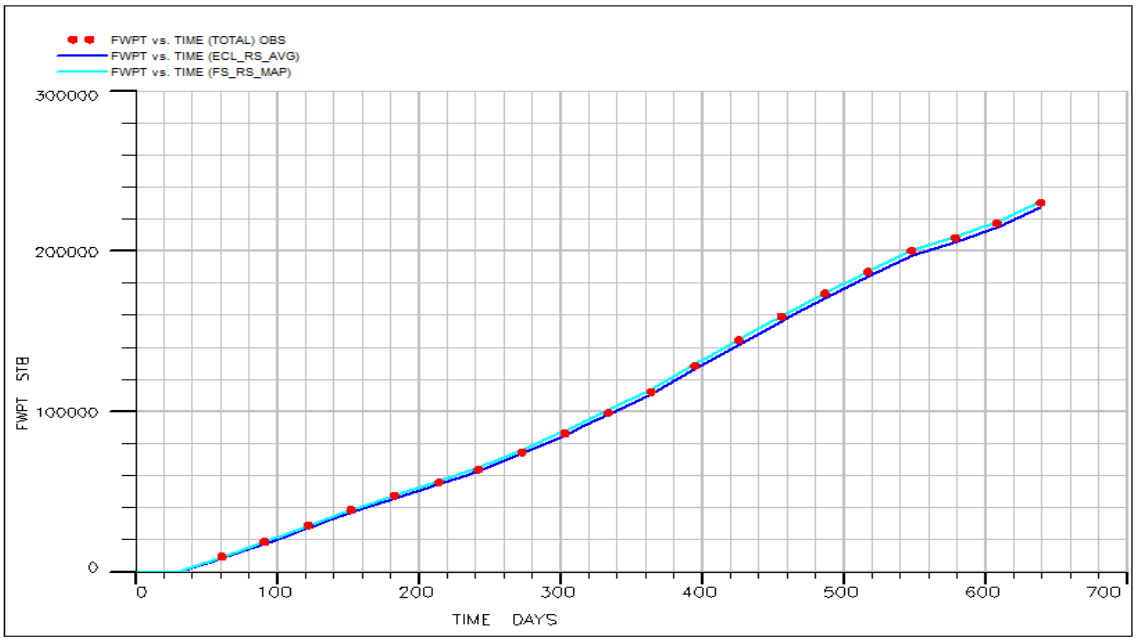

Fig. 80: Simulator Comparison For Cumulative Water Production

4.5. Summary of Dual-Porosity Streamline Simulation

A brief summary of observations from the dual-porosity streamline simulation study is listed:

1. The main controlling parameters for history matching were determined as initial water saturation, fracture porosity, and fracture permeability from initial sensitivity analysis.
2. The extremely high-water-saturation example proves that actual matrix-fracture interaction in the field is much lower than calculated sigma based on fracture spacing. Fracture mineralization seems to be the main reason for limited counter-current flow between the matrix and fracture in spite of a closely spaced fracture system.
3. According to the base model properties, water saturation in the matrix is higher than expected. This could be due to either initial fluid distribution settled during pre- or post-deposition of the reservoir or an external water source flowing to the field where the matrix had been watered before any field production started. To a certain extent, both are believed to be valid.
4. Matrix contribution is still significant in spite of a low sigma value. The overestimation in oil production is believed to be due to the use of higher than actual matrix capillary pressures.
5. Flow domination in field production and high tracer responses strongly agree on the presence of highly conductive fracture systems in the E-W

and NE-SW directions. However, a very poor fracture system was observed in N-S direction, while almost no fracture system exists in the NW-SE direction according to tracer recovery.

6. Rather than the oriented fracture system, the dipping of the reservoir and pressure difference could be the reason for flow tendency, which was proved by both higher liquid production and more tracer recovery toward the W and N-E directions.
7. High tracer response does not necessarily mean more allocated water, as in the case of Sherrod 1807.
8. In off-trend wells, the production capacity of newly drilled wells is larger than old wells because of an unswept drainage area.
9. The history-matched model successfully regenerated historical production performance for oil and water at both the field and well scale.
10. A deficiency of gas production resulted in a low GOR and high voidage replacement ratio. However, the trend and magnitude of the latter is quite similar to observed data. Thus, errors due to lower gas production could be evaluated as uncertainty.
11. TOF visualizes tracer breakthrough time match, except for Sherrod 1807; however, its production performance was perfectly matched.
12. Certain differences exist between finite-difference and streamline base simulation in calculating individual phase production for this particular dual-porosity model.

CHAPTER V

IMPROVED WATERFLOOD MANAGEMENT

Not only the reservoir itself but also nearby wellbore effects, creates heterogeneity in fluid flow, which designates the success of the displacement process. Understanding the displacement process in a broader sense requires accurate quantification of the relationship between the injector and producer. Unlike finite difference simulators, a unique feature of streamline simulation allows determining this relationship. In the literature, optimization of waterflooding with the aid of streamline simulation has been applied by many authors (Ghori et al., 2007; Grinestaff, 1999; Grinestaff and Caffrey, 2000) for some of the largest fields in the world.

The PFM suite of FrontSim provides an automated way of optimizing streamline waterflood simulations. In order to improve waterflood performance, PFM determines the amount of water to allocate to injectors by using streamline simulation properties from the history-matched model. Based on that model, it recommends injection and production rates well by well under field operation limitations in such a way that oil production is enhanced while delaying water breakthrough and reducing water production, increasing ultimate recovery. Fields with a large number of wells and high-resolution reservoir models are the best candidates for FrontSim PFM usage.

5.1. Optimization Theory

In general, the ultimate goal for optimizing field performance via simulation is minimizing the defined objective function. However, the current approach doesn't consider whether it is an optimal solution or not, and it only adjusts well rates in order to increase oil production or reduce water cycling. The basic idea is so simple that more water is allocated to efficient producers while the amount of injected water received by poor producers is reduced. The described optimization workflow below is a brief summary of the paper written by Thiele and Batycky (2006). Further description on both optimization workflow and equations can be found in SPE 84080.

The initial step is calculating average injection efficiency for the field or pattern according to Eq. 5.1. As seen, injection efficiency is a dynamic parameter that changes during the time of simulation or the field life. Similarly, it also has a different value for each well pair at each time step. Because streamline simulation calculates individual phase rates from the solution of the 1D transport equation for each time step, the dynamic well allocation factor or dynamic injection efficiency is already provided.

$$IE = e = \frac{Offset\ Oil\ Production}{Water\ Injection}$$

Eq. 5.1

After obtaining injection efficiency for the field average and for individual well pairs from the well allocation factor, which is a distinguishing feature of streamline

simulation compared with finite difference, injection efficiencies are ranked according to average field efficiency, which is a reference point to classify producers. When classification is finished, a new target rate for each well is assigned based on Eq. 5.2. The sign of the weight depends on well classification. If a well has an injection efficiency less than average, it is evaluated as a poor producer and the production rate is reduced. In other words, *w* is smaller than zero. Similarly, if the well has a higher injection efficiency, *w* becomes positive and the production rate target will increase. The critical point in this optimization routine is keeping the difference between cumulative rate increase and cumulative rate decrease as close as to zero as possible to honor the underlying assumption. The proposed functional form for weight is shown by Eq. 5.3. It defines the shape of the weighting function for different alpha exponents between minimum and maximum weight limit. Basically, it accelerates or slows down the difference between calculated new rate and old rate. Fig. 81 clearly explains weight function and its shape for the corresponding alpha (α) exponent.

$$q_{new} = (1 + w) * q_{old}$$

Eq. 5.2

$$e_i > \bar{e}: \; w_i = min\left[w_{max}, w_{max}\left(\frac{e_i - \bar{e}}{e_{max} - \bar{e}}\right)^{\alpha}\right]$$

$$e_i < \bar{e}: \; w_i = max\left[w_{min}, w_{min}\left(\frac{\bar{e} - e_i}{\bar{e} - e_{max}}\right)^{\alpha}\right]$$

Eq. 5.3

, where e_i = injection efficiency for well; $\bar{e}$ = average field injection efficiency; w_i = increase/decrease in weight; w_{max} = maximum weight at e_{max}; w_{min} = minimum weight at e_{min}; e_{max} = upper injection efficiency limit; e_{min} = lower injection efficiency limit; and α = exponent.

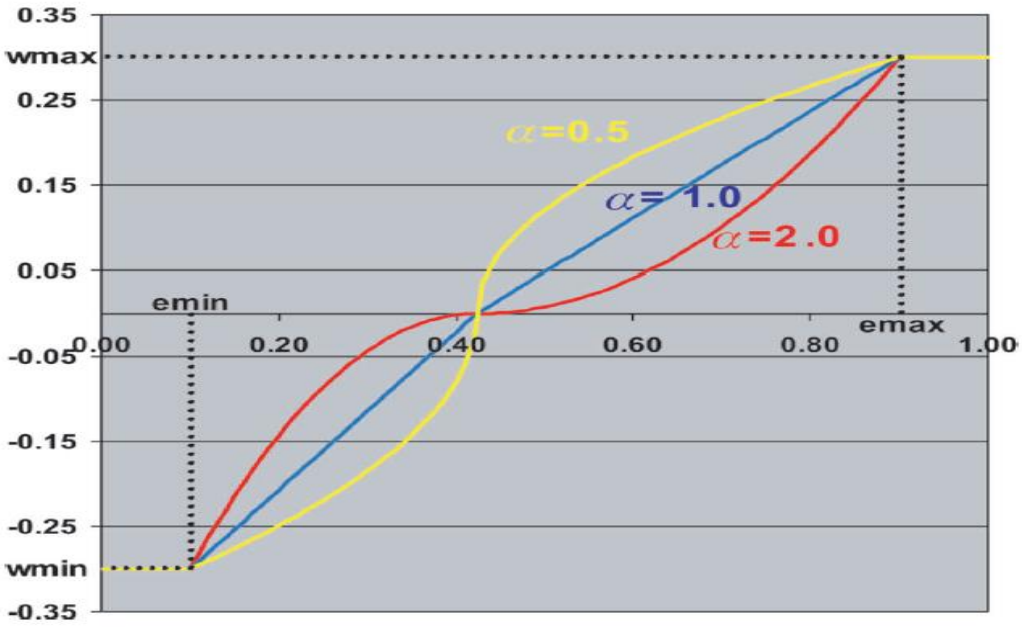

Fig. 81: Weight Functions For Varying (α) Exponent, Thiele and Batycky (2006)

Once a new target rate for wells is determined, a simulation model is run for the prediction period. At the end of that period, a new well allocation factor for wells is generated by streamline simulation. All calculations mentioned above are repeated for the next prediction period, and this routine will continue until the end of the required prediction period. Another important point is the length of the prediction period because

the accuracy of calculated phase rates from streamlines depends on the frequency of the solution update. Therefore, each prediction period shouldn't be so long as to lose confidence in the solution.

5.2. Application of Pattern Flood Management

The PFM suite of FrontSim works under the same optimization logic mentioned in the previous section. However, it has three different strategies to be followed in terms of optimization. The first one is called Pattern Voidage Replacement (VREP), which adjusts the injection rate for the injector to achieve the requested voidage replacement ratio for the regions where voidage is occurring. The second strategy, Pattern Recovery Balancing (RECOV), calculates the remaining mobile oil in each bundle of streamlines between producer and injector and injects more water to well pairs with higher remaining mobile oil. Unlike the second strategy, Reducing Water Recycling (INJEFF) computes oil cut for each bundle instead of remaining mobile oil and allocates more water to well pairs with higher oil cut (FrontSim Technical Description, Version 2013.1).

RECOV and INJEFF were applied to the history-matched model obtained in Chapter IV as optimization strategies. To sustain optimization accuracy, the prediction period was kept at 1 year because the quality of the history-matched model is crucial to confidently apply optimization. Therefore, the 1-year prediction period is reasonable for this short-term history matching. However, overestimation and underestimation of well

allocation factors used during optimization were eliminated by monthly updates for solutions. Well rates were altered depending on optimization strategy and were kept constant for the "Do Nothing" scenario from the end of history matching until the end of the prediction period. The keyword WECON was used for the economic limit, which is 1 bbl/day in order to prevent negative interference of low-rate producers to optimization.

According to Fig. 82, cumulative oil production was enhanced by almost 8,000 bbl for optimized cases, while 10,000 bbl less water was produced, as shown by Fig. 83. Therefore, the optimization logic efficiently allocated available water to increase oil production and reduce water production. Fig. 84 to Fig. 91 show well-by-well cumulative oil production for optimized and non-optimized strategies. Green represents oil production for the "Do Nothing" scenario while blue illustrates optimized oil production. Before the prediction period end, optimization suggests shutting-in or reducing the production rate of Sherrod 1003, Sherrod 1004, Sherrod 1207, and Sherrod 1208. The queue of shutting time is based on the economic limit specified by the WECON keyword, and shutting time for wells is different from each other. As can be seen from Fig. 84 and Fig. 85, Sherrod 1003 was shut-in just at the start of optimization and then Sherrod 1207 was shut-in after 1 month. Similarly, Sherrod 1004 couldn't meet the economic limit and was shut-in after three months. However, Sherrod 1208 stayed active almost 9 months after optimization started. On the other hand, a change in water allocation led to more oil production for Sherrod 1011, Sherrod 1807, Sherrod 1812, and Sherrod 1902.

Because our history-matched model was created based on production and tracer data, shutting-in those wells is consistent with tracer response in terms of injection efficiency, except Sherrod 1004. In other words, high tracer recovery shows that most of the injected water directly flows to these wells without observing a significant increase in oil production. Also, the reason for shutting-in Sherrod 1004 could be explained by low production performance and moderately high water production, confirmed with tracer recovery compared with other poorly performing producers due to injector. Unlike these low-recovery wells, more water allocation to Sherrod 1011, Sherrod 1807, Sherrod 1812, and Sherrod 1902 enhanced oil production, as illustrated in Fig. 88 to Fig. 91. This allocation strategy is reasonable and consistent with tracer response in terms of injecting more water toward unswept regions. In this regard, the only exception is Sherrod 1807, which showed high tracer response. However, the amount of received water from the injector is very low for Sherrod 1807, as mentioned earlier.

To sum up, PFM classified Sherrod 1003, Sherrod 1004, Sherrod 1207, and Sherrod 1208 as low-efficiency wells and Sherrod 1011, Sherrod 1807, Sherrod 1812, and Sherrod 1902 as high-efficiency wells. Better allocation of injected water by PFM resulted in 8,000 bbl of oil production enhancement and a reduction of 10,000 bbl of recycled water.

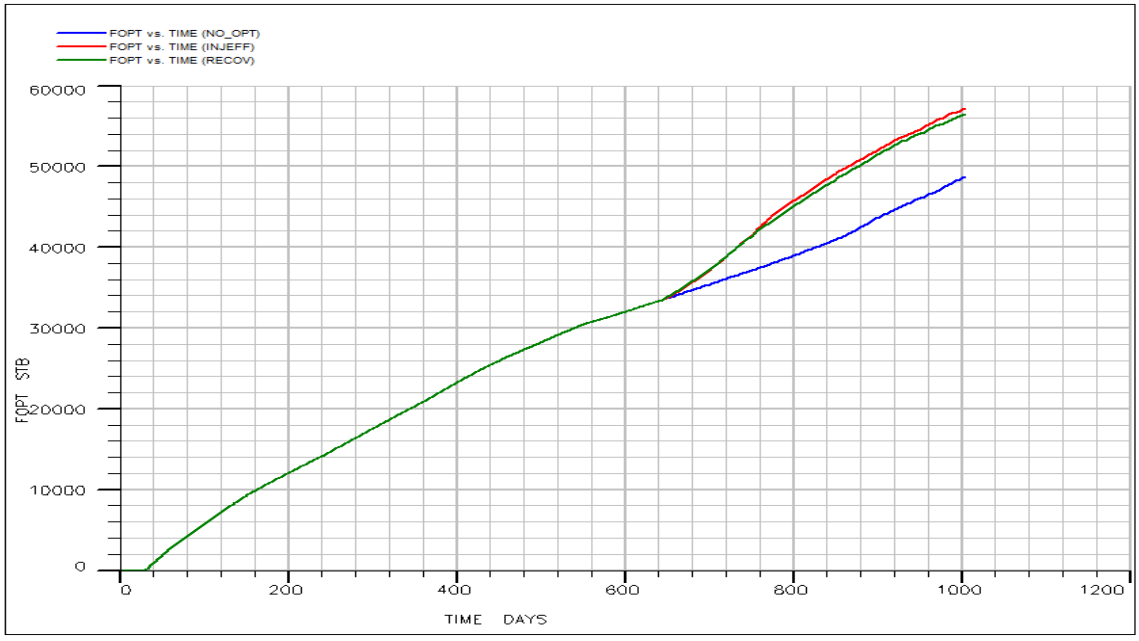

Fig. 82: Cumulative Oil Production For 1-Year Optimization

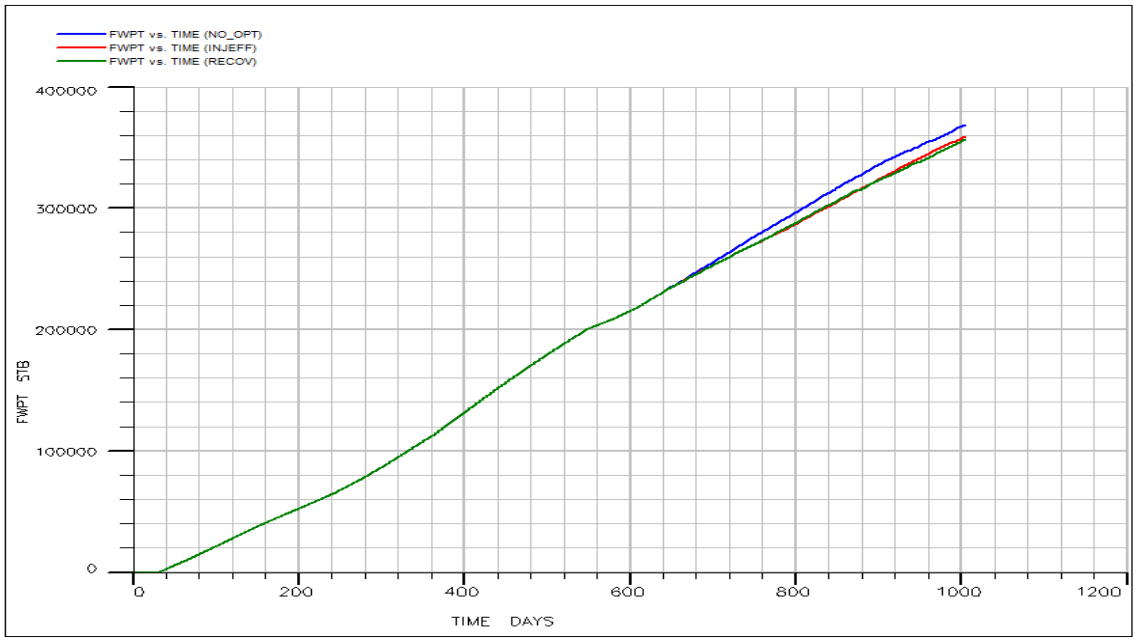

Fig. 83: Cumulative Water Production For 1-Year Optimization

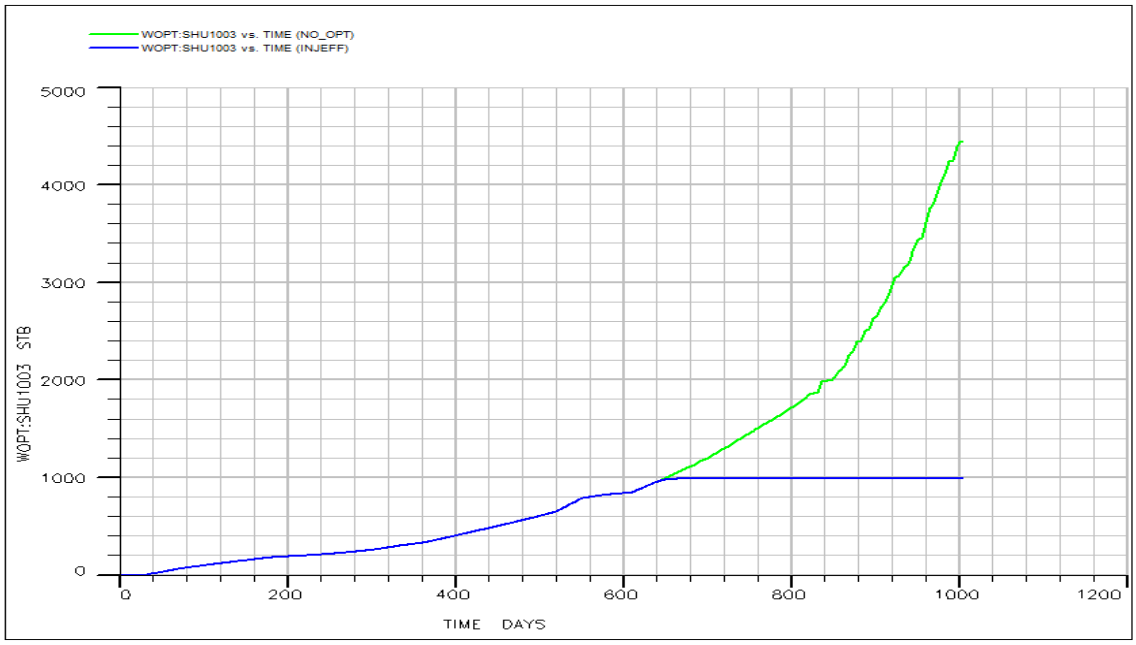

Fig. 84: Cumulative Oil Production For Sherrod 1003, "INJEFF" vs. "Do Nothing"

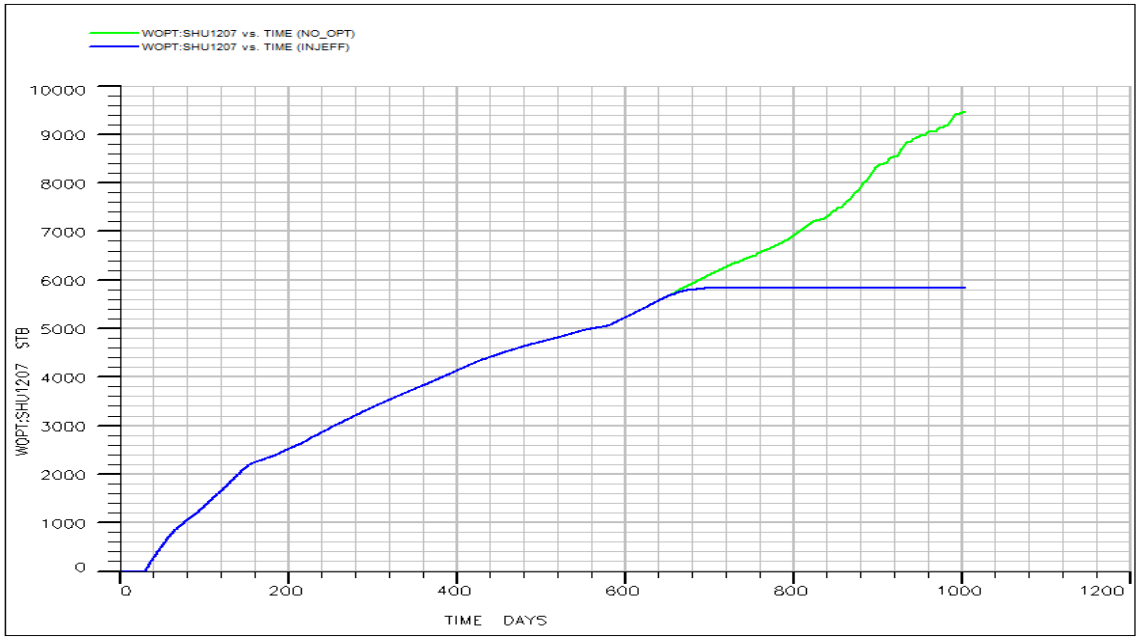

Fig. 85: Cumulative Oil Production For Sherrod 1207, "INJEFF" vs. "Do Nothing"

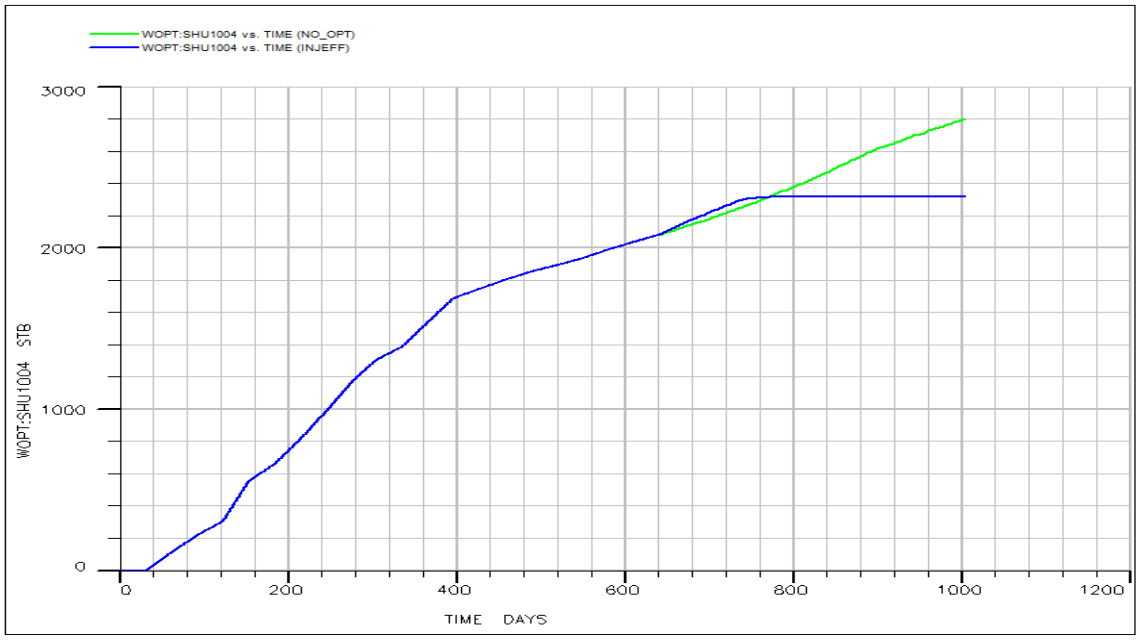

Fig. 86: Cumulative Oil Production For Sherrod 1004, "INJEFF" vs. "Do Nothing"

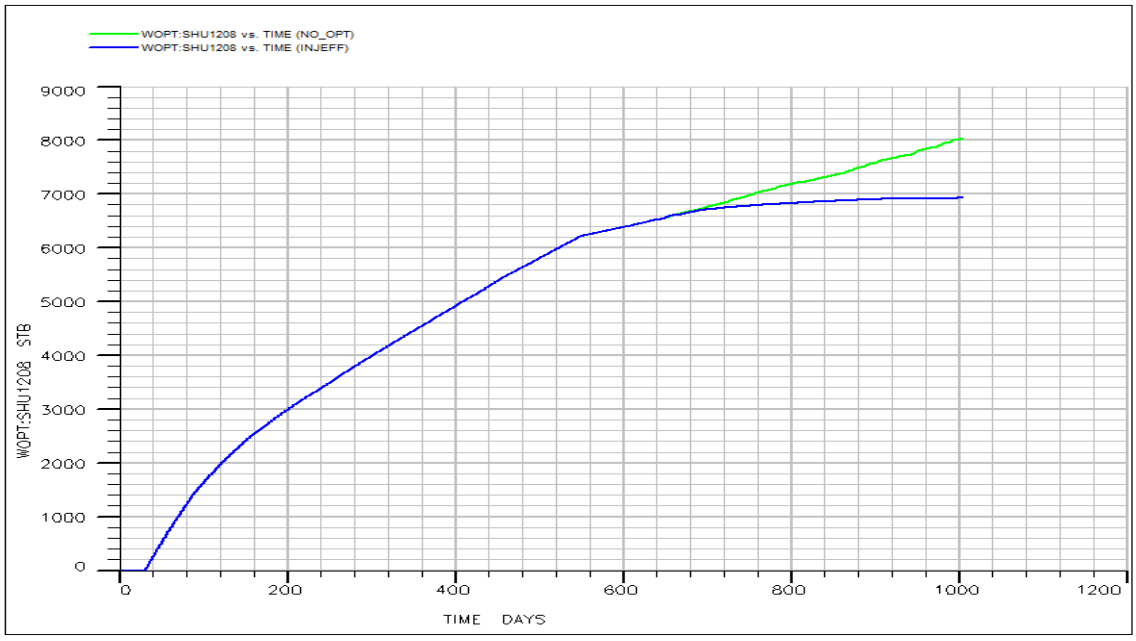

Fig. 87: Cumulative Oil Production For Sherrod 1208, "INJEFF" vs. "Do Nothing"

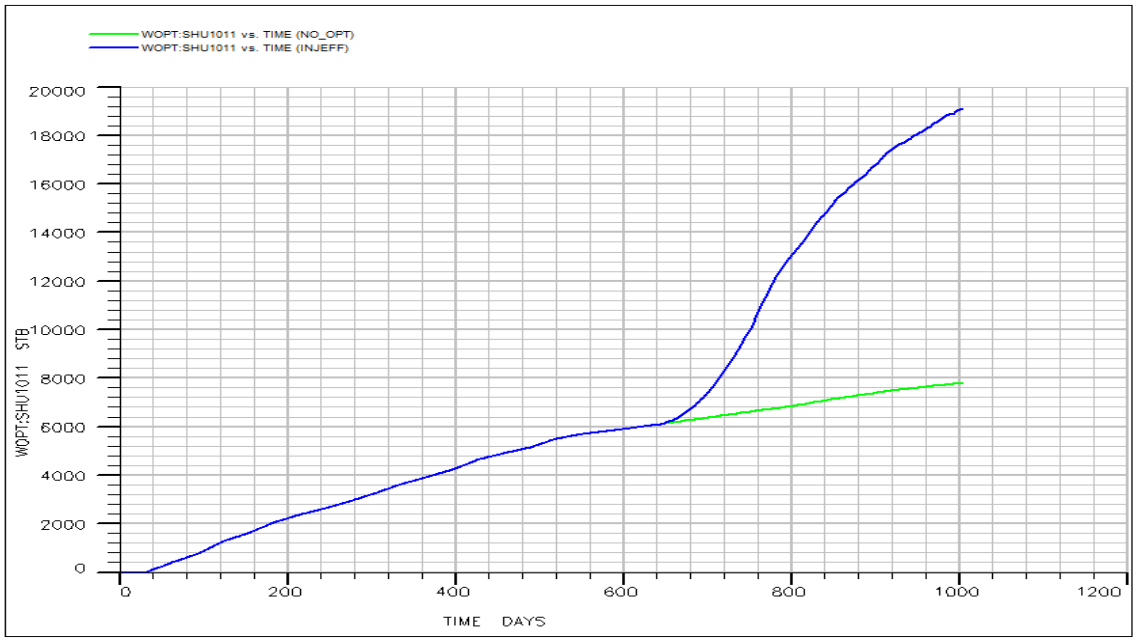

Fig. 88: Cumulative Oil Production For Sherrod 1011, "INJEFF" vs. "Do Nothing"

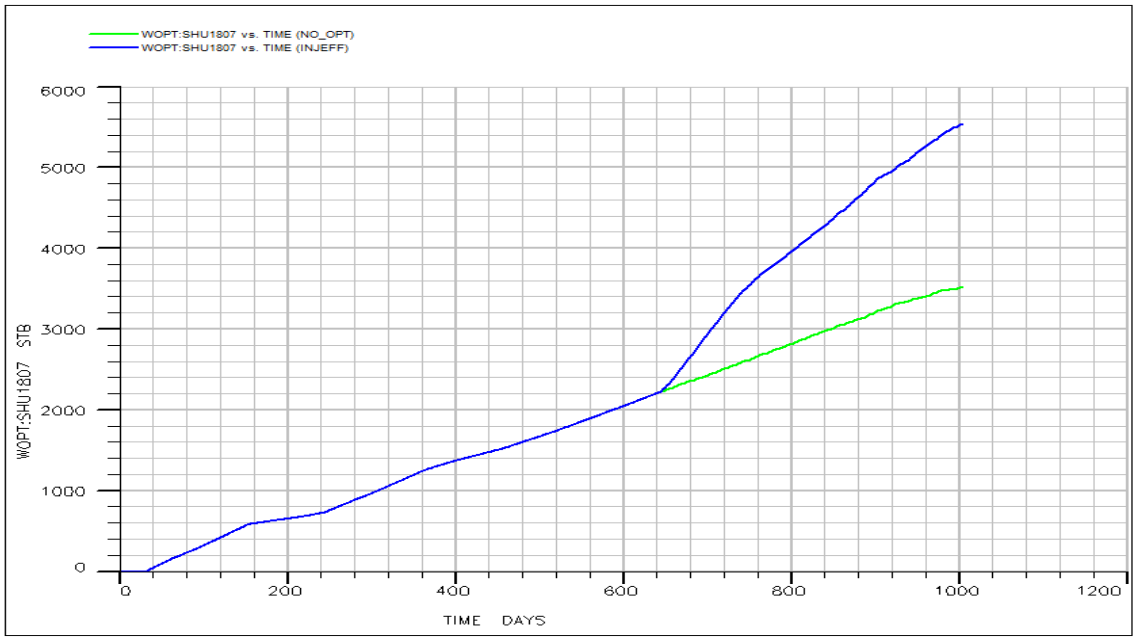

Fig. 89: Cumulative Oil Production For Sherrod 1807, "INJEFF" vs. "Do Nothing"

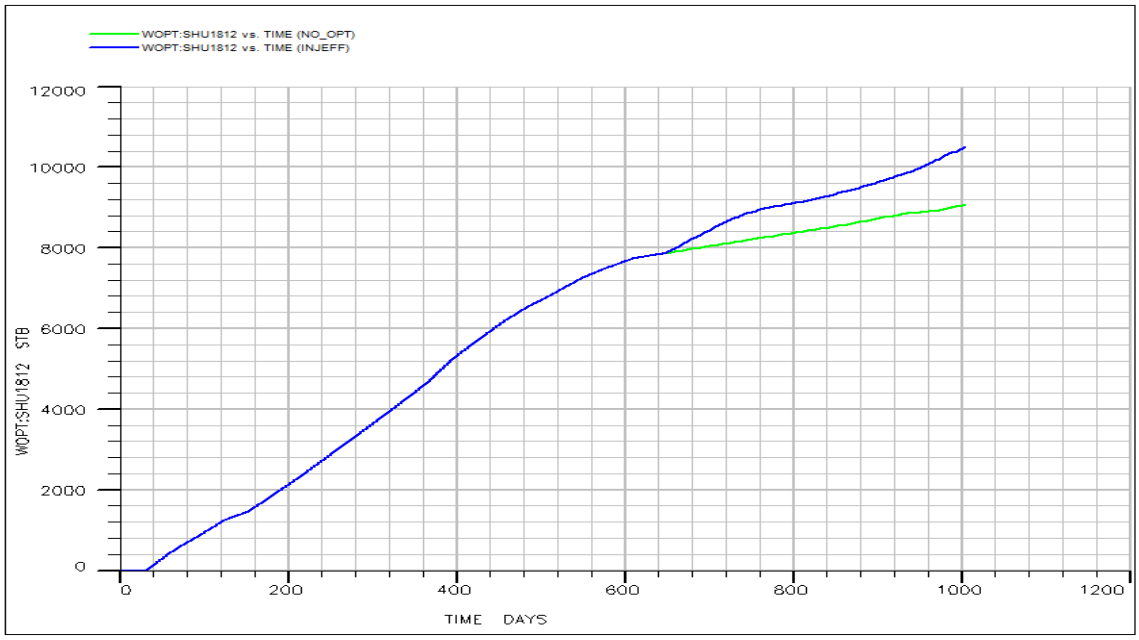

Fig. 90: Cumulative Oil Production For Sherrod 1812, "INJEFF" vs. "Do Nothing"

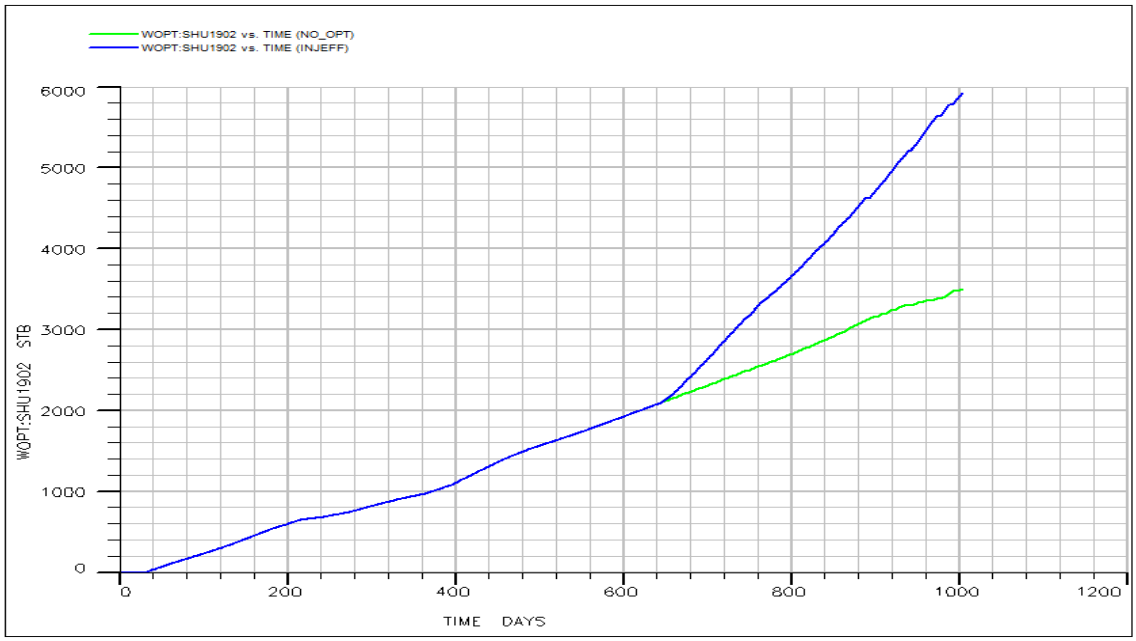

Fig. 91: Cumulative Oil Production For Sherrod 1912, "INJEFF" vs. "Do Nothing"

5.3. Sensitivity on Injection Rate

In order to test PFM capability, injection rate for forecasting period was doubled and tripled. The optimization was still able to improve oil production but essential benefit of it is seen on water production. For doubled injection rate, oil production was increased by 4,000 bbl under "INJEFF" optimization strategy while almost 60,000 bbl of less water was produced than "Do Nothing" case as shown Fig. 92 and Fig. 93, respectively. Similarly, Fig. 94 and Fig. 95 illustrate that almost 70,000 bbl of extra water was not being produced in addition to 5,000 bbl enhancement in oil production with optimized well rates.

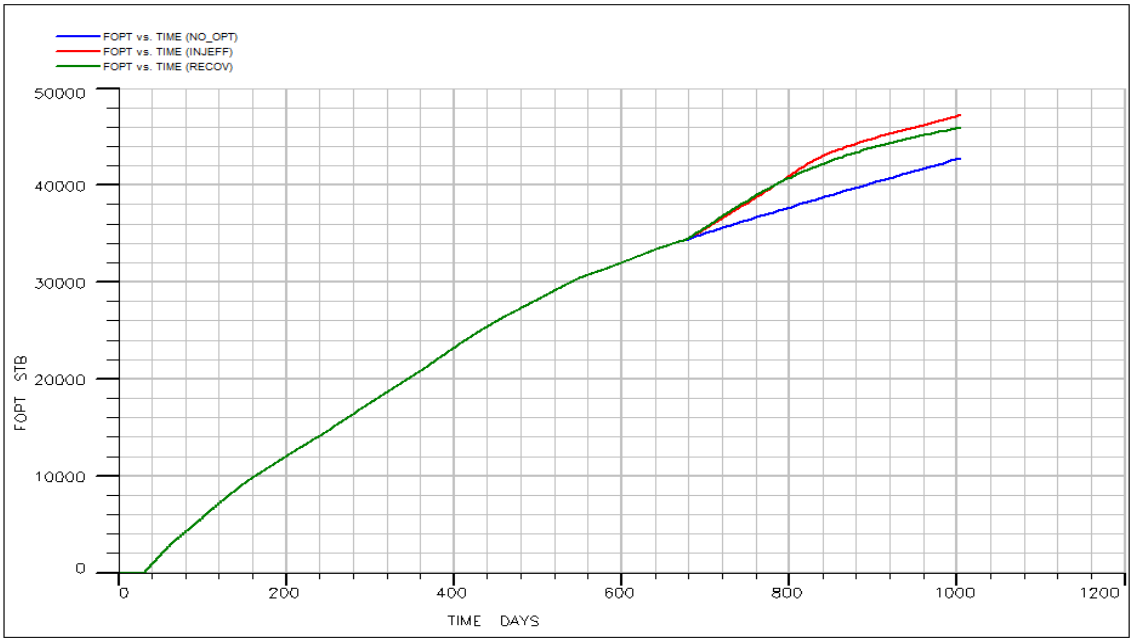

Fig. 92: Optimized Oil Production For Doubled Injection Rate

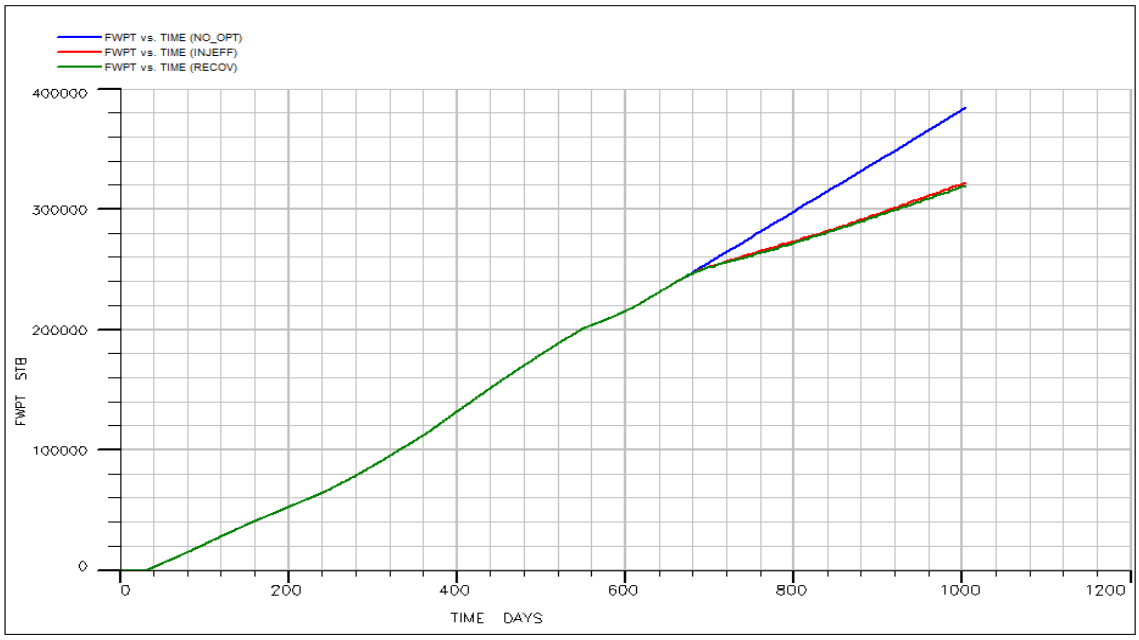

Fig. 93: Optimized Water Production For Doubled Injection Rate

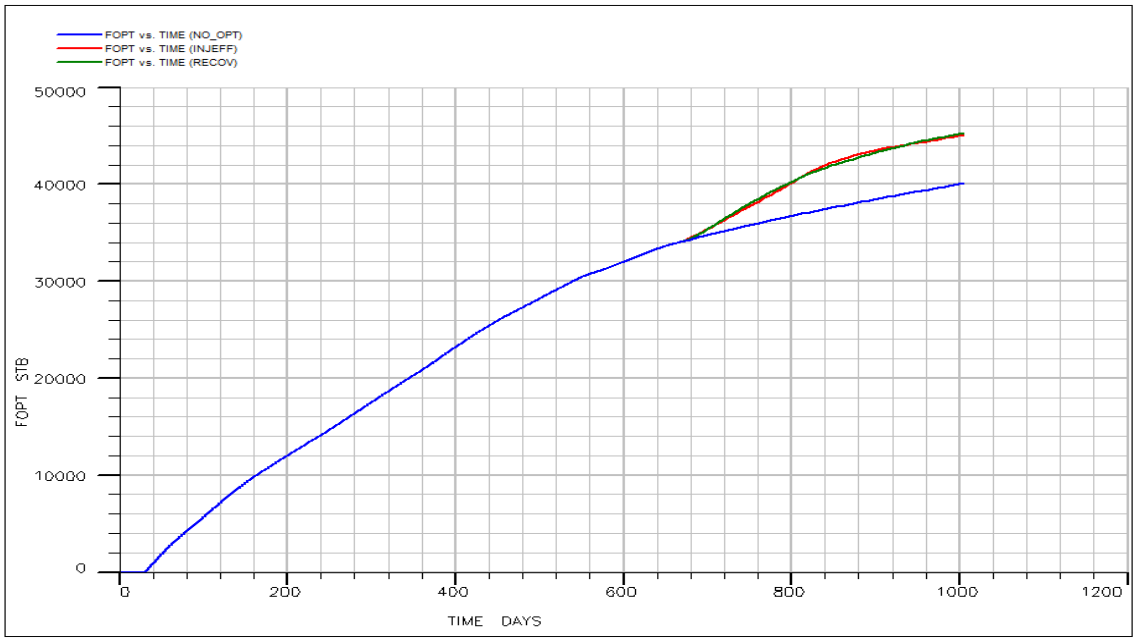

Fig. 94: Optimized Oil Production For Tripled Injection Rate

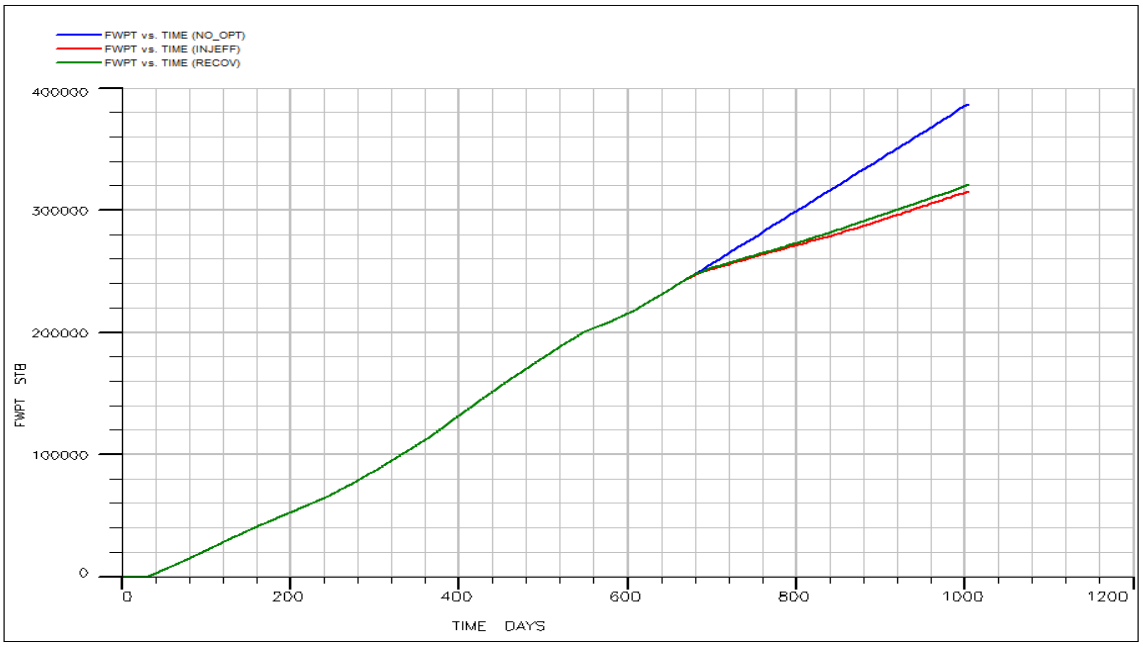

Fig. 95: Optimized Water Production For Tripled Injection Rate

Furthermore, a manual sensitivity on injection rate was conducted for "Do Nothing" scenario. Increasing injection rate adversely affects both cumulative oil and cumulative water production for this particular history matched model. As can be seen from Fig. 96, more water injection causes less oil production while accelerates water production shown by Fig. 97. Therefore, it is suggested to keep injection rate at reasonable level.

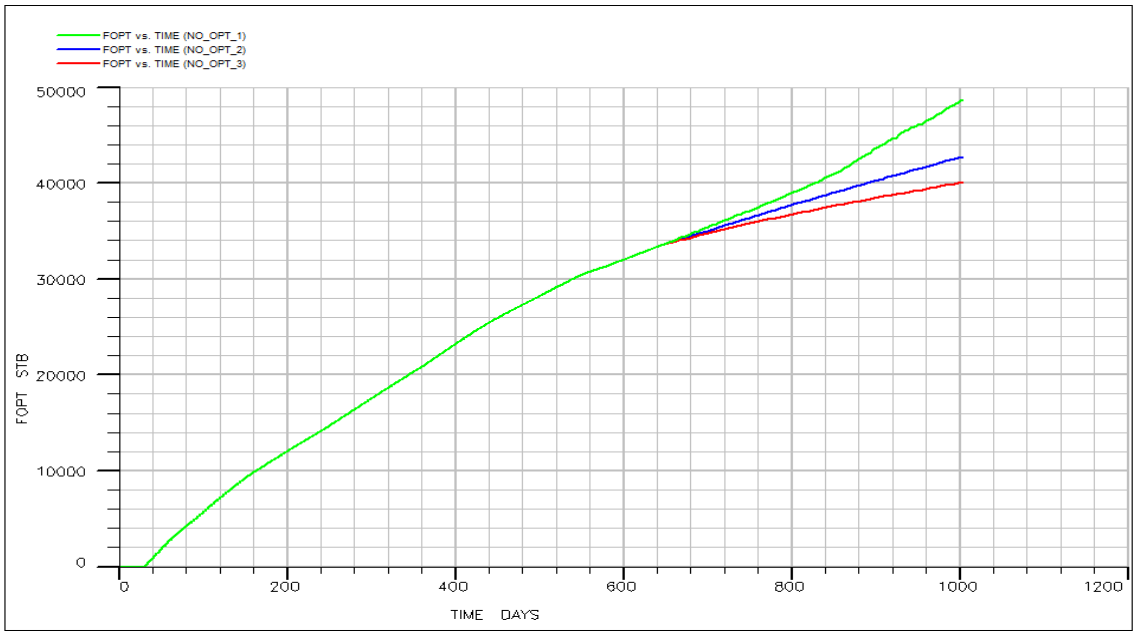

Fig. 96: Cumulative Oil Production For Increasing Injection Rate

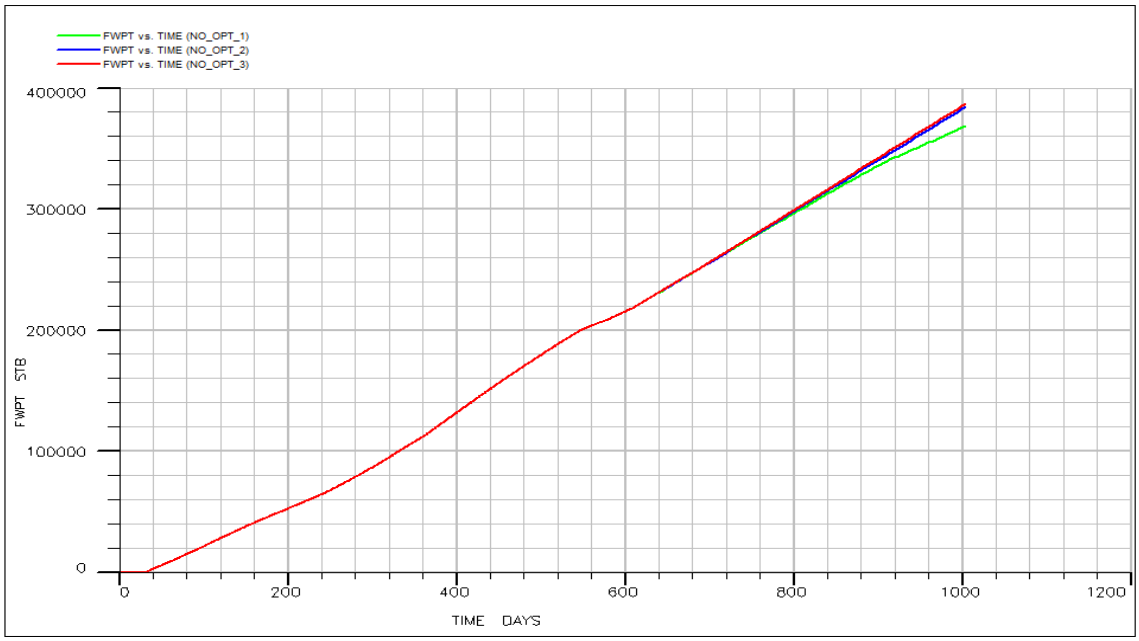

Fig. 97: Cumulative Water Production For Increasing Injection Rate

5.4. Summary of Improved Waterflood Management

The main interpretations from the optimization study for waterflood management are listed:

1. Sherrod 1003, Sherrod 1004, Sherrod 1207, and Sherrod 1208 were classified as less efficient wells with respect to oil production per water production due to injector. Conversely, PFM assigned Sherrod 1011, Sherrod 1807, Sherrod 1812, and Sherrod 1902 as more efficient wells according to the same criteria.
2. Well classification mostly agreed with tracer response in such a way that high tracer responses correspond with low injection efficiency, while low-tracer-response wells produce more oil per amount of injected water.
3. Once ranking of injection efficiencies for wells was finished, optimized well rates generated by the PFM suite succeeded in enhancing oil recovery up to 8,000 bbl and reducing water production by 10,000 bbl for this particular model.
4. High injection rates clearly highlighted the advantage of applying well rate optimization in reducing recycled water production.
5. A negative impact of increasing injection rate on cumulative oil production was demonstrated for the “Do Nothing” case by manual sensitivity analysis.

CHAPTER VI

CONCLUSIONS AND RECOMMENDATIONS

6.1. Conclusions

In this study, dynamic reservoir characterization of the Sherrod Unit, a naturally fractured reservoir, was done based on field production performance and tracer responses. To accomplish accurate reservoir characterization, a variety of different approaches such as analytical, streamline-based flow simulation, and production optimization were incorporated into this analysis. Before starting simulation work, tracer responses were categorized in terms of tracer recovery, breakthrough time, velocity, and traced water production by analytical interpretation techniques and were then mapped in order to identify preferential flow trends. A 3D, three-phase, dual-porosity model was simulated by a streamline simulator to replicate historical production performance of inverted nine-spot and breakthrough time of injected tracer. After matching production history, well rates in the history-matched model were optimized to enhance oil production and reduce the amount of recycled water. Main conclusions from this research can be summarized as follows:

1. Field-wide tracer recoery is less than 10% for any injected tracer, which is too low for highly conductive fractures commonly seen in the Spraberry Trend Area. Injected tracer was not confined in the Sherrod Unit and most likely flowed outside the well, as it might be produced by non-sampled wells

because of poor matrix-fracture interaction. Another reason could be excessive dilution of tracer, which was shown for the Sherrod 1003-1012W well pair.

2. Mapping categorized tracer recovery based on its distribution is helpful to assess direction of the dominating fracture system. Even though the map of tracer recovery in the range of 0.1–0.5% shows a very complex fracture system, it disappeared by mapping tracer recovery higher than 0.5%, and then the presence of an E-W fracture trend became obvious. Furthermore, the map of those two categories in a pattern base was helpful to confidently detect a NE-SW fracture system.
3. Calculated water production due to injector based on tracer response is much lower than actual because injected tracer was excessively diluted, which was proved for the Sherrod 1003-1012W well pair. For accurate estimation of water contribution from injector, water production of the well should be monitored before and after the injection period, if it is present.
4. In spite of the recognition of underestimated water production based on tracer response, water influx to the Sherrod can be still one of the reasons for abnormally high water cuts observed in the field for many wells.
5. Breakthrough time analysis showed that water recycling has an influence on low-recovery wells' response after the first 2 weeks, while its effect does not exist for high-tracer-recovery wells, at least during the first 2 weeks. To be

confident, it is suggested to only use tracer responses during the first 2 weeks for interpretation of fracture sets.

6. Neither distribution of overall tracer velocities nor distribution of high-recovery tracer velocities provides any useful information that could be used for fracture characterization because of inconsistent trends.
7. An extremely high-water-saturation example proves that the actual matrix-fracture interaction in the field is much lower than calculated sigma based on fracture spacing. Fracture mineralization seems to be the main reason for limited counter-current flow between the matrix and fracture, in spite of a closely spaced fracture system.
8. According to the base model properties, water saturation in the matrix is higher than expected. This could be due to either initial fluid distribution settled during pre- or post-deposition of the reservoir, in which the matrix had been watered before any field production started or to an external water source flowing to the field after field production. To a certain extent, both of them are believed to be valid.
9. Flow domination in field production and high tracer responses strongly agree on the presence of highly conductive fracture systems in the E-W and NE-SW directions. However, a very poor fracture system was observed in the N-S direction, while almost no fracture system exists in the NW-SE direction according to tracer recovery.

10. The tendency of flow observed with both higher liquid production and more tracer recovery toward the W and N-E directions could be a result of reservoir dipping and pressure difference rather than oriented fracture system.
11. High tracer response does not necessarily mean more allocated water, as in the case of Sherrod 1807.
12. In off-trend wells, production capacity of newly drilled wells is larger than old wells because of an unswept drainage area.
13. Regeneration of historical production performance was achieved by the constructed model based on dynamic data for oil and water at both the field and well scale.
14. Deficiency of gas production resulted in a low GOR and high voidage replacement ratio. However, trend and magnitude of the latter is quite similar to observed data. Thus, errors due to lower gas production could be evaluated as uncertainty.
15. PFM classified on-trend wells as less efficient wells with respect to oil production per water production due to injector, except Sherrod 1004. On the other hand, off-trend wells, except Sherrod 1807, were classified as more efficient wells according to the same criteria.
16. An enhancement of 8,000 bbl of oil and a reduction of 10,000 bbl of recycled water production was achieved for this particular model by allocating more water toward off-trend wells while lowering or shutting-in on-trend wells.

17. High injection rates underlined the benefits of applying well rate optimization in clearly reducing recycled water production.

6.2. Recommendations for Reservoir Management

It is clear that injected water doesn't yield a considerable increment in oil production, and a large portion of injected water is recycled by on-trend wells. The short-term objective should be controlling water movement in the fracture, while the long-term objective should be increasing matrix contribution to oil recovery. Some of the suggestions from this study are as follows:

1. The adverse impact of highly conductive fractures on waterflood efficiency can be minimized by shutting-in or lowering the flow rate of on-trend wells, which allows more water movement toward off-trend wells.
2. Besides on-trend wells, well rate for off-trend producers and injectors should also be optimized to improve waterflooding.
3. The computation efficiency of streamline simulation and its visual robustness are useful for applying rate optimization at the full-field scale as a surveillance model.
4. A poor matrix-fracture transfer mechanism limits overall waterflood efficiency. Therefore, other kinds of applications that can enhance the interaction between the two media should be considered a long-term objective.

6.3. Recommendations for Future Work

1. Validation of the matched model and reducing uncertainty in reservoir properties with additional data
2. Construction of a base fracture model for the field according to high tracer recovery
3. Matching historical production performance at the field scale and conducting different optimization strategies under economic limits based on the shown workflow to improve waterflooding

REFERENCES

Abbaszadeh-Dehghani, M. and Brigham, W.E., 1984. Analysis of Well-to-Well Tracer Flow to Determine Reservoir Layering. Journal of Petroleum Technology, 36(10): 1753-1762.

Agca, C., 1987. Field Tracer Studies Using a Compositional Simulator. M.S. Thesis, The University of Texas at Austin.

Agca, C., Pope, G.A. and Sepehrnoori, K., 1990. Modelling and Analysis of Tracer Flow in Oil Reservoirs. Journal of Petroleum Science and Engineering, 4(1): 3-19.

Akin, S., 2001. Analysis of Tracer Tests with Simple Spreadsheet Models. Computers & Geosciences, 27(2): 171-178.

Al-Najem, A.A., Siddiqui, S., Soliman, M. and Yuen, B., 2012. Streamline Simulation Technology: Evolution and Recent Trends, SPE Saudi Arabia Section Technical Symposium and Exhibition. Society of Petroleum Engineers, Al-Khobar, Saudi Arabia.

Allison, S.B., Pope, G.A. and Sepehrnoori, K., 1991. Analysis of Field Tracers for Reservoir Description. Journal of Petroleum Science and Engineering, 5(2): 173-186.

Altinay, E.I., 2005. Application of inverse modeling to partitioning interwell tracer tests for estimating oil saturation. M.S. Thesis, The University of Texas at Austin.

Asakawa, K., 2005. A Generalized Analysis of Partitioning Interwell Tracer Tests. Ph.D. Thesis, The University of Texas at Austin, 239-239 p. pp.

Baker, R.O., 1996. Reasons for the Relatively Low Recovery of the Spraberry Waterfloods. PRRC Spraberry Database, New Mexico.

Baker, R.O., Contreras, R.A. and Sztukowski, D., 2000. Characterization of the Dynamic Fracture Transport Properties in a Naturally Fractured Reservoir, SPE Permian Basin Oil and Gas Recovery Conference. Copyright 2000, Society of Petroleum Engineers Inc., Midland, Texas.

Baldwin Jr., D.E., 1966. Prediction of Tracer Performance in a Five-Spot Pattern. Journal of Petroleum Technology, 18(4): 513-517.

Banik, A.K. and Schechter, D.S., 1996. Characterization of the Naturally Fractured Spraberry Trend Shaly Sands Based on Core and Log Data, Permian Basin Oil and Gas Recovery Conference. Copyright 1996, Society of Petroleum Engineers Inc., Midland, Texas.

Barenblatt, G.I., Zheltov, I.P. and Kochina, I.N., 1960. Basic Concepts in the Theory of Seepage of Homogeneous Liquids in Fissured Rocks [Strata]. Journal of Applied Mathematics and Mechanics, 24(5): 1286-1303.

Barfield, E.C., Jordan, J.K. and Moore, W.D., 1959. An Analysis of Large-Scale Flooding in the Fractured Spraberry Trend Area Reservoir. Journal of Petroleum Technology, 11(4): 15-19.

Batycky, R.P., 1997. A Three-Dimensional Two-Phase Field Scale Streamline Simulator. Ph.D. Thesis, Stanford University, 163-163 p. pp.

Batycky, R.P., Blunt, M.J. and Thiele, M.R., 1997. A 3D Field-Scale Streamline-Based Reservoir Simulator. SPE Reservoir Engineering, 12(4): 246-254.

Beraldo, V.T., Blunt, M.J. and Schiozer, D.J., 2008. Compressible Streamline-Based Simulation with Changes in Oil Composition, SPE Annual Technical Conference and Exhibition. Society of Petroleum Engineers, Denver, Colorado, USA.

Beraldo, V.T., Blunt, M.J., Schiozer, D.J. and Qi, R., 2007. Streamline Simulation With an API Tracking Option, EUROPEC/EAGE Conference and Exhibition. Society of Petroleum Engineers, London, U.K.

Berenblyum, R.A., Shapiro, A.A., Jessen, K., Stenby, E.H. and Franklin M. Orr, J., 2003. Black Oil Streamline Simulator With Capillary Effects, SPE Annual Technical Conference and Exhibition. Society of Petroleum Engineers, Denver, Colorado.

Brigham, W.E. and Smith Jr., D.H., 1965. Prediction of Tracer Behavior in Five-Spot Flow, Conference on Production Research and Engineering. Society of Petroleum Engineers Tulsa, Oklahoma.

Brownscombe, E.R. and Dyes, A.B., 1952. Water-Imbibition Displacement-A Possibility for the Spraberry, Drilling and Production Practice. American Petroleum Institute, Washington, DC.

Cheng, H., Oyerinde, A.S., Datta-Gupta, A. and Milliken, W.J., 2006. Compressible Streamlines and Three-Phase History Matching, SPE/DOE Symposium on Improved Oil Recovery. Society of Petroleum Engineers, Tulsa, Oklahoma.

Chowdhury, T., 2002. Improving Dual-Porosity Simulation of Waterflood Performance in the Naturally Fractured Spraberry Trend Area. M.S. Thesis, Texas A&M University.

Christie, R.S. and Blackwood, J.C., 1952. Characteristic and Production Performance of the Spraberry, Drilling and Production Practice. American Petroleum Institute, Washington, DC

Cooke, C.E.J., 1971. Method of Determining Residual Oil Saturation in Reservoirs, U.S. Patent No. 3590923

Danckwerts, P.V., 1953. Continuous Flow Systems: Distribution of Residence Times. Chemical Engineering Science, 2(1): 1-13.

Datta-Gupta, A. and King, M.J., 1995. A Semianalytic Approach to Tracer Flow Modeling in Heterogeneous Permeable Media. Advances in Water Resources, 18(1): 9-24.

Datta-Gupta, A. and King, M.J., 2007. Streamline Simulation: Theory and Practice. Society of Petroleum Engineers, Richardson, Texas.

Datta-Gupta, A., Yoon, S., Vasco, D.W. and Pope, G.A., 2002. Inverse Modeling of Partitioning Interwell Tracer Tests: A Streamline Approach. Water Resources Research, 38(6): 15-1-15-17.

Deans, H.A., 1978. Using Chemical Tracers to Measure Fractional Flow and Saturation In-Situ, SPE Symposium on Improved Methods of Oil Recovery. Copyright 1978, American Institute of Mining, Metallurgical, and Petroleum Engineers, Inc., Tulsa, Oklahoma.

Deans, H.A. and Carlisle, C.T., 1986. Single-Well Tracer Test in Complex Pore Systems, SPE Enhanced Oil Recovery Symposium. Copyright 1986, Society of Petroleum Engineers, Inc., Tulsa, Oklahoma.

Deans, H.A. and Shallenberger, L.K., 1974. Single-Well Chemical Tracer Method to Measure Connate Water Saturation, SPE Improved Oil Recovery Symposium. Copyright 1974, American Institute of Mining, Metallurgical and Petroleum Engineers Inc., Tulsa, Oklahoma.

Dershowitz, B., LaPointe, P., Eiben, T. and Wei, L., 2000. Integration of Discrete Feature Network Methods With Conventional Simulator Approaches. SPE Reservoir Evaluation & Engineering, 3(2): 165-170.

Dershowitz, W.S. and Doe, T.W., 1988. Practical Applications of Discrete Fracture Approaches in Hydrology, Mining, and Petroleum Extraction, International Conference on Fluid Flow in Fractured Rocks. Georgia State University, Atlanta, pp. 381-396.

Donato, G.D., Huang, W. and Blunt, M., 2003. Streamline-Based Dual Porosity Simulation of Fractured Reservoirs, SPE Annual Technical Conference and Exhibition. Society of Petroleum Engineers, Denver, Colorado.

Dyes, A.B. and Johnston, O.C., 1953. Spraberry Permeability From Build-Up Curve Analyses. Journal of Petroleum Technology, 5(5): 135-138.

Elkins, L.F., 1953. Reservoir Performance and Well Spacing, Spraberry Trend Area Field of West Texas. Journal of Petroleum Technology, 5(7): 177-196.

Elkins, L.F. and Skov, A.M., 1960. Determination of Fracture Orientation from Pressure Interference. Petroleum Transactions, AIME, 219: 301-304.

Elkins, L.F. and Skov, A.M., 1962. Large Scale Waterflood Performance Sprayberry Field, West Texas, Fall Meeting of the Society of Petroleum Engineers of AIME. Society of Petroleum Engineers Los Angeles, California.

Fay, C.H. and Pratts, M., 1951. The Application of Numerical Methods to Cycling and Flooding Problems, 3rd World Petroleum Congress. World Petroleum Congress, The Hague, the Netherlands.

Ghori, S.G., Jilani, S.Z., Alhuthali, A., Krinis, D. and Kumar, A.T.A., 2007. Improving Injector Efficiencies Using Streamline Simulation: A Case Study in a Giant Middle East Field, SPE Middle East Oil and Gas Show and Conference. Society of Petroleum Engineers, Kingdom of Bahrain.

Gilman, J.R. and Kazemi, H., 1983. Improvements in Simulation of Naturally Fractured Reservoirs. Society of Petroleum Engineers Journal, 23(4): 695-707.

Grinestaff, G.H., 1999. Waterflood Pattern Allocations: Quantifying the Injector to Producer Relationship with Streamline Simulation, SPE Western Regional Meeting. Society of Petroleum Engineers, Anchorage, Alaska.

Grinestaff, G.H. and Caffrey, D.J., 2000. Waterflood Management: A Case Study of the Northwest Fault Block Area of Prudhoe Bay, Alaska, Using Streamline Simulation and Traditional Waterflood Analysis, SPE Annual Technical Conference and Exhibition. Copyright 2000, Society of Petroleum Engineers Inc., Dallas, Texas.

Grove, D.B. and Beetem, W.A., 1971. Porosity and Dispersion Constant Calculations for a Fractured Carbonate Aquifer Using the Two Well Tracer Method. Water Resources Research, 7(1): 128-134.

Guan, L., Du, Y., Johnson, S.G. and Choudhary, M.K., 2005. Advances of Interwell Tracer Analysis in the Petroleum Industry. Journal of Canadian Petroleum Technology, 44(5).

Guo, B. and Schechter, D.S., 1997. Use of a Simple Mathematical Model for Estimating Formation Damage in Wells Intersecting Long Fractures, SPE European Formation Damage Conference. Copyright 1997, Society of Petroleum Engineers, Inc., The Hague, Netherlands.

Guo, B., Schechter, D.S. and Baker, R.O., 1998. An Integrated Study of Imbibition Waterflooding in the Naturally Fractured Spraberry Trend Area Reservoirs, SPE Permian Basin Oil and Gas Recovery Conference. Society of Petroleum Engineers, Midland, Texas.

Gupta, A.D., Lake, L.W., Pope, G.A. and King, M.J., 1995. A Type-Curve Approach to Analyzing Two-Well Tracer Tests. SPE Formation Evaluation, 10(1): 40-48.

Higgins, R.V. and Leighton, A.J., 1962. Computer Prediction of Water Drive of Oil and Gas Mixtures Through Irregularly Bounded Porous Media Three-Phase Flow. Journal of Petroleum Technology, 14(9): 1048-1054.

Iliassov, P.A., Datta-Gupta, A. and Vasco, D.W., 2001. Field-Scale Characterization of Permeability and Saturation Distribution Using Partitioning Tracer Tests: The Ranger Field, Texas, SPE Annual Technical Conference and Exhibition. Copyright 2001, Society of Petroleum Engineers Inc., New Orleans, Louisiana.

Jensen, C.L. et al., 1998. Field Simulation of Naturally Fractured Reservoirs Using Effective Permeabilities Derived From Realistic Fracture Characterization, SPE Annual Technical Conference and Exhibition. Copyright 1998, Society of Petroleum Engineers Inc., New Orleans, Louisiana.

Jessen, K. and Orr, F.M., 2002. Compositional Streamline Simulation, SPE Annual Technical Conference and Exhibition. Copyright 2002, Society of Petroleum Engineers Inc., San Antonio, Texas.

Lange, A., Basquet, R. and Bourbiaux, B., 2004. Hydraulic Characterization of Faults and Fractures Using a Dual Medium Discrete Fracture Network Simulator, Abu Dhabi International Conference and Exhibition. Society of Petroleum Engineers, Abu Dhabi, United Arab Emirates.

Lange, A., Bourbiaux, B.J. and Bouzian, J., 2005. Tracer-Test Simulation on Discrete Fracture Network Models for the Characterization of Fractured Reservoirs, SPE Europec/EAGE Annual Conference. Society of Petroleum Engineers, Madrid, Spain.

Lee, S.H., Durlofsky, L.J., Lough, M.F. and Chen, W.H., 1997. Finite Difference Simulation of Geologically Complex Reservoirs With Tensor Permeabilities, SPE Reservoir Simulation Symposium. Copyright 1997, Society of Petroleum Engineers, Inc., Dallas, Texas.

Lee, S.H. and Lough, M.F., 1999. An Efficient Finite Difference Model For Flow In a Reservoir With Multiple Length-Scale Fractures, SPE Annual Technical Conference and Exhibition. Society of Petroleum Engineers, Houston, Texas.

Lichtenberger, G.J., 1991. Field Applications of Interwell Tracers for Reservoir Characterization of Enhanced Oil Recovery Pilot Areas, SPE Production Operations Symposium. Copyright 1991, Society of Petroleum Engineers, Inc., Oklahoma City, Oklahoma.

Long, J.C.S., Gilmour, P. and Witherspoon, P.A., 1985. A Model for Steady Fluid Flow in Random Three-Dimensional Networks of Disc-Shaped Fractures. Water Resour. Res. Water Resources Research, 21(8): 1105-1115.

McDonald, P., Lorenz, J.C., Sizemore, C., Schechter, D.S. and Sheffield, T., 1997. Fracture Characterization Based on Oriented Horizontal Core From the Spraberry Trend Reservoir: A Case Study, SPE Annual Technical Conference and Exhibition. Copyright 1997, Society of Petroleum Engineers, Inc., San Antonio, Texas.

Moreno, J., Kazemi, H. and Gilman, J.R., 2004. Streamline Simulation of Countercurrent Water-Oil and Gas-Oil Flow in Naturally Fractured Dual-Porosity Reservoirs, SPE Annual Technical Conference and Exhibition. Society of Petroleum Engineers, Houston, Texas.

Muskat, M. and Wyckoff, R.D., 1934. A Theoretical Analysis of Water-Flooding Networks. Transactions of the AIME, 107(1): 62-76.

Osako, I. and Datta-Gupta, A., 2007. A Compositional Streamline Formulation With Compressibility Effects, SPE Reservoir Simulation Symposium. Society of Petroleum Engineers, Houston, Texas.

Ouenes, A. and Hartley, L.J., 2000. Integrated Fractured Reservoir Modeling Using Both Discrete and Continuum Approaches, SPE Annual Technical Conference and Exhibition. Copyright 2000, Society of Petroleum Engineers Inc., Dallas, Texas.

Oyerinde, A.S., 2005. A Composite Tracer Analysis Approach to Reservoir Characterization. M.S. Thesis, Texas A&M University.

Peddibhotla, S., Cubillos, H., Datta-Gupta, A. and Wu, C.H., 1996. Rapid Simulation of Multiphase Flow Through Fine-Scale Geostatistical Realizations Using a New, 3-D, Streamline Model: A Field Example, Petroleum Computer Conference. Copyright 1996, Society of Petroleum Engineers, Inc., Dallas, Texas.

Ramirez-S., J., Samaniego V., F., Rodriguez, F. and Rivera-R., J., 1995. Tracer-Test Interpretation in Naturally Fractured Reservoirs. SPE Formation Evaluation, 10(3): 186-192.

Ramirez, J., Samaniego, F.V., Rivera, J.R. and Rodriguez, F., 1993. Tracer Flow in Naturally Fractured Reservoirs, Low Permeability Reservoirs Symposium. Copyright 1993, Society of Petroleum Engineers, Inc., Denver, Colorado.

Rodriguez, P.G., Segura, M.K. and Moreno, F.J.M., 2003. Streamline Methodology Using an Efficient Operator Splitting for Accurate Modelling of Capillarity and Gravity Effects, SPE Reservoir Simulation Symposium. Copyright 2003, Society of Petroleum Engineers Inc., Houston, Texas.

Rosenbrock, H.H., 1960. An Automatic Method for Finding the Greatest or Least Value of a Function. The Computer Journal, 3(3): 175-184.

Samaniego, F. et al., 2005. A Tracer Injection-Test Approach to Reservoir Characterization: Theory and Practice, International Petroleum Technology Conference. International Petroleum Technology Conference, Doha, Qatar.

Sarda, S., Jeannin, L., Basquet, R. and Bourbiaux, B., 2002. Hydraulic Characterization of Fractured Reservoirs: Simulation on Discrete Fracture Models. SPE Reservoir Evaluation & Engineering, 5(2): 154-162.

Sato, K. and Abbaszadeh, M., 1996. Tracer Flow and Pressure Performance of Reservoirs Containing Distributed Thin Bodies. SPE Formation Evaluation, 11(3): 185-193.

Schechter, D., 2002. Waterflooding and CO2 Injection in the Naturally Fractured Spraberry Trend Area. Journal of Canadian Petroleum Technology, 41(10).

Schechter, D.S., McDonald, P., Sheffield, T. and Baker, R., 1996a. Reservoir Characterization and CO2 Pilot Design in the Naturally Fractured Spraberry Trend Area, Permian Basin Oil and Gas Recovery Conference. Copyright 1996, Society of Petroleum Engineers, Inc., Midland, Texas.

Schechter, D.S., McDonald, P., Sheffield, T. and Baker, R.O., 1996b. Integration of Laboratory and Field Data for Development of a CO2 Pilot in the Naturally Fractured Spraberry Trend, SPE Annual Technical Conference and Exhibition. Copyright 1996, Society of Petroleum Engineers, Inc., Denver, Colorado.

Shinta, A.A. and Kazemi, H., 1993. Tracer Transport in Characterization of Dual-Porosity Reservoirs, SPE Annual Technical Conference and Exhibition. Copyright 1993, Society of Petroleum Engineers, Inc., Houston, Texas.

Shook, G.M., Pope, G.A. and Asakawa, K., 2009. Determining Reservoir Properties and Flood Performance From Tracer Test Analysis, SPE Annual Technical Conference and Exhibition. Society of Petroleum Engineers, New Orleans, Louisiana.

Stalgorova, E. and Babadagli, T., 2011. Field Scale Modeling of Tracer Injection in Naturally Fractured Reservoirs using the Random-Walk Simulation, SPE Western North American Region Meeting. Society of Petroleum Engineers, Anchorage, Alaska.

Tang, D.H., Frind, E.O. and Sudicky, E.A., 1981. Contaminant Transport in Fractured Porous Media: Analytical Solution for a Single Fracture. Water Resources Research, 17(3): 555-564.

Thiele, M., Batycky, R., Pöllitzer, S. and Clemens, T., 2010. Polymer-Flood Modeling Using Streamlines. SPE Reservoir Evaluation & Engineering, 13(2): pp. 313-322.

Thiele, M., Rao, S. and Blunt, M., 1996. Quantifying Uncertainty in Reservoir Performance Using Streamtubes. Math Geol, 28(7): 843-856.

Thiele, M.R. and Batycky, R.P., 2006. Using Streamline-Derived Injection Efficiencies for Improved Waterflood Management. SPE Reservoir Evaluation & Engineering, 9(2): pp. 187-196.

Thomas, L.K., Dixon, T.N. and Pierson, R.G., 1983. Fractured Reservoir Simulation. Society of Petroleum Engineers Journal, 23(1): 42-54.

Tomich, J.F., Dalton Jr., R.L., Deans, H.A. and Shallenberger, L.K., 1973. Single-Well Tracer Method To Measure Residual Oil Saturation. Journal of Petroleum Technology, 25(2): 211-218.

Tyler, N. and Gholston, J.C., 1988. Heterogeneous Deep-Sea Fan Reservoirs, Shackelford and Preston Waterflood Units, Spraberry Trend, West Texas. Bureau of Economic Geology, University of Texas at Austin, Austin, Tex.

Vasco, D.W., Yoon, S. and Datta-Gupta, A., 1999. Integrating Dynamic Data Into High-Resolution Reservoir Models Using Streamline-Based Analytic Sensitivity Coefficients. SPE Journal, 4(4): 389-399.

Wagner, O.R., 1977. The Use of Tracers in Diagnosing Interwell Reservoir Heterogeneities - Field Results. Journal of Petroleum Technology, 29(11): 1410-1416.

Warn, G.F. and Sidwell, R., 1953. Petrology of the Spraberry Sands of West Texas. Journal of Sedimentary Research, 23(2): 67-74.

Warren, J.E. and Root, P.J., 1963. The Behavior of Naturally Fractured Reservoirs. SPE Journal, 3(3): 245-255.

Yoon, S., Barman, I., Datta-Gupta, A. and Pope, G.A., 1999. In-Situ Characterization of Residual NAPL Distribution Using Streamline-Based Inversion of Partitioning Tracer Tests, SPE/EPA Exploration and Production Environmental Conference. Copyright 1999,Society of Petroleum Engineers, Inc., Austin, Texas.

Yuen, D.L., Brigham, W.E. and Cinco-L, H., 1979. Analysis of Five-Spot Tracer Tests to Determine Reservoir Layering. Dept. of Energy [Washington]; Springfield, Va.

APPENDIX A

MODIFIED HISTORY MATCH DATA FILE

A sample file for history matched model properties is provided below.

```
================================

RUNSPEC

FRONTSIM

TITLE

    FRONTSIM FRACTURED RESERVOIR DUAL-PORO MODEL

DIMENS

   76   76   6  /

DUALPORO

OIL

WATER

GAS

DISGAS

FIELD

START

  1 'JUL' 2010 /

UNIFOUT

UNIFIN

GRID
```

==========

DPGRID

NODPPM

INIT

DXV

76*50 /

DYV

76*50 /

DEPTHZ

5929*6930 /

DZV

10 140 10 /

PORO

5776*0.1

5776*0

5776*0.1

5776*0.004

5776*0

5776*0.004

/

PERMX

5776*0.5

5776*0.0

5776*0.5

5776*700

5776*0

5776*500 /

SIGMAV

17328*0.001 /

COPY

'PERMX' 'PERMY' /

/

COPY

'PERMX' 'PERMZ' /

/

GRIDFILE

2 /

PROPS

==========

SWOF

0.22 0.000 1.00 20

0.24 0.001 0.90 14

0.27 0.006 0.76 11

0.31 0.027 0.60 9

0.37 0.096 0.39 6

0.42 0.197 0.26 4

0.495 0.438 0.12 2

0.57 0.8 0 0

/

0.0 0.0 1.0 0

0.5 0.5 0.5 0

1.0 1.0 0.0 0

/

SGOF

0 0 1 0

0.04 0 0.81 0

0.1 0.05 0.58 0.1

0.2 0.13 0.31 0.25

0.3 0.225 0.15 0.4

0.35 0.35 0.00 1.25

/

0 0 1 0

1 1 0 0

/

PVTW

2300 1 3.5E-006 1 0 /

PVDG

14.7 204.631 0.011035

141.7 20.7247 0.011193

268.7 10.6667 0.011415

395.8 7.0649 0.011686

522.8 5.2140 0.012007

649.8 4.0878 0.012379

776.8 3.3315 0.012807

903.8 2.7900 0.013296

1030.9 2.3846 0.013850

1157.9 2.0715 0.014475

1284.9 1.8242 0.015174

1411.9 1.6256 0.015949

1538.9 1.4644 0.016796

1666.0 1.3324 0.017712

1793.0 1.2235 0.018687

1920.0 1.1333 0.019712

2136.0 1.0125 0.021534

2352.0 0.9220 0.023411

2568.0 0.8529 0.025298

2784.0 0.7990 0.027159

3000.0 0.7561 0.028974 /

PVTO

```
0.176   118     1.1740 1.3429 /
0.26    300     1.2160 1.2268 /
0.36    600     1.2580 1.0594 /
0.45    900     1.2960 0.9219 /
0.535   1200    1.3330 0.8143 /
0.621   1500    1.3690 0.7366 /
0.689   1750    1.3990 0.6946 /
0.735   1920    1.4230 0.6680
        2100    1.4202 0.6700
        2400    1.4152 0.6800
        2700    1.4105 0.6900
        3000    1.4059 0.7100 /
/
ROCK
2300 4.0E-006 /
DENSITY
52.3000  62.4300 .05140 /
REGIONS
============================================================
SATNUM
 17328*1 17328*2
/
```

PVTNUM

34656*1

/

EQLNUM

34656*1

/

FIPNUM

34656*1

/

SOLUTION

==========

PRESSURE

34656*2300 /

SWAT

17328*0.51

17328*0.73/

SGAS

34656*0 /

RS

34656*0.735 /

RPTSOL

RESTART=2 /

```
SUMMARY
=====================================================================
WLPT
/
WOPT
/
WWPT
/
WGPT
/
WWCT
/
WGOR
/
WWIR
'SHU1012W' /
FPR
FLPR
FOPT
FWPT
FGPT
FWCT
```

```
FGOR

SCHEDULE

============================================================

RPTRST

 BASIC=3 / 'PRES' 'SWAT' 'SOIL' 'TOF' 'ALLOC' 'FLUXDENS' 'FLOWTOT' /

RPTSLN

LINES=300 BASIC FLOWS ALLOC /

RPTSCHED

  FIP=3 WELLS=2  RESTART=2 SUMMARY=1 CPU=1 ALLOC=3 /

TUNEFSPR

PresFreq MaxMBE MaxNewtCnv MaxLinCnv MaxNewtIt MaxLinIt

    1     0.02    2E-4        2E-5        5      /

WELSPECS

'SHU1012W'  1*      35      38      1*      WAT   5*  AVG /

'SHU1003'     1*      13      44      1*      OIL     5*  AVG /

'SHU1004'     1*      32      13      1*      OIL     5*  AVG /

'SHU1011'     1*      6       19      1*      OIL     5*  AVG /

'SHU1207'     1*      64      32      1*      OIL     5*  AVG /

'SHU1208'     1*      58      5       1*      OIL     5*  AVG /

'SHU1807'     1*      20      72      1*      OIL     5*  AVG /

'SHU1812'     1*      50      68      1*      OIL     5*  AVG /

'SHU1902'     1*      71      59      1*      OIL     5*  AVG /
```

/

COMPDAT

'SHU1012W' 2* 4 4 3* 1 /

'SHU1003' 2* 4 4 3* 1 /

'SHU1004' 2* 4 4 3* 1 /

'SHU1011' 2* 4 4 3* 1 /

'SHU1207' 2* 4 4 3* 1 /

'SHU1208' 2* 4 4 3* 1 /

'SHU1807' 2* 4 4 3* 1 /

'SHU1812' 2* 4 4 3* 1 /

'SHU1902' 2* 4 4 3* 1 /

'SHU1012W' 2* 6 6 3* 1 /

'SHU1003' 2* 6 6 3* 1 /

'SHU1004' 2* 6 6 3* 1 /

'SHU1011' 2* 6 6 3* 1 /

'SHU1207' 2* 6 6 3* 1 /

'SHU1208' 2* 6 6 3* 1 /

'SHU1807' 2* 6 6 3* 1 /

'SHU1812' 2* 6 6 3* 1 /

'SHU1902' 2* 6 6 3* 1 /

/

WCONHIST

```
'SHU1003'    'OPEN''LRAT'0      0      0      5*     /
'SHU1004'    'OPEN''LRAT'0      0      0      5*     /
'SHU1011'    'OPEN''LRAT'0      0      0      5*     /
'SHU1012W'   'OPEN''LRAT'0      0      0      5*     /
'SHU1207'    'OPEN''LRAT'0      0      0      5*     /
'SHU1208'    'OPEN''LRAT'0      0      0      5*     /
'SHU1807'    'OPEN''LRAT'0      0      0      5*     /
'SHU1812'    'OPEN''LRAT'0      0      0      5*     /
'SHU1902'    'OPEN''LRAT'0      0      0      5*     /
/
INCLUDE
'LRAT.SCH' /
END
```

==========

APPENDIX B

INITIAL AND FINAL MAPS FOR HISTORY MATCH

Since simulation started in 2010, it is impossible to get a match with uniform reservoir model. Therefore, certain parameters of fracture system were only changed until reasonable match was obtained. Fracture and matrix water saturation, pressure in fracture and gas saturation in fracture are shown in below at beginning of simulation and after history match.

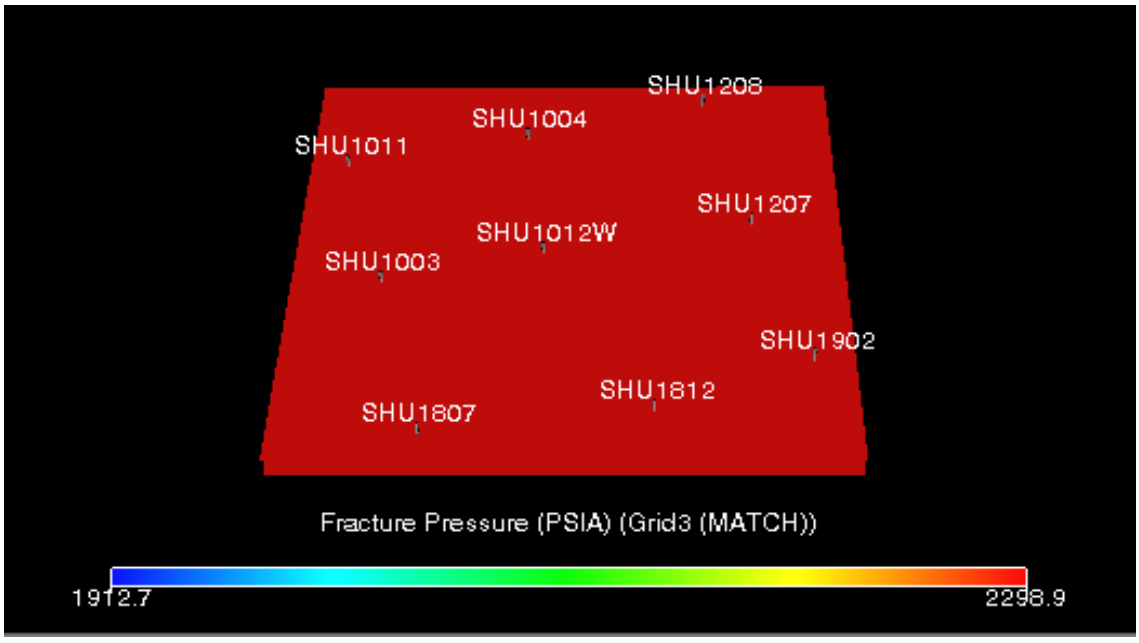

Figure 1: Initial Fracture Pressure, psi

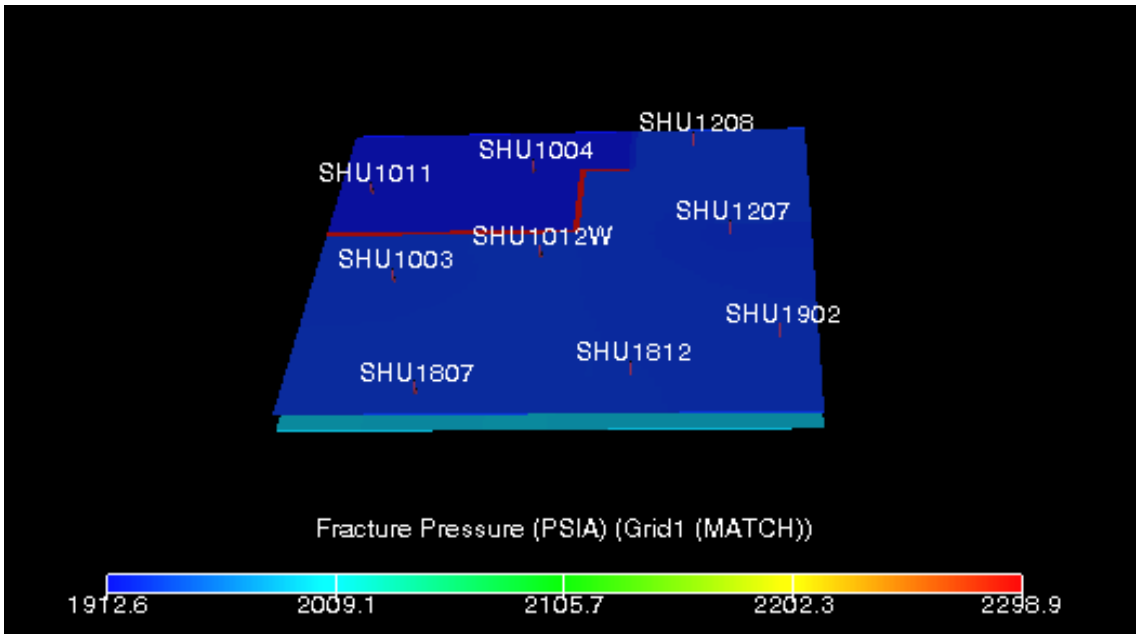

Figure 2: Final Fracture Pressure, psi

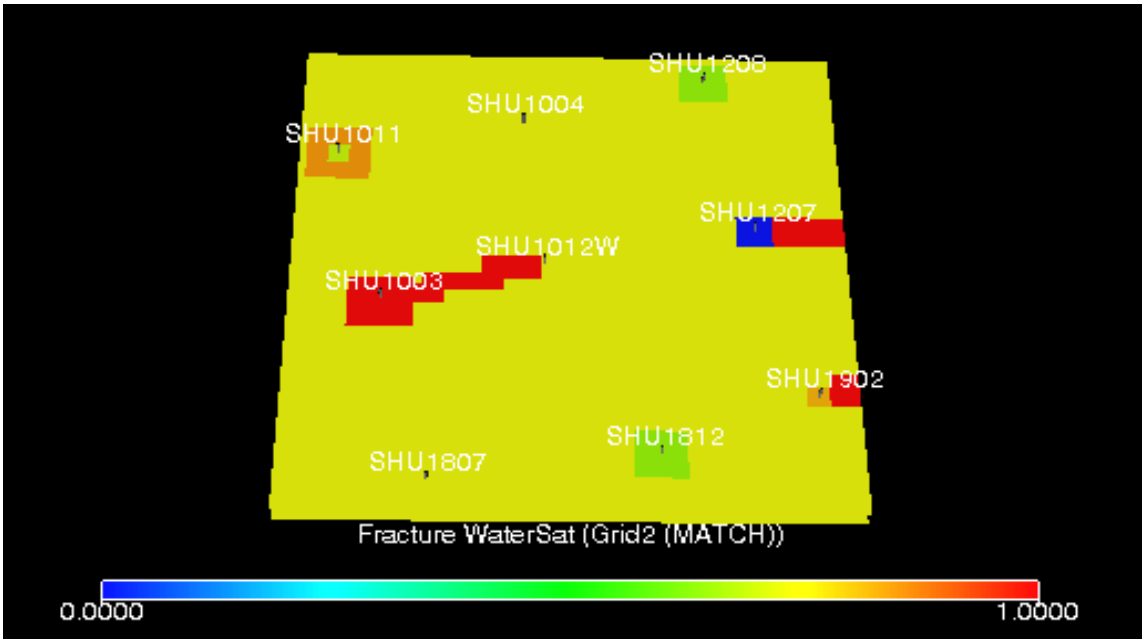

Figure 3: Initial Water Saturation in Fracture

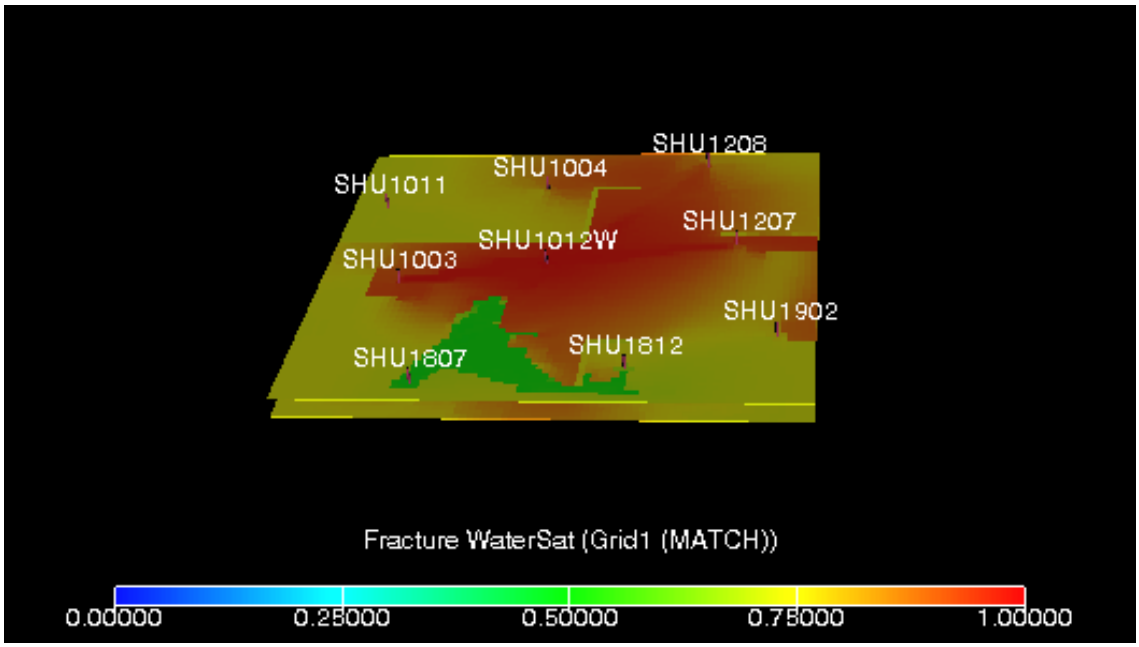

Figure 4: Final Water Saturation in Fracture

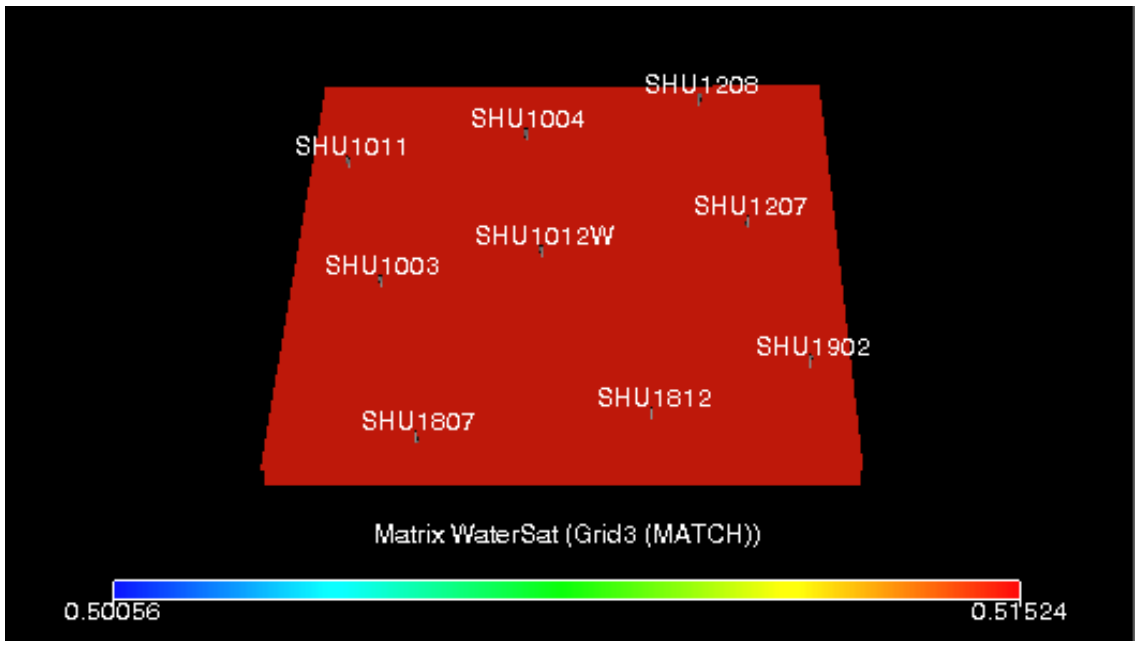

Figure 5: Inital Water Saturation in Matrix

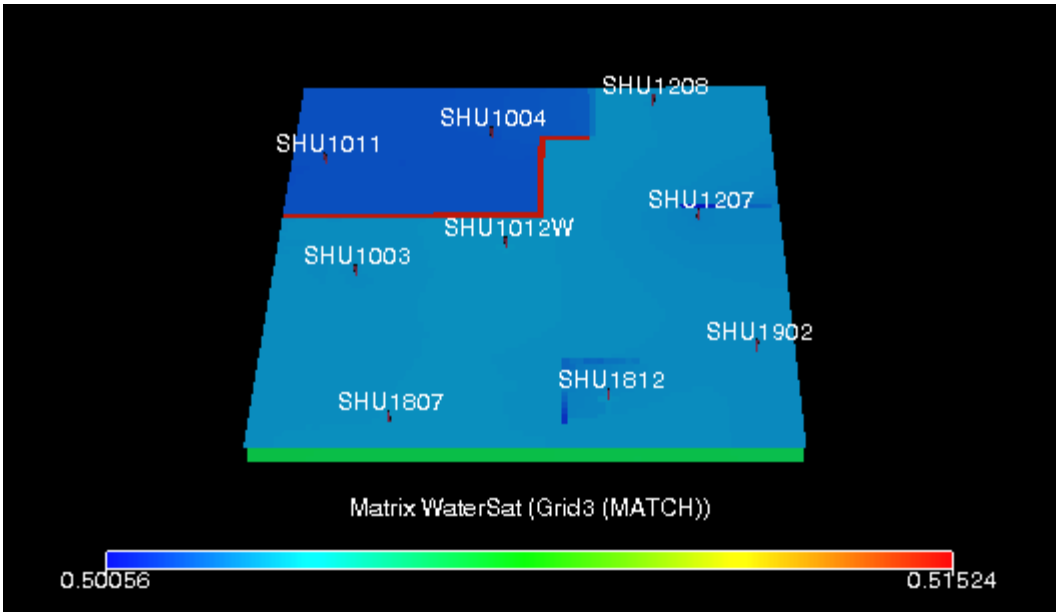

Figure 6: Final Water Saturation in Matrix

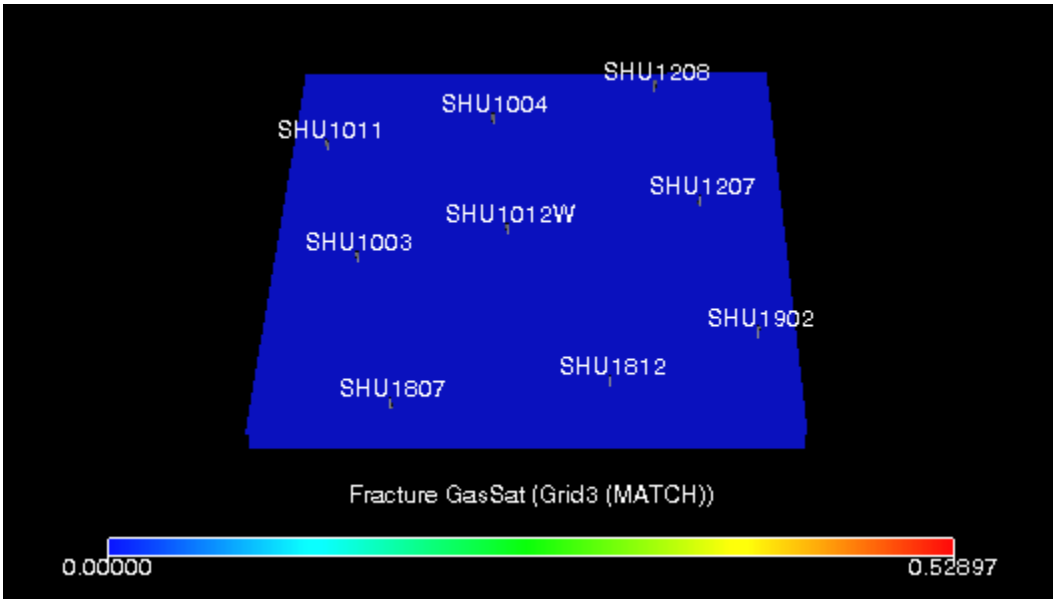

Figure 7: Initial Fracture Gas Saturation

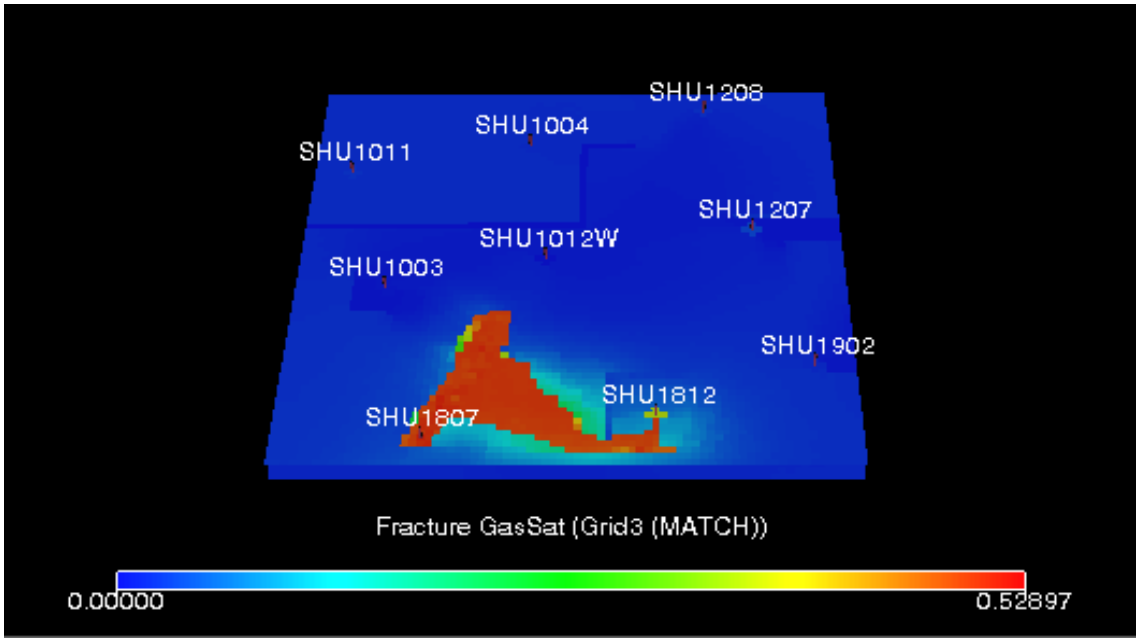

Figure 8: Final Fracture Gas Saturation